Aus der

Klinik und Poliklinik für Psychiatrie und Psychotherapie

Klinik der Universität München

Direktor: Prof. Dr. med. Peter Falkai

Functional genomic screens to identify and validate neuro-developmental modulators of immediate early genes, Arc and Bdnf

Dissertation

zum Erwerb des Doktorgrades der Humanbiologie

an der Medizinischen Fakultät

der Ludwig-Maximilians-Universität zu München

vorgelegt von

Vivek Kumar Sahoo

aus

Odisha, India

Jahr

2024

Mit Genehmigung der Medizinischen Fakultät
der Universität München

Berichterstatter:	Prof. Dr. Moritz Rossner
Mitberichterstatter:	Prof. Dr. Frank Weber Prof. Dr. Anne-Laure Boulesteix
Mitbetreuung durch den promovierten Mitarbeiter:	
Dekan:	Prof. Dr. med. Thomas Gudermann
Tag der mündlichen Prüfung:	17.12.2024

LMU LUDWIG-MAXIMILIANS-UNIVERSITÄT MÜNCHEN

Dean's Office Medical Faculty
Faculty of Medicine

Affidavit

Sahoo, Vivek Kumar

Surname, first name

I hereby declare, that the submitted thesis entitled

Functional genomic screens to identify and validate neuro-developmental modulators of immediate early genes, Arc and Bdnf

is my own work. I have only used the sources indicated and have not made unauthorised use of services of a third party. Where the work of others has been quoted or reproduced, the source is always given.

I further declare that the dissertation presented here has not been submitted in the same or similar form to any other institution for the purpose of obtaining an academic degree.

München, 20.05.2025

Place, Date

Vivek Kumar Sahoo

Signature doctoral candidate

1 Table of Contents

1 Table of Contents 1

Abstract 5

List of figures 6

List of tables 7

List of abbreviations 8

2 Introduction 10

2.1 TargetFinder assay 12

2.1.1 What can be a genetic sensor? 12

2.1.2 *Arc* gene 13

2.1.3 *Bdnf* gene 16

2.1.4 TargetFinder concept 20

2.1.5 TargetFinder is a pooled screening assay 22

2.2 shRNA-Perturb-seq 22

2.2.1 Single-cell RNA sequencing (scRNA-seq) 22

2.2.2 Pooled perturbation screens 26

2.2.3 Pooled perturbation screen for neurons 27

3 Material and Methods 28

3.1 Chapter 1 28

3.1.1 TargetFinder assay using E-SARE as sensor. 28

3.1.2 Cloning shRNA-Perturb-seq parent vector 30

3.1.3 Cloning individual shRNA to shRNA-Perturb-seq parent vector 30

3.1.4 Individual plasmid and AAV library preparation 30

3.1.5 Single nuclei Perturb-seq assay 31

3.1.6 Data analysis 32

3.2 Chapter 2 38

3.2.1 Creating three potential BDNF sensor TargetFinder libraries 38

3.2.2 Evaluation of sensor activity of three potential BDNF sensors 39

3.2.3 Determining optimal time for *mE840 BDNF* sensor maximum activity 40

3.2.4 Creating shRNA-BC library for A452 41

3.2.5 Identifying neuronal modulators of mBDNF E840 sensor 43
3.3 General Methods 46
3.3.1 Cell culture and maintenance 46
3.3.2 AAV production and genomic copies (GC) titer 46
3.3.3 Primary culture of Mouse cortical neurons 48
3.3.4 In-suspension transduction protocol for primary CNs 49
3.3.5 Molecular cloning 49
3.3.6 RNA isolation and cDNA synthesis 51
3.3.7 Quantitative real-time PCR (qRT-PCR) 51
3.3.8 qRT-PCR, primer efficiency testing 52
3.4 Materials 53
3.4.1 Reagents, Kits, Equipment's and Software 53
3.4.2 Oligonucleotide 55
3.4.3 Plasmids 59
3.4.4 AAV 60
3.4.5 Perturb-seq barcodes 61
4 Results 62
4.1 Chapter 1 62
4.1.1 Identification of modulators of the E-SARE sensor. 62
4.1.2 Establishment of shRNA-Perturb-seq 63
4.1.3 shRNA-Perturb-seq experiment 66
4.2 Chapter 2 93
4.2.1 Identification of an optimal BDNF sensor 93
4.2.2 TargetFinder assay with BDNF-E840 as sensor 95
5 Discussion 102
5.1 Chapter 1 102
5.1.1 TargetFinder assay on E-SARE sensor identifies genetic modulators of neuronal activity from developmental perspective 102
5.1.2 Optimization of shRNA-Perturb-seq methodology 102
5.1.3 shRNA-Perturb-seq quality assessment 103
5.1.4 Annotating Cell Types and Overcoming Challenges in Cluster Characterization 104
5.1.5 Treatment-Specific transcriptional responses 104
5.1.6 Pseudo-bulk differential analysis identifies perturbation only and combined treatment and perturbation transcriptional response 104

5.1.7 GSEA reveals Perturbation effect upon AMPA treatment 105
5.1.8 Differential Analysis and Pathway Enrichment results helps validating the modulators of E-SARE sensor 105
5.1.9 Methodological Insights and Future Directions 106
5.2 Chapter 2 107
5.2.1 Characterization of BDNF-E840 as sensor 107
5.2.2 TargetFinder assay with BDNF-E840 as sensor 107
5.3 Limitations 109
5.3.1 Sensitivity and Specificity of Genetic Sensors 109
5.3.2 Temporal Resolution and Timing of Interventions 109
5.3.3 Variability in *in-vitro* Culture Conditions 109
5.3.4 Technical Limitations of shRNA-Mediated Knockdown 109
5.3.5 Limitations in Single-Cell RNA Sequencing 110
5.3.6 Transition from NGS to Image-Based Readouts in Single-Cell Assays 110
References 112
Acknowledgements 121

Abstract

Objective:

This study aims to address the scalability challenges in functional genomics research on neuronal cells by using TargetFinder and shRNA-Perturb-seq to explore the molecular mechanisms of neuronal plasticity and survival within the context of neurodevelopment, focusing on the immediate early genes (IEGs), *Arc* and *Bdnf*.

Methods:

The TargetFinder assay was utilized as the initial screening tool, focusing on identifying potential modulators of the pathway sensor under investigation. Through systematic perturbation of gene expression, TargetFinder allowed for the exploration of a wide array of genetic factors that may influence the activity or output of the pathway sensor. Complementing this, Perturb-seq provided a deeper examination of the functional consequences of genetic perturbations identified through the initial screen. Perturb-seq enabled a closer look at the transcriptomic changes induced by these modulators, offering mechanistic insights into their effects at the molecular level.

Results and discussion:

In this study, we identified neuronal modulators of the E-SARE and BDNF-E840 genetic sensors using the TargetFinder assay. To characterize modulators of the E-SARE sensor, we developed an shRNA-Perturb-seq assay, successfully adapting Perturb-Seq methodologies from previous studies to primary mouse cortical neurons. To address the unique challenges posed by *in vitro* primary neuron cultures, we devised novel strategies, including direct gene expression capture through robust Pert-BC expression and a protocol for in-suspension transduction and cell pooling.

We created a marker gene list for cell-type cluster annotation, which will serve as a template for future primary mouse cortical neurons snRNA-seq experiments. By effectively capturing primary and delayed response genes, we observed distinct transcriptional profiles following BIC cocktail and AMPA stimulation. The perturbation effect induced by AMPA showed negative enrichment in pathways related to long-term potentiation, axon guidance, synaptic membrane regions, and post-synaptic signal transmission. Furthermore, studying the combined effects of perturbation and treatment revealed positive enrichment in nervous system developmental pathways, indicating that all perturbations result in neuron development delay. This supports our initial hypothesis of capturing near-developmental modulators of the E-SARE sensor. Further empirical validation is required to gain a deeper mechanistic understanding of both sensors.

List of figures

FIGURE 1 SARE, A REGULATORY ELEMENT OF ARC/ARG-3.1 PROMOTER. 14
FIGURE 2 DESIGN AND CHARACTERIZATION OF THE ARTIFICIAL E-SARE SENSOR. 15
FIGURE 3 FUNCTION OF BDNF/TRKB SIGNALING IN THE CNS 16
FIGURE 4 SCHEMATIC ILLUSTRATION OF THE HUMAN BDNF PROTEIN AND ITS INTRACELLULAR TRAFFICKING... 17
FIGURE 5 BDNF PROTEIN SEQUENCE IS EVOLUTIONARILY CONSERVED ACROSS PRIMATES AND RODENTS. 18
FIGURE 6 TRANSCRIPTIONAL REGULATORY ELEMENTS GOVERNING BDNF/BDNF PROMOTERS I AND IV ACTIVITY. 20
FIGURE 7 SCHEMATIC REPRESENTATION OF THE TARGETFINDER ASSAY CONCEPT. 21
FIGURE 8 POOLED SCREENING EMPLOYING MOLECULAR BARCODES. 22
FIGURE 9 TIMELINE OF MILESTONES IN SINGLE-CELL SEQUENCING TECHNOLOGY. 23
FIGURE 10 SCHEMATIC WORKFLOW OF SINGLE-CELL RNA SEQUENCING (SCRNA-SEQ). 24
FIGURE 11 SCHEMATIC OF DATA ANALYSIS PIPELINE FOR PERTURBATION IDENTIFICATION 34
FIGURE 12 SCHEMATIC OF CLONING STRATEGY FOR TARGETFINDER LIBRARIES 38
FIGURE 13 SCHEMATIC OF DATA ANALYSIS PIPELINE FOR THE TARGETFINDER ASSAY 45
FIGURE 14 TARGETFINDER ASSAY IDENTIFIES DEVELOPMENTAL MODULATORS OF SYNAPTIC ACTIVITY 62
FIGURE 15 FUNCTIONAL TESTING OF SHRNA-PERTURB-SEQ VECTOR IN PRIMARY MOUSE CORTICAL NEURONS. .. 64
FIGURE 16 QUANTIFICATION OF FUNCTIONAL GENOMICS COPIES 64
FIGURE 17 IN-SUSPENSION TRANSDUCTION AND OPTIMIZATION OF CELL POOLING 65
FIGURE 18 SHRNA-PERTURB-SEQ EXPERIMENT. 66
FIGURE 19 NGS READ ANALYSIS 67
FIGURE 20 RELATIVE DISTRIBUTION OF PERTURBATION IDENTITY CONTRIBUTED BY TWO METHODS 68
FIGURE 21 VISUALIZING QC METRICS OF SNRNA-SEQ DATA 68
FIGURE 22 SHRNA-PERTURB-SEQ IDENTIFIES NEURONAL CELL TYPES. 71
FIGURE 23 DIFFERENTIAL GENE EXPRESSION ANALYSIS IDENTIFIES TREATMENT SPECIFIC TRANSCRIPTS IN GLUTAMATERGIC CLUSTER. 72
FIGURE 24 QUALITY CONTROL FOR PSEUDO-BULK DIFFERENTIAL EXPRESSION ANALYSIS. 73
FIGURE 25 CORRELATION HEATMAP PER TREATMENT CONDITION. 74
FIGURE 26 DIFFERENTIAL EXPRESSION OF GENES FROM PERTURBATION ONLY EFFECT ACROSS VARIOUS PERTURBATIONS AND TREATMENT GROUPS 77
FIGURE 27 DIFFERENTIAL EXPRESSION OF GENES FROM TREATMENT AND PERTURBATION COMBINED EFFECT ACROSS VARIOUS PERTURBATIONS AND TREATMENT GROUPS 80
FIGURE 28 UPSET PLOTS COMPARING DEGS FROM PERTURBATION ONLY EFFECT BETWEEN DIFFERENT PERTURBATIONS AND TREATMENT GROUPS. 81
FIGURE 29 UPSET PLOTS COMPARING DEGS FROM PERTURBATION AND TREATMENT EFFECT BETWEEN DIFFERENT PERTURBATIONS AND TREATMENT GROUPS. 82
FIGURE 30 HISTOGRAM DEPICTING ENRICHED PATHWAYS IDENTIFIED DURING GSEA 83
FIGURE 31 HEATMAP REPRESENTATION OF ENRICHMENT SCORE AND SIGNIFICANCE VALUES FOR PERTURBATION EFFECTS ACROSS ALL PERTURBATIONS 84
FIGURE 32 HEATMAP REPRESENTATION OF ENRICHMENT SCORE AND SIGNIFICANCE VALUES FOR TREATMENT AND PERTURBATION COMBINED EFFECTS COMPARED TO SCRAMBLE UNTREATED SAMPLES ACROSS ALL PERTURBATIONS 88
FIGURE 33 HEATMAP REPRESENTATION OF ENRICHMENT SCORE AND SIGNIFICANCE VALUES FOR TREATMENT AND PERTURBATION COMBINED EFFECTS COMPARED TO SCRAMBLE TTX SAMPLES ACROSS ALL PERTURBATIONS 92
FIGURE 34 BDNF-E840 IS IDENTIFIED TO BE THE MOST EFFECTIVE BDNF SENSOR 93
FIGURE 35 TEMPORAL QUANTITATIVE PCR WAS PERFORMED TO IDENTIFY ADEQUATE STIMULATION TIME 94
FIGURE 36 TARGETFINDER ASSAY IDENTIFIES MODULATORS OF BDNF-E840 SENSOR 96
FIGURE 37 TARGETFINDER ASSAY BDNF-E840 SAMPLES QUALITY ASSESSMENT 97
FIGURE 38 DIFFERENTIAL ANALYSIS IDENTIFIES MODULATORS OF BDNF-E840 SENSOR. 99
FIGURE 39 DOT PLOT SHOWING RESULTS OF OVER-REPRESENTATION ANALYSIS. 100

List of tables

TABLE 1 LIST OF REAGENTS, KITS, EQUIPMENT'S AND SOFTWARE'S 53
TABLE 2 LIST OF OLIGONUCLEOTIDES USED. 55
TABLE 3 LIST OF PLASMIDS USED. 59
TABLE 4 LIST OF ADENO-ASSOCIATED VIRUS (AAV) USED. 60
TABLE 5 LIST OF PERUTURBSEQ SHRNA-BC TO TARGET GENE ASSOCIATION USING SANGER SEQUENCING. 61

List of abbreviations

AAV	Adeno-Associated Virus
Arc	Activity-Regulated Cytoskeleton-Associated Protein
BC	Barcodes
Bdnf	Brain-Derived Neurotrophic Factor
BIC	Bicuculline
CaMKIV	Calcium/Calmodulin-Dependent Protein Kinase IV
CaMKs	Ca2+/Calmodulin-Dependent Protein Kinases
CaREs	Calcium Response Elements
CFU	Colonies Forming Units
CNS	Central Nervous System
CREB	cAMP Response Element-Binding Protein
CRISPR	Clustered Regularly Interspaced Short Palindromic Repeats
DEGs	Differentially Expressed Genes
DSMs	Differentially Sensor Modulators
ERK	Extra-cellular Signal Regulated Kinases
FBS	Fetal Bovine Serum
GC	Genomic Copy
GDNF	Glial Cell Line-Derived Neurotrophic Factor
gRNA	Guide RNA
HATs	Histone Acetyltransferases
HDACs	Histone Deacetylases
IEGs	Immediate Early Genes
ITRs	Inverted Terminal Repeats
KD	Knock Down
LTD	Long-Term Depression
LTP	Long-Term Potentiation
MAPKs	Mitogen-Activated Protein Kinases
MEF2	Myocyte Enhancer Factor 2
MOI	Multiplicity Of Infection
NFAT	Nuclear Factor of Activated T Cells
NGS	Next-Generation Sequencing
NMDA	N-Methyl-D-Aspartate
NMDARs	NMDA-Type Glutamate Receptors
ORF	Open Reading Frame
PBS	Phosphate-Buffered Saline
PDL	Poly-D-Lysin
PEI	Polyethyleneimine
PKA	Protein Kinase A
PLL	Poly-L-Lysine

PMA	Phorbol-12-myristat-13-acetat
qPCR	Quantitative PCR
RNAi	RNA Interference
SARE	Synaptic Activity Response Element
scPCR	Single-Cell PCR
scRNA	Single-Cell RNA Sequencing
Shc	SHC (Src-Homology 2-Domain-Containing) Transforming Protein 2
shRNA	Short Hairpin RNA
snRNA-seq	Single-Nuclei RNA Sequencing
SRF	Serum-Responsive Factor
SH-SY5Y	SK-N-SH neuroblastoma cell line
Trk	Tropomyosin Receptor Kinase
t-SNE	T-Distributed Stochastic Neighbor Embedding
TTX	Tetrodotoxin
UMAP	Uniform Manifold Approximation and Projection
UMI	Unique Molecular Identifiers
VGCCs	Voltage-Gated Calcium Channels

2 Introduction

The elucidation of gene function stands as a cornerstone in our quest to comprehend the intricate machinery orchestrating cellular processes, development, and disease (Alberts B, 2002). Across recent decades, strides in molecular biology and genomics have furnished us with potent tools to dissect the roles of individual genes within the vast landscape of the genome. Among these techniques, functional genomic screens have emerged as indispensable instruments for systematically probing gene function on a large scale (Przybyla and Gilbert, 2022).

Functional genomic screens present a holistic approach to unraveling the intricate interplay between genes and cellular phenotypes (Przybyla and Gilbert, 2022). By perturbing gene expression or activity systematically and observing resultant changes in cellular behavior, these screens yield invaluable insights into the underlying genetic determinants governing biological processes (Replogle et al., 2022). Whether aimed at pinpointing genes vital for cell survival, untangling signaling pathways implicated in disease progression, or uncovering potential therapeutic targets, functional genomic screens offer a potent means to decode the functional landscape of the genome (Herholt et al., 2022; Rauscher et al., 2017).

Yet, when it comes to neurons, functional genomic screens encounter distinctive hurdles owing to the intricate nature of the nervous system (Beirute-Herrera et al., 2024). Characterized by cellular heterogeneity and complex regulatory networks finely tuned for neuronal cells, the nervous system poses unique challenges to researchers (Jin et al., 2020; Santinha et al., 2023). Furthermore, technical aspects such as culturing methods, delivery systems, and the scalability of assays compound these challenges, necessitating innovative approaches to overcome them (Ahmed et al., 2023).

Despite these obstacles, recent advancements in technologies such as RNA interference (RNAi), CRISPR-based techniques, and viral-based gene transfer have provided some respite (Beirute-Herrera et al., 2024). These tools enable precise genetic manipulation and perturbation within neuronal populations, empowering researchers to explore gene function with enhanced precision and accuracy (Jin et al., 2020; Santinha et al., 2023). Additionally, the advent of molecular barcoding techniques has revolutionized the efficiency and throughput of functional genomic screens in neurons (Herholt et al., 2022, 2018). By allowing the tagging and tracking of individual genetic elements within a pooled library, molecular barcoding enables the parallel screening of large numbers of genes or genomic regions (Ahmed et al., 2023; Beirute-Herrera et al., 2024).

Furthermore, the integration of next-generation sequencing has revolutionized the field by augmenting our capacity to comprehensively profile gene expression and regulatory elements in neurons (Herholt et al., 2022). This comprehensive analysis

furnishes invaluable insights into the molecular landscape governing neuronal function and dysfunction, aiding in our understanding of neurological disorders (Herholt et al., 2022).

However, the most transformative breakthrough may lie in the emergence of droplet-based single-nucleus RNA sequencing (snRNA-seq) (Macosko et al., 2015). This groundbreaking approach has substantially enhanced the scalability and efficiency of transcriptomic profiling in neuronal populations. By enabling the simultaneous analysis of thousands of individual nuclei, snRNA-seq permits the identification of rare cell types, exploration of cellular heterogeneity, and characterization of transcriptional dynamics with unprecedented resolution (Replogle et al., 2022).

While functional genomic screens in neurons confront unique challenges, the convergence of innovative technologies and methodologies promises to unlock new frontiers in our understanding of the genetic underpinnings of neuronal function and dysfunction (Jin et al., 2020; Santinha et al., 2023). These advancements hold immense potential for advancing neuroscience and paving the way for targeted therapeutic interventions in neurological disorders. In this study, we employed two complementary functional genomics approaches: TargetFinder assay (Herholt et al., 2018) and Perturb-seq (Adamson et al., 2016; Dixit et al., 2016). Each method was strategically chosen to provide distinct yet synergistic insights into the modulation of a specific pathway sensor within neuronal cells.

The TargetFinder assay served as the initial screening tool, focusing on the identification of potential modulators of the pathway sensor under investigation. By systematically perturbing gene expression, TargetFinder allowed us to explore a wide range of genetic factors that may influence the activity or output of the pathway sensor (Herholt et al., 2018). This high-throughput screening approach provided us with a comprehensive overview of candidate genes or regulatory elements involved in pathway modulation.

Complementing the TargetFinder assay, Perturb-seq offered a deeper dive into the functional consequences of genetic perturbations identified through the initial screen (Adamson et al., 2016; Dixit et al., 2016). Perturb-seq enabled us to zoom in on the transcriptomic changes induced by the identified modulators, providing mechanistic insights into how these genetic factors alter the activity of the pathway sensor at the molecular level. By linking genetic perturbations to specific changes in gene expression profiles, Perturb-seq facilitated the elucidation of functional relationships between genes and the pathway of interest (Adamson et al., 2016; Dixit et al., 2016; Jin et al., 2020; Replogle et al., 2022; Santinha et al., 2023). By integrating data from both TargetFinder and Perturb-seq, we gained a comprehensive understanding of the regulatory network governing the pathway sensor in neuronal cells. This integrative approach not only identified novel modulators of the pathway but also elucidated the molecular mechanisms underlying their regulatory effects.

Furthermore, the identification of druggable targets among the newly discovered modulators holds promise for accelerating drug discovery efforts targeting neuronal pathways.

2.1 TargetFinder assay

Upon synaptic stimulation, intricate intracellular signaling cascades are initiated, ultimately leading to alterations in gene transcription (Guzowski et al., 1999; Link et al., 1995; Lyford et al., 1995). These changes in gene expression play a pivotal role in determining critical phenotypic outcomes, such as neuronal survival and/or plasticity (McClung and Nestler, 2008). Despite considerable efforts over the past three decades to elucidate the mechanisms underlying these transcriptional changes and their impact on neuronal phenotype, a significant obstacle persists: scalability (Herholt et al., 2018). The prevailing focus of most studies on individual or a limited number of genes hampers our ability to gain a comprehensive understanding of the complex transcriptional landscape governing neuronal function. This limitation represents a substantial bottleneck in the identification of druggable targets, particularly in the realm of psychiatric diseases (Herholt et al., 2022). To address this challenge, innovative approaches such as the TargetFinder assay have emerged. This pooled screening assay is specifically designed to identify modulators of a genetic sensor for a specific phenotype in primary cortical neurons, offering promise in expanding our understanding of synaptic-to-nucleus signaling and facilitating the discovery of potential therapeutic targets (Herholt et al., 2018).

2.1.1 What can be a genetic sensor?

The genetic sensor employed in the TargetFinder assay can assume the guise of either an enhancer or a promoter, carefully chosen through empirical data to specifically target a phenotype of interest. Ideally, candidates for serving as a genetic sensor encompass genetic regulators of immediate early genes (IEGs). In the context of synaptic input reception, calcium ions ingress into the cytoplasm via NMDA-type glutamate receptors (NMDARs) at activated synapses and voltage-gated calcium channels (VGCCs) upon neuronal firing. Subsequently, this instigates the activation of various calcium-dependent kinase cascades, including Ca2+/calmodulin-dependent protein kinases (CaMKs) (Bito et al., 1996; Fujii et al., 2013) and mitogen-activated protein kinases (MAPKs) (Dolmetsch et al., 2001; Zhai et al., 2013). Ultimately, the activation of these kinase cascades leads to the site-specific modulation of activity-dependent transcription factors such as CREB (Bito et al., 1996), myocyte enhancer factor-2 (MEF2), and serum-responsive factor (SRF), thereby facilitating the rapid transcription of downstream IEGs.

Two immediate early genes (IEGs) utilized in this study are *Arc* and *Bdnf*, specifically selected for their pivotal roles in neuronal plasticity and their responsiveness to synaptic activity-induced transcriptional alterations. By strategically employing these genetic sensors and delineating downstream IEG targets, the TargetFinder assay endeavors to unravel the intricate molecular mechanisms governing neuronal plasticity and survival within the context of neurodevelopment.

2.1.2 *Arc* gene

The activity-regulated cytoskeleton-associated protein (*Arc*), also known as *Arg3.1*, represents a pivotal molecule in the dynamic regulation of synaptic plasticity—a fundamental mechanism underlying learning and memory processes in the brain (Link et al., 1995; Lyford et al., 1995). Initially identified as an immediate early gene (IEG) induced by neuronal activity, *Arc* has since garnered significant attention for its multifaceted roles in synaptic function, dendritic morphology, and neural circuit dynamics. One of the hallmark features of *Arc* is its rapid and robust upregulation in response to various forms of synaptic activity, including excitatory neurotransmission, synaptic potentiation, and sensory stimulation (Guzowski et al., 1999; Link et al., 1995; Lyford et al., 1995). Upon induction, *Arc* mRNA undergoes rapid transport to dendrites, where it is locally translated in close proximity to activated synapses (Steward et al., 1998). This unique spatiotemporal regulation enables *Arc* to serve as a molecular sensor, linking neuronal activity with dynamic changes in synaptic structure and function.

2.1.2.1 Regulatory mechanisms governed by the SARE element

Central to the regulatory mechanisms governing *Arc* expression are specific cis-acting elements within its promoter region, notably the synaptic activity response element (SARE). The SARE sequence, located approximately 7 kb upstream of the *Arc* gene transcription initiation site, acts as a critical molecular switch (Kawashima et al., 2009). This ~100-bp element is characterized by its enrichment of binding sites for activity-dependent transcription factors, including Serum Response Factor (SRF), Myocyte Enhancer Factor 2 (MEF2), and cAMP Response Element-binding protein (CREB) (Figure 1E) (Kawashima et al., 2009). These factors are known to be activated by various signaling cascades triggered by neuronal activity, such as calcium influx and activation of protein kinase pathways (Thomas and Huganir, 2004).

Trans-acting factors play crucial roles in mediating the transcriptional activation of *Arc* via the SARE element in response to synaptic activity. Upon neuronal stimulation, intracellular signaling cascades converge on these transcription factors, leading to their activation and subsequent binding to the SARE element. Trans-acting factors involved in *Arc* regulation include CREB, which is phosphorylated and activated by various kinases, including protein kinase A (PKA) and calcium/calmodulin-dependent protein

kinase IV (CaMKIV), in response to synaptic activity. Activated CREB then binds to the SARE element, initiating *Arc* transcription (Shaywitz and Greenberg, 1999).

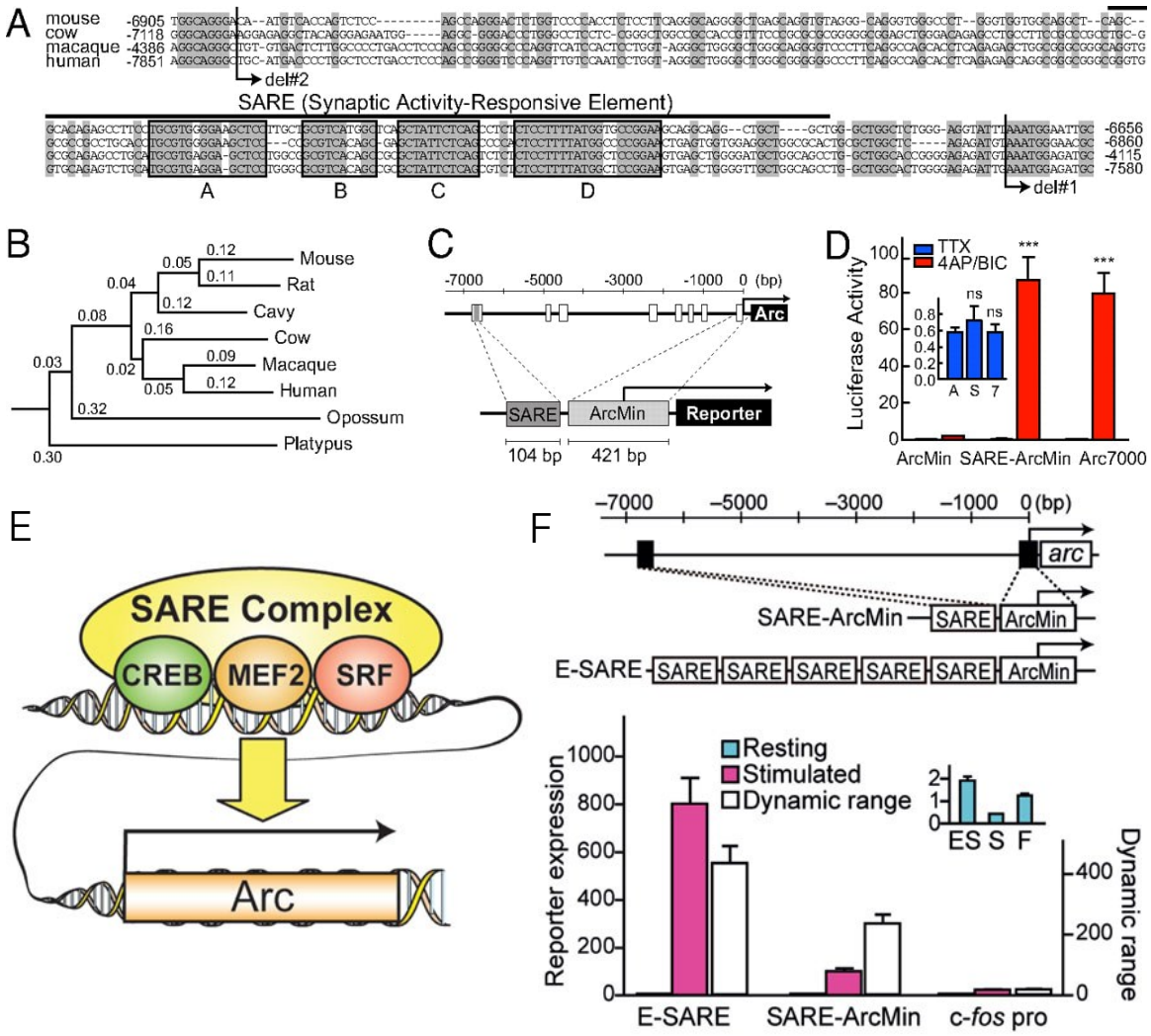

Figure 1 SARE, a regulatory element of Arc/Arg-3.1 promoter.

(A) Comparison of *Arc/Arg-3.1* SARE activity across multiple mammalian species.

(B) Dendrogram depicting the divergence of SARE sequences across mammalian species.

(C) Schematic representation of the SARE-ArcMin reporter vector, where SARE is fused upstream of ArcMin, containing a TATA-containing sequence at the *Arc/Arg-3.1* transcription initiation site.

(D) SARE-ArcMin replicates Arc7000 promoter activity.

(E) Transcription factors CREB, MEF2, and SRF binds to SARE enhancer element and regulate activity-dependent expression of Arc/Arg3.1.

(F) Comparison of E-SARE with SARE-ArcMin and *c-fos* promoters by luciferase reporter assay in cultured neurons under resting (blue) and stimulated (pink) conditions.

Original: A-D were used from Kawashima et al. PNAS 2009 (Figure 3); E-F were used from Kawashima et al. Front Neural Circuits. 2014 (Figure 1)

Additionally, SRF and MEF2 are activated downstream of intracellular signaling pathways, such as the Rho GTPase and calcium signaling pathways, respectively (Inoue

et al., 2010; Kawashima et al., 2009). These transcription factors bind to their respective consensus sequences within the SARE element, further enhancing *Arc* transcriptional activation. Furthermore, other co-factors and chromatin modifiers, such as histone acetyltransferases (HATs) and histone deacetylases (HDACs), modulate chromatin accessibility and transcription factor binding at the *Arc* promoter, fine-tuning *Arc* expression in response to synaptic activity (Kawashima et al., 2013).

2.1.2.2 E-SARE served as a sensor in the TargetFinder assay

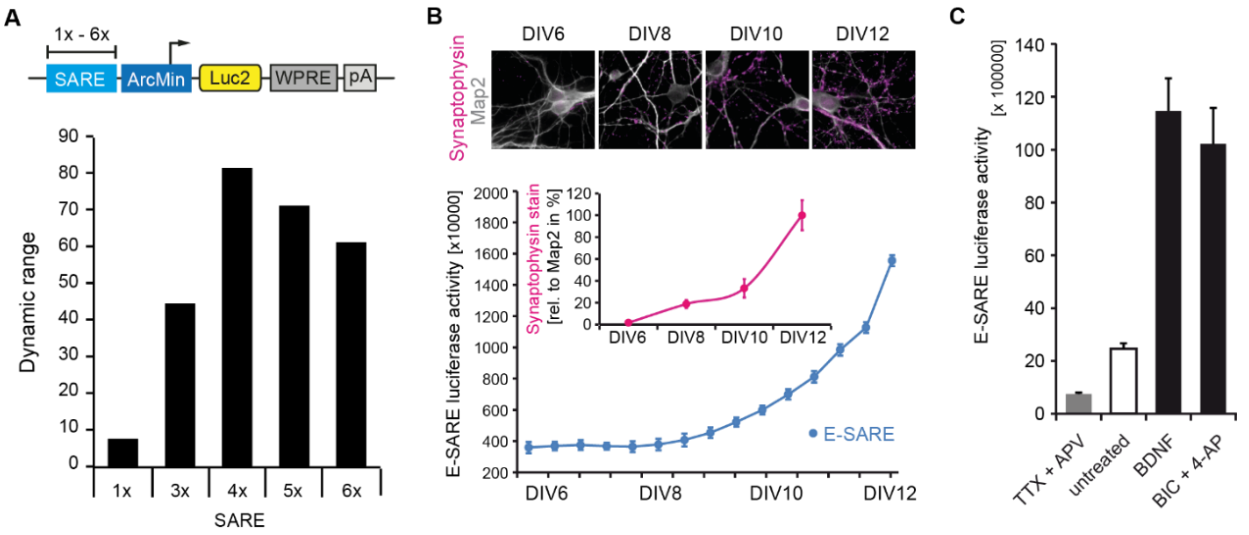

Figure 2 Design and characterization of the artificial E-SARE sensor.

(A) Comparative analysis of luciferase activity from clustered SARE reporters post-stimulation with PMA in SH-SY5Y cells (n=6). 4 times SARE cluster has the maximum dynamic range and referred as E-SARE.

(B) Sequential assessment of basal E-SARE activity in developing primary neurons from DIV6-12. E-SARE luciferase activity increases as the culture matures.

(C) Evaluation of E-SARE activity in primary neurons under conditions of silencing (TTX/APV), basal activity (untreated), and stimulation (BDNF, BIC/4-AP) at DIV14). E-SARE activity response changes upon drug treatment.

Original: PhD thesis Alexander Herholt 2016 (Figure 12)

The SARE sequence serves as a key molecular switch controlling *Arc* transcription in response to synaptic activation. The close proximity and cooperative nature of the binding sites within SARE are crucial for its exceptional sensitivity to even minor fluctuations in neuronal activity (Inoue et al., 2010). A groundbreaking advancement in synthetic promoter engineering emerged recently with the development of the E-SARE construct, derived from the SARE enhancer element within the *Arc* promoter (Figure 1C,D) (Kawashima et al., 2013). To capitalize on this modularity, multiple SARE elements were concatenated in tandem with an optimized linker. Remarkably, combinations featuring a five-tandem repeat yielded a seven-fold enhancement in reporter expression levels. Consequently, the resultant synthetic promoter, E-SARE, exhibited over 20-fold higher expression levels and a 30-fold higher induction ratio compared to the *c-fos* promoter (Figure 1F). In 2018, Herholt et al recharacterized the tandem of

SARE element and used it as a sensor of neuronal activity. In the first TargetFinder experiment, 4 times SARE was used as a sensor (Figure 2A) (Herholt et al., 2018).

2.1.3 *Bdnf* gene

Brain-derived neurotrophic factor (*Bdnf*), a paramount neurotrophin abundantly expressed in the central nervous system (CNS) (Aid et al., 2007; Pruunsild et al., 2007; Tirassa et al., 2000), emanates not only from neurons and oligodendrocytes but also from platelets (Małczyńska et al., 2019), immune cells (e.g., T and B lymphocytes, monocytes/macrophages) (Kerschensteiner et al., 1999), and actively contracting muscles, augmenting its peripheral reservoir (Hanson et al., 1992). Despite expression of BDNF is reported in diverse cell type, *Bdnf* is not expressed in inhibitory neurons (Gorba and Wahle, 1999; Rocamora et al., 1996).

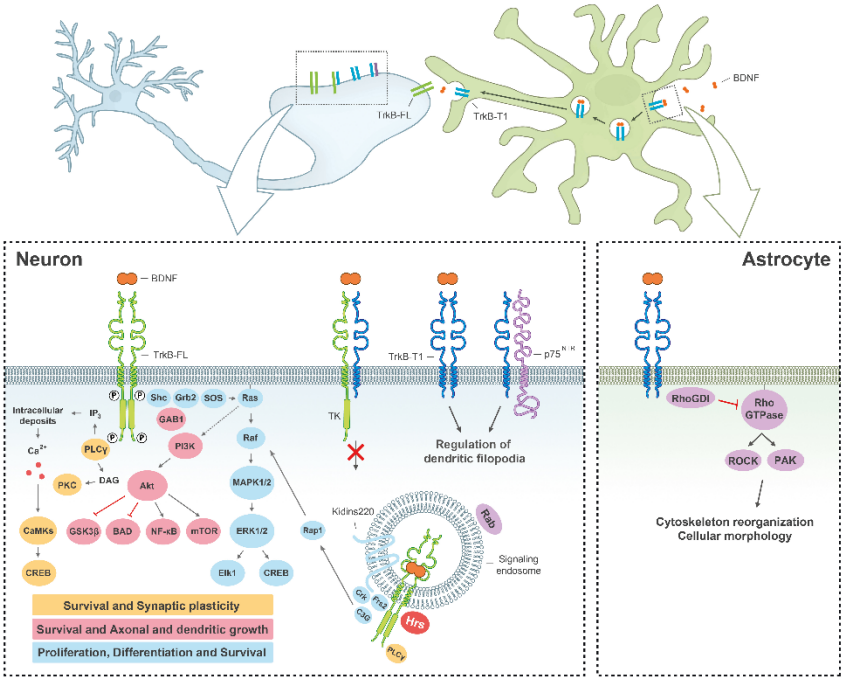

Figure 3 Function of BDNF/TrkB Signaling in the CNS

BDNF (Brain-Derived Neurotrophic Factor) binds to the full-length TrkB receptor (TrkB-FL) in neurons (left diagram), initiating receptor homodimerization and subsequent activation. This activation triggers three primary signaling pathways: MAPK/ERK (blue), PI3K (pink), and PLCγ (yellow), which collectively regulate numerous processes critical to neuronal function. The ligand-receptor complex can undergo internalization and continue to function within signaling endosomes. Alternatively, TrkB-T1, a truncated isoform of the receptor, can form heterodimers with TrkB-FL, inhibiting its transduction cascades. TrkB-T1 also plays a role in modulating local BDNF concentration (upper diagram) and influencing cell morphology, both in neurons and astrocytes (illustrated in the left and right diagrams, respectively). Phosphorylation sites (denoted as P) are crucial for receptor activation.

Original: Image used from Tejeda, G.S et al. Int. J. Mol. Sci. 2017 (Figure 1).

Bdnf exerts its effects through interaction with two receptor types: tropomyosin receptor kinase (Trk) receptors, possessing tyrosine kinase activity, and p75 neurotrophin receptor (p75NTR), characterized by low binding affinity (Figure 3) (Thomas and Davies, 2005). Upon activation, TrkB receptors initiate three principal downstream signaling pathways. Phosphorylation of the Tyr515 residue on full-length TrkB enables the recruitment of Src-homology 2-domain-containing adapter protein (Shc), subsequently activating the PI3K/Akt cascade and the MAPK/ERK pathway (Huang and Reichardt, 2003). These pathways play pivotal roles in modulating neuronal differentiation and/or survival. Additionally, recruitment and activation of phospholipase C γ (PLC γ) by TrkB phosphorylation at Tyr816 promote neuronal survival, neurite outgrowth, and synaptic plasticity (Minichiello et al., 2002).

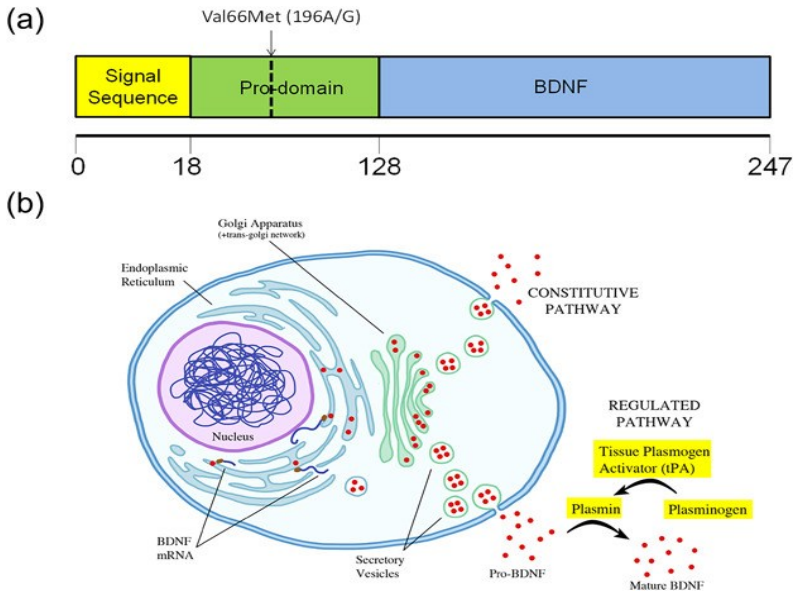

Figure 4 Schematic illustration of the human BDNF protein and its intracellular trafficking.

(A) Representation of human pre-pro-BDNF protein, where the signal peptide undergoes cleavage at amino acid 18. The pro-domain harbors the rs6265 single nucleotide polymorphism at nucleotide 196, substituting "A" with "G" and leading to a valine to methionine alteration. Cleavage of the pro-domain occurs at amino acid 128, yielding mature BDNF.

(B) Diagram depicting the intracellular trafficking pathway of BDNF.

Original: Image used Hing et al., 2018 American J of Med Genetics 2017 (Figure 1)

Furthermore, BDNF exhibits interactions with various isoforms of TrkB, expressed at distinct developmental stages and in selective compartments, contributing to the modulation of diverse cellular functions (Hing et al., 2018).

The synthesis of BDNF involves a complex process starting with the production of a precursor, pre-pro-BDNF, in the endoplasmic reticulum. Following the removal of the signal peptide, pro-BDNF, a 32 kDa protein, is formed (Lessmann et al., 2003). Proteolytic cleavage of pro-BDNF generates mature BDNF within the cell (Mowla et al., 2001). Interestingly, pro-BDNF can also undergo proteolytic cleavage extracellularly, leading to bioactive actions. Notably, both immature pro-BDNF and mature BDNF exhibit distinct binding properties and diverse biological functions (Ancot et al., 2009).

Mature BDNF promotes neuronal survival, cell differentiation, synaptic plasticity, and long-term potentiation (LTP), while pro-BDNF may induce apoptosis, reduce dendritic spine density, and facilitate long-term depression (LTD) at the hippocampal level (Yeh et al., 2012). However, separate studies show, function of pro-BDNF and mature BDNF is dependent on developmental stage, neuron cell types and also different areas of neurons (Figure 4) (Matsumoto et al., 2008; Orefice et al., 2013; Woo et al., 2005; Yang et al., 2014, 2009).

2.1.3.1 Evolutionary conservation and isoform complexity

From an evolutionary standpoint, the orthologs of the BDNF protein exhibit remarkable conservation between primate and rodent species (Pruunsild et al., 2007). However, even within the same species, various isoforms of BDNF have been documented (Figure 5) (Pruunsild et al., 2007). Notably, disparate transcripts can give rise to identical protein products following post-translational modifications. This phenomenon arises from the intricacies of the genetic architecture governing *Bdnf* expression, characterized by multiple promoters. These promoters play a pivotal role in orchestrating temporal and spatial regulation, as different brain regions and cell types selectively utilize distinct promoter regions for transcriptional initiation (Hing et al., 2018). Such complexity underscores the nuanced control mechanisms governing *Bdnf* expression and highlights the dynamic nature of its regulatory landscape across evolutionary time scales and within diverse biological contexts.

Figure 5 BDNF protein sequence is evolutionarily conserved across primates and rodents.

Constraint-based Multiple Alignment Tool(Cobalt) was used to align all reported proteins from *Homo sapiens*, *Mus musculus* and *Rattus norvegicus*. Alignment was done with default parameters and coloring parameter is "Conservation". Red color represents highly conserved regions.

Cobalt RID ZNCK96D1212 (40 seqs)

2.1.3.2 Regulatory mechanisms of *Bdnf* expression

The *Bdnf* gene is characterized by a complex genetic structure, featuring 11 exons in humans and 9 in rodents, along with nine alternative promoters for both species (Aid et al., 2007; Pruunsild et al., 2007). Despite this complexity, only the last

exon, exon IX, which encodes the BDNF pre-pro-peptide, undergoes translation. The remaining exons serve as untranslated regions, with start codons located in exons I, VII, VIII, and IX in the human *BDNF* gene (You and Lu, 2023). Downstream exons are spliced to exon IX, ensuring its presence in all *BDNF* mRNA isoforms. The multitude of promoters likely facilitates precise spatiotemporal regulation of *BDNF* gene expression (You and Lu, 2023).

Moreover, these different promoters enable *Bdnf* to respond to a wide array of stimuli. Regulatory elements within *Bdnf* promoters recruit transcription factors to modulate their activity in response to specific stimuli. In this study, we utilized two well-characterized *Bdnf* promoters, promoter I (*Rn* pI) and promoter IV (*Rn* pIV), along with enhancer -840 (*Mm* E840), a novel enhancer with unexplored functionality. Notably, activation of L-type voltage-gated calcium channels (L-VGCCs) or N-methyl-D-aspartate (NMDA) receptors triggers intracellular calcium signaling, crucial for diverse brain functions by activating promoter I and/or promoter IV (Paoletti et al., 2013; Simms and Zamponi, 2014).

Upstream of *Bdnf* promoter I, a cAMP-responsive element (CRE) or CRE-like element has been identified in both rat and human orthologs (Pruunsild et al., 2011). In rats, CRE is implicated in neuron depolarization and is upregulated during such events (Tabuchi et al., 2002; Tao et al., 1998). However, mutation studies in human *BDNF* promoter I suggest involvement of upstream activator protein 1 (AP-1)-like and asymmetric E-box-like elements, rather than CRE, in response to neuron depolarization (Figure 6A) (Pruunsild et al., 2011), indicating species-specific regulatory mechanisms.

Similarly, *BDNF* promoter IV harbors multiple regulatory elements involved in neuron depolarization. In rats, three calcium response elements (CaREs) upregulate *Bdnf* expression upon depolarization, each binding different transcription factors. CaRE1-dependent transcription factor (CaRF) binds to CaRE1 (Tao et al., 2002) upstream stimulating factor (USF) 1 and USF2 binds to CaRE2 (Chen et al., 2003) and cAMP-response element binding protein (CREB) binds to CaRE3 (Shieh et al., 1998) upon depolarization. Other regulatory regions, such as NF-κβ regulatory region, NFAT regulatory region, and basic helix-loop-helix-PAS transcription factor response element (PasRE), also enhance BDNF expression upon NMDA receptor activation (Jiang et al., 2008; Lipsky et al., 2001; Vashishta et al., 2009). Additionally, a negative regulatory element, class B E-box, suppresses *BDNF* promoter IV activity prior to cell stimulation by binding to BHLHB2 (Figure 6B) (Jiang et al., 2008). In human *BDNF* promoter IV, similar different regulatory regions.

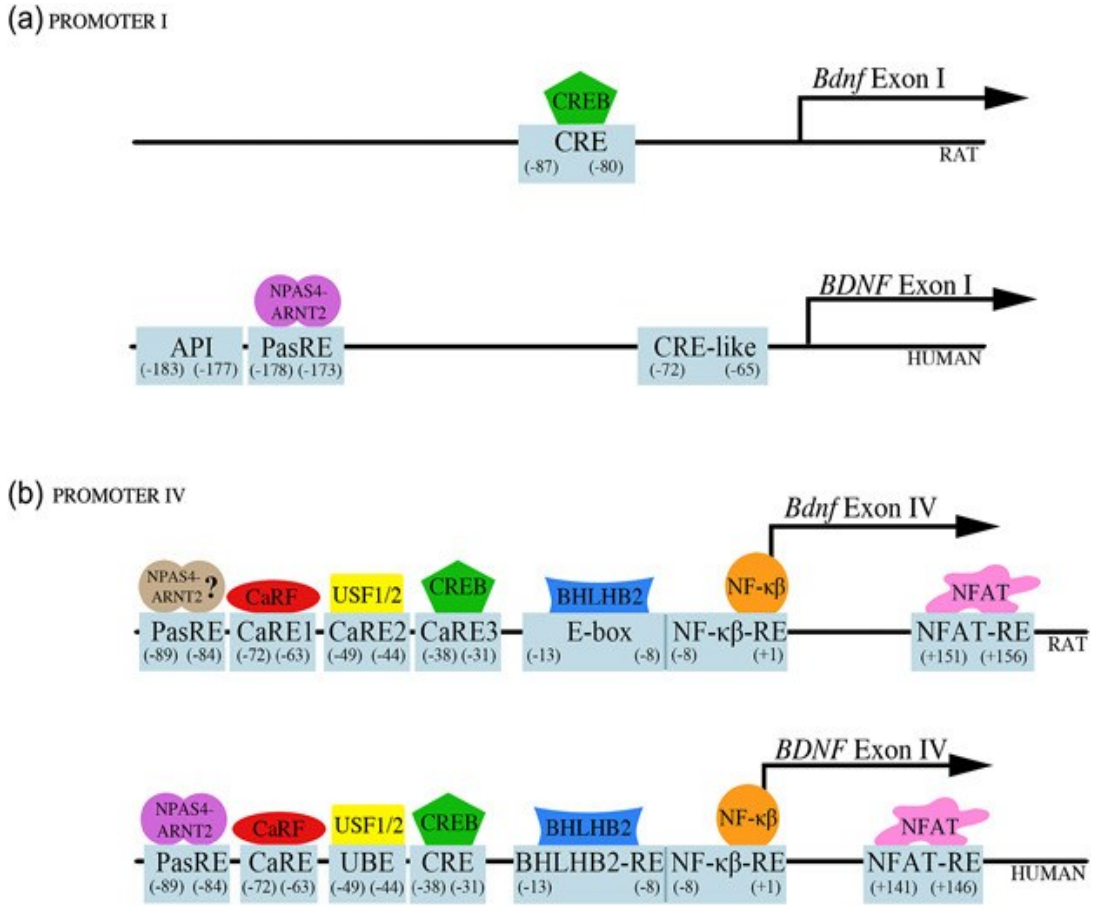

Figure 6 Transcriptional regulatory elements governing BDNF/Bdnf promoters I and IV activity.

(A) Illustration of Promoter I and

(B) Promoter IV, highlighting the transcription factors responsible for modulating promoter activity in response to neuronal activation.

Original: Image used Hing et al., 2018 American J of Med Genetics 2017 (Figure 3)

2.1.4 TargetFinder concept

The TargetFinder construct consists of two key components: the Sensor cassette and the Effector cassette (Figure 7A). The Sensor cassette contains a phenotype-specific sensor that drives the expression of a reporter gene upon stimulation. Conversely, the Effector cassette comprises a constitutive human U6 promoter driving the expression of short hairpin RNA (shRNA) targeting a specific transcript. The entire construct is flanked by Adeno-associated virus (AAV) inverted terminal repeats (ITRs).

Upon introduction into neurons, the Effector cassette constitutively knocks down a specific transcript. Upon stimulation, a signaling cascade is initiated, leading to sensor activity. There are three possible scenarios (Figure 7B):

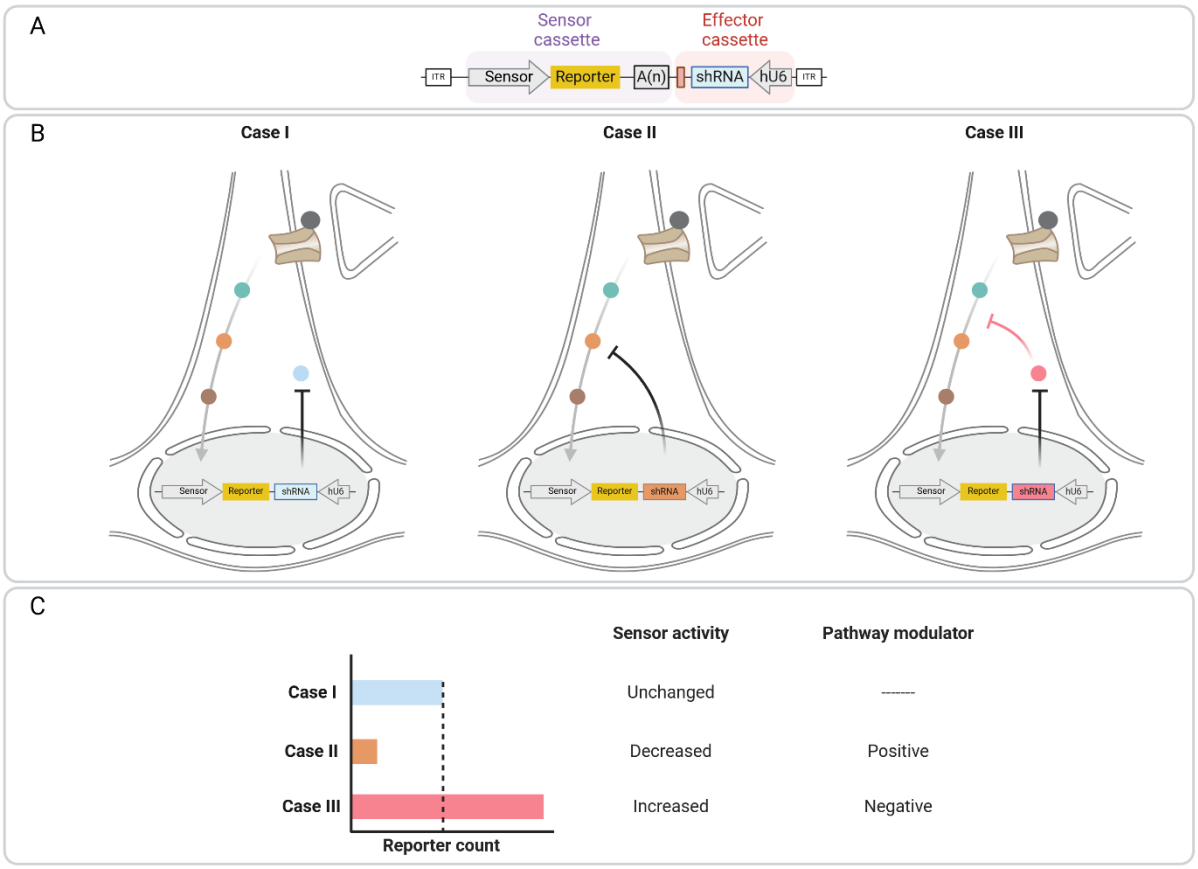

Figure 7 Schematic representation of the TargetFinder assay concept.

(A) Diagram depicting the TargetFinder assay plasmid structure, highlighting the Sensor and Effector cassette along with their components. Effector cassette comprises of a constitutive Pol III promotor, hU6 driving the expression of shRNA targeting specific transcript. Sensor cassette comprises of a pathway specific genetic sensor driving the expression of reporter gene. Entire construct is flanked by AAV ITRs.

(B) Illustration presenting the three potential scenarios of plasmid response within a cell. Briefly, effector cassette knockdown a specific transcript and sensor cassette acts as proxy to measure effect of transcript knockdown on pathway.

(C) Visualization demonstrating the alteration in sensor activity caused by knockdown via the effector cassette, facilitating the identification of pathway modulators based on the direction of change in sensor activity.

Case I: If the shRNA targets a gene unrelated to the signaling cascade, normal sensor activity is observed.

Case II: If the shRNA targets a gene positively modulating the signaling cascade, sensor activity decreases relatively. The targeted gene is identified as a positive modulator of the signaling cascade.

Case III: If the shRNA targets a gene negatively regulating the signaling cascade, knocking down the gene removes the negative regulation. Consequently, an increase in sensor activity is observed.

Through this process, the TargetFinder assay enables the identification of both positive and negative modulators of phenotype-specific sensors (Figure 7C). By systematically manipulating gene expression and monitoring sensor activity, this

approach offers valuable insights into the regulatory mechanisms governing specific phenotypes in neuronal cells.

2.1.5 TargetFinder is a pooled screening assay

To address scalability, the read-out of the assay relies on Next-generation sequencing (NGS), enabling high-throughput analysis of sensor activity changes. Each reporter is linked to a molecular barcode that is uniquely coupled to one specific shRNA. This molecular barcode system allows for the simultaneous monitoring of multiple shRNA-transcript interactions within the same sample, enhancing the efficiency and scalability of the assay. By employing NGS technology coupled with molecular barcoding, the TargetFinder assay can systematically screen a large number of genes and identify their effects on phenotype-specific sensor (Figure 8) (Herholt et al., 2022, 2018).

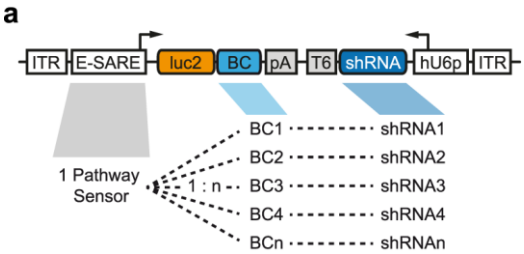

Figure 8 Pooled screening employing molecular barcodes.

A common pathway sensor is linked to a stretch of nucleotide sequence uniquely associated with shRNA targeting various transcripts. Sensor activity is assessed based on the alteration in molecular barcode reads using NGS as read-out.

Original: Image used Herholt et al., 2018 Sci Rep (Figure 2)

2.2 shRNA-Perturb-seq

Perturb-seq, the perturbation of gene expression is often achieved using CRISPR-based gene editing or RNA interference (RNAi) techniques to either knock out (inactivate) or knock down (reduce expression of) specific genes. Subsequently, single cell sequencing techniques are employed to simultaneously measure gene expression profiles and phenotypic characteristics across a large number of individual cells within the perturbed population (Adamson et al., 2016; Dixit et al., 2016; Replogle et al., 2022).

2.2.1 Single-cell RNA sequencing (scRNA-seq)

Single-cell RNA sequencing (scRNA-seq) has revolutionized our ability to explore the transcriptomes of individual cells with unprecedented resolution, providing insights into cellular heterogeneity, dynamics, and regulatory networks. This innovative technology has its roots in the development of traditional bulk RNA sequencing

methods and the need to overcome the limitations associated with analyzing gene expression in heterogeneous cell populations (Han et al., 2022).

The origins of scRNA-seq can be traced back to the early 2000s when pioneering studies first demonstrated the feasibility of analyzing gene expression at the single-cell level (Tang et al., 2009). One of the earliest methods, known as single-cell PCR (scPCR), allowed for the quantification of mRNA transcripts in individual cells using quantitative PCR (qPCR) assays. However, scPCR had limitations in terms of scalability and throughput, making it impractical for genome-wide expression profiling.

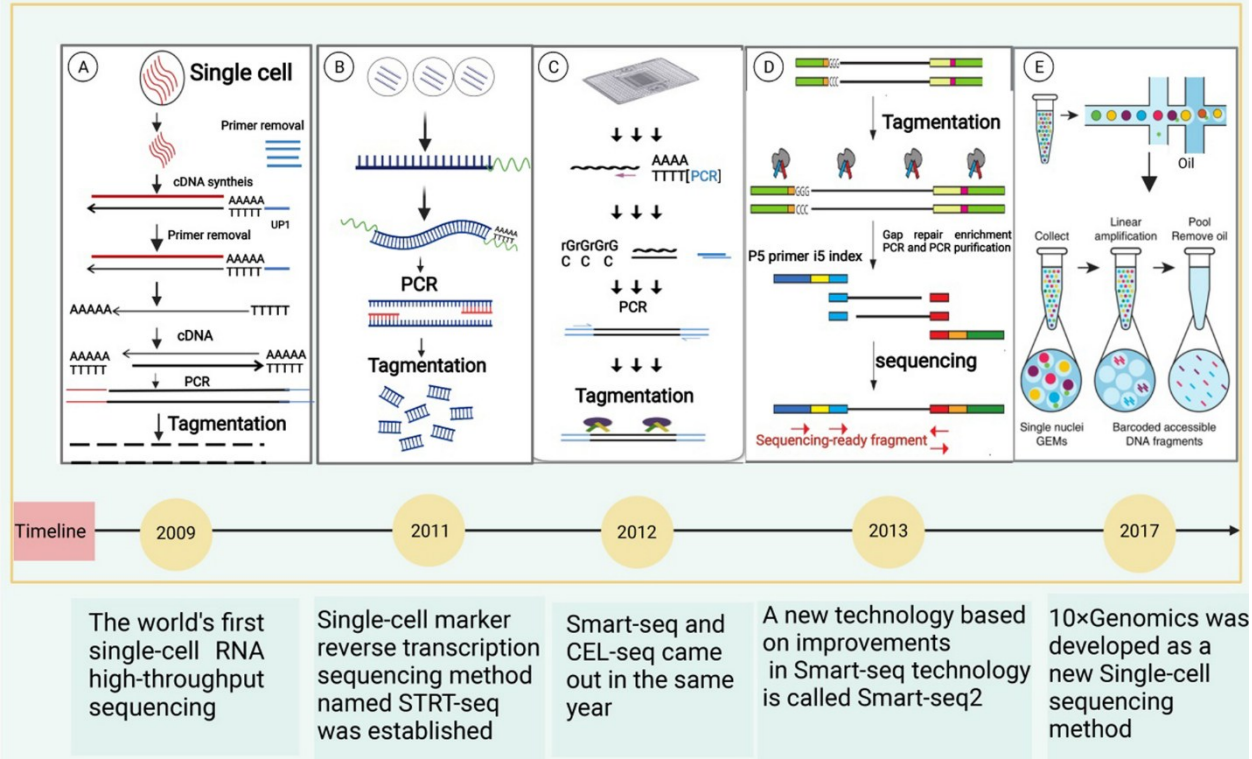

Figure 9 Timeline of milestones in single-cell sequencing technology.

(A) Tang et al. 2009, introduced the first single-cell transcriptional sequencing technology, mRNA-seq.

(B) Islam et al. 2011, established the single-cell labeled reverse transcription sequencing method, STRT-seq.

(C) Ramsköld et al. 2012, developed Smart-seq, a novel single-cell sequencing technology; concurrently, Hashimshony et al. introduced single-cell RNA-Seq by multiplexed linear amplification, named CEL-seq.

(D) Picelli et al. 2013, implemented enhancements to the Smart-seq technology, resulting in Smart-seq2.

(E) 10× Genomics technology emerged as a new single-cell transcriptome sequencing method in 2017.

Original: Image used Han et al., 2022 Journal of Hematology & Oncology (Figure 2)

The breakthrough in scRNA-seq came with the development of high-throughput sequencing technologies, particularly RNA sequencing (RNA-seq) (Tang et al., 2009), which enabled the simultaneous profiling of thousands of genes in individual cells. The first scRNA-seq protocols were introduced in the late 2000s and early 2010s, leveraging RNA-seq to analyze gene expression in single cells. These early methods, such as

Smart-seq (Ramsköld et al., 2012) and STRT-seq (Islam et al., 2011), offered unprecedented insights into cellular heterogeneity and dynamics in various biological systems.

Subsequent advancements in scRNA-seq methodologies, including Smart-seq2 (Picelli et al., 2013), Drop-seq (Macosko et al., 2015), and 10x Genomics Chromium, have further improved throughput, sensitivity, and cost-effectiveness. Drop-seq introduced the use of microfluidics to encapsulate individual cells in nanoliter droplets, enabling parallel processing of thousands of cells (Macosko et al., 2015). Similarly, the 10x Genomics Chromium platform utilizes droplet-based technology to generate single-cell libraries with high throughput and scalability.

2.2.1.1 Methodology of scRNA-seq

The general workflow of scRNA-seq involves several key steps:

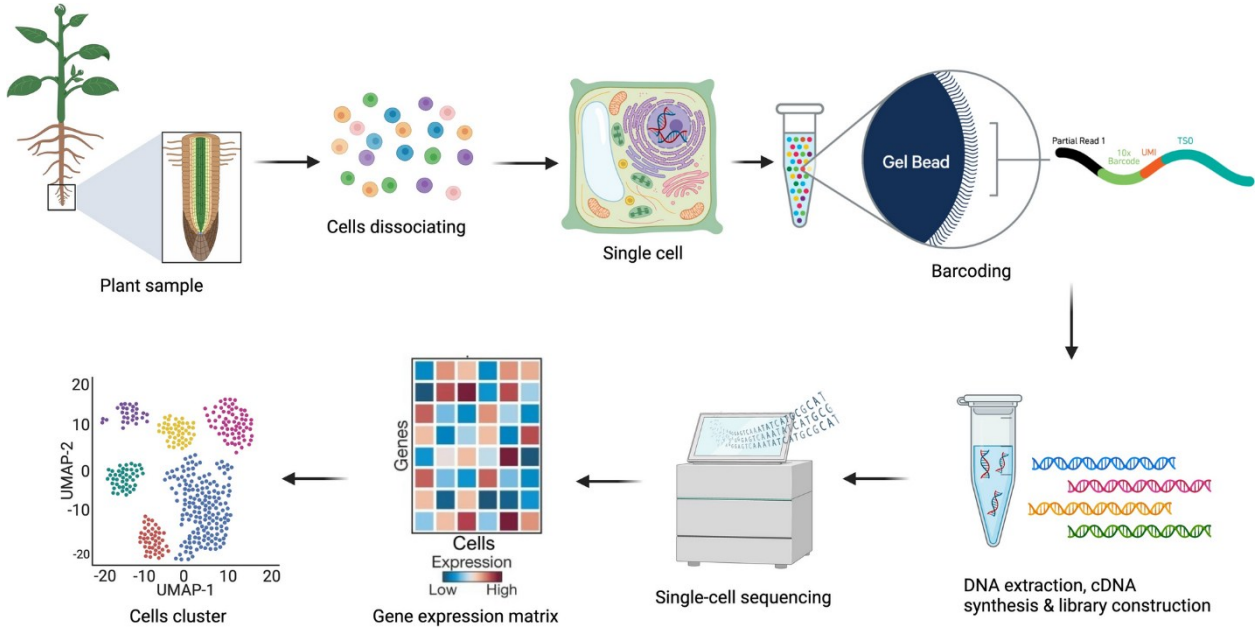

Figure 10 Schematic Workflow of Single-Cell RNA Sequencing (scRNA-seq).

Tissue samples are initially dissected into smaller fragments and treated with appropriate dissociation enzymes to yield single cells. These cells are encapsulated into gel beads in emulsion (GEMs) using a microfluidic system, along with barcode-containing gel beads, cell mixtures, and oil. Within the GEMs, cells are lysed, and gel beads dissolve, releasing barcoded mRNA sequences. Reverse transcription incorporates 10X barcodes and unique molecular identifiers (UMIs) for cDNA synthesis. The synthesized cDNA is then utilized for library construction, followed by sequencing. The sequenced data undergo quality checks, cell clustering, and gene expression analysis, along with normalization and mapping against a reference genome to identify individual cells and analyze gene expression patterns in diverse tissue samples.

Original: Image used Ali et al., 2024 Plant Cell Reports (Figure 3)

Cell isolation: Individual cells are isolated from a heterogeneous population using methods such as fluorescence-activated cell sorting (FACS), microfluidic devices, or manual picking under a microscope.

RNA capture and reverse transcription: RNA molecules are extracted from each cell and converted into cDNA using reverse transcription. Different scRNA-seq methods employ various strategies for RNA capture, including oligo-dT priming for polyadenylated transcripts or random priming for total RNA.

Library preparation: The cDNA is amplified and fragmented to generate sequencing libraries. Unique molecular identifiers (UMIs) or molecular barcodes are often incorporated during library preparation to distinguish between genuine mRNA transcripts and amplification artifacts.

Sequencing: The prepared libraries are sequenced using next-generation sequencing platforms, generating millions of short sequence reads per cell.

Data analysis: Bioinformatic analysis pipelines are employed to process and analyze the sequencing data, including read alignment, gene expression quantification, dimensionality reduction, clustering, and visualization.

Description modified from (Ali et al., 2024)

2.2.1.2 Applications of scRNA-seq

scRNA-seq has been widely applied across diverse fields of biology and medicine, including developmental biology, neuroscience, immunology, oncology, and regenerative medicine. Some key applications of scRNA-seq include:

Characterization of cell types and states: scRNA-seq enables the identification and classification of cell types based on their gene expression profiles, facilitating the discovery of rare or novel cell populations (Jovic et al., 2022).

Analysis of cellular heterogeneity: By profiling individual cells within a population, scRNA-seq reveals cellular heterogeneity and dynamic changes in gene expression patterns, shedding light on cellular states, transitions, and regulatory networks (Jovic et al., 2022).

Investigation of disease mechanisms: scRNA-seq has provided insights into the molecular mechanisms underlying various diseases, including cancer, neurodegenerative disorders, and autoimmune diseases, by elucidating disease-associated cell types, pathways, and biomarkers (Van de Sande et al., 2023).

Drug discovery and personalized medicine: scRNA-seq enables the identification of cell-specific drug targets and biomarkers, paving the way for the development of targeted therapies and personalized treatment strategies (Van de Sande et al., 2023).

Despite its transformative potential, scRNA-seq still faces several challenges, including technical variability, data analysis complexity, and the need for standardized

protocols and computational tools. Future advancements in scRNA-seq technologies and analytical methods are expected to address these challenges and further enhance the utility of single-cell transcriptomics in understanding the complexity of biological systems and advancing biomedical research and clinical applications (Adil et al., 2021).

2.2.2 Pooled perturbation screens

Initially pooled genetic screens were confined to investigating relatively straightforward phenotypes, like cell viability or reporter gene activity in mixed population of cells (Herholt et al., 2018). However, these approaches often require follow-up studies to fully elucidate gene functions. Recently, three distinct studies have combined CRISPR-based genetic perturbations with scRNA-seq to achieve in-depth molecular characterization (Adamson et al., 2016; Dixit et al., 2016; Jaitin et al., 2016).

In these studies (Adamson et al., 2016; Dixit et al., 2016; Jaitin et al., 2016), researchers reasoned that conducting scRNA-seq on cells subjected to various CRISPR-induced perturbations would furnish single-cell resolution to validate target gene suppression and reveals the change in transcriptomic profile due to each genetic alterations. They developed innovative methodologies where mammalian cells are transduced with lentiviral constructs expressing guide RNA (gRNA) that guide the Cas9 enzyme to specific genomic locations. Each gRNA is linked to a unique barcode integrated in a poly(A) transcript, allowing identification via scRNA-seq libraries constructed from poly(A)-positive RNA.

CRISP-seq, a technique designed to study the regulatory networks and cellular diversity in innate immunity, was introduced using bone marrow cells harvested from Cas9-transgenic mice to achieve precise genome editing at specific loci (Jaitin et al., 2016). They targeted transcription factors (TFs) linked to immune system regulation through various setups, including single genes, pairs, and up to 22 genes, analyzing transcriptional changes resulting from these perturbations and responses to lipopolysaccharide (LPS) stimulation *in vitro* and *in vivo*, highlighting response variability among cell subpopulations and niches. This study demonstrated the benefits of using scRNA-seq over conventional bulk-RNA-seq approach (Jaitin et al., 2016).

Perturb-seq, a conceptually similar approach to CRISP-seq but focused towards increasing throughput and used droplet microfluidic approaches for the construction of scRNA-seq libraries (Dixit et al., 2016; Adamson et al., 2016). In the first study, multiple screens were conducted in Cas9-expressing human cells, analyzing the transcriptional effects of single and combined perturbations. The perturbed transcription factors (TFs) and their transcriptional profiles were grouped into functional categories; genetic interactions were explored and mechanisms influencing cell fitness and cell cycle changes were determined (Dixit et al., 2016). In the second study,

genetically engineered K562 cells expressing a catalytically inactive Cas9 (dCas9) fused with the KRAB transcriptional repressor was used. They applied CRISPR interference (CRISPRi) with gRNA libraries to investigate the unfolded protein response (UPR) (Adamson et al., 2016). Their methodology involved initial large-scale screening with CRISPRi gRNA libraries, followed by in-depth analysis using Perturb-seq for both broad and focused screens (Adamson et al., 2016).

In addition to experimental complexities, all studies developed novel bioinformatic pipelines to handle the size and noise of scRNA-seq datasets (Adamson et al., 2016; Dixit et al., 2016; Hao et al., 2021; Jin et al., 2020; Santinha et al., 2023). These advancements provide powerful resources for exploring gene function and molecular dynamics in various biological contexts.

2.2.3 Pooled perturbation screen for neurons

Primary cortical neurons, differentiated polar cells at *Day-in-vitro* 12 (*DIV 12*), represent a crucial model system for studying neuronal development and function (Herholt et al., 2018). However, when investigating these cells within the context of brain tissue, new challenges arise, such as difficulties in capturing cells within oil droplets. Recent advances in in-vivo Perturb-seq have emerged as the new standard for studying complex brain tissue, as evidenced by studies by (Jin et al., 2020) and (Santinha et al., 2023). In these investigations, adeno-associated virus (AAV) libraries targeting candidate genes associated with autism spectrum disorder (ASD) or genes related to the 22q11.2 deletion syndrome were injected into mice, followed by the isolation of nuclei from specific brain regions to assess perturbation effects in various cell types. Notably, all these studies utilized the CRISPR-Cas9 tool for genetic manipulation.

In this study, our objective was to investigate the transcriptomic profile of modulators of SARE sensors in primary cortical neurons. Inspired by previous Perturb-seq methodologies (Adamson et al., 2016; Dixit et al., 2016; Jin et al., 2020; Replogle et al., 2022; Santinha et al., 2023), particularly in vector design and analysis, we made custom modifications tailored to the use of short hairpin RNA (shRNA) and primary cortical neurons. By leveraging insights from these previous methodologies and adapting them to our experimental context, we aimed to elucidate the regulatory mechanisms underlying SARE sensor modulation in neuronal cells.

3 Material and Methods

3.1 Chapter 1

3.1.1 TargetFinder assay using E-SARE as sensor.

3.1.1.1 Cell culture

To identify modulators of E-SARE sensor, TargetFinder assay was performed. Primary cortical cultures were prepared from E15.5 C57BL/6 mice embryo as described in Section 3.3.3 and 10 million cells were seeded on 15 cm dishes. Cultures were separately infected with A59-3 on *DIV* 1 with an MOI of 1200. Cultures were separated into two groups containing three dishes each. Group 1 was silenced on *DIV* 11 by using TTX cocktail [1 µM TTX; 100 µM D-AP5] for 24 hours and Group 2 was stimulated on *DIV* 11 using BIC cocktail [50 µM Bicuculline; 100µM 4-AP; 100µM Glycine; 1µM Strychnine] for 4 hours.

3.1.1.2 RNA harvest, cDNA synthesis

First spent media containing TTX were collected for safe disposal and the cells were washed with 10 ml ice-cold 1 x PBS. To lyse the cells, 2.4 ml of RLT buffer was added. Cells were scrapped from the plate using cell scrapper. Lysates were homogenized using a 19-gauge needle and a syringe. RNA was harvested using RNA Easy Mini Kit as per manufactures protocol. Considering the binding capacity of columns, three columns were used per lysate. RNA concentration was measured using a spectrophotometer. To remove genomic DNA, TURBO DNase kit was used as per manufactures protocol. Each sample was cleaned again using RNA Easy Mini Kit as per manufactures protocol. As the RNA concentration before DNase digest step was ~60µg, one column was used at this step.

cDNA synthesis was done using High-Capacity c-DNA Reverse Transcription Kit and as per manufactures protocol. However, the reaction was scaled up considering per reaction limit was 2 µg RNA to cDNA.

3.1.1.3 Quality control for stimulation by qRT-PCR

qRT-PCR was performed as described in Section 3.3.7. Oligonucleotides are used for targets *Luc*, *BDNF exon IV* and *Hprt1* (housekeeping). Sequences are available in Table 2.

3.1.1.4 Barcode enrichment PCR (PCR1)

cDNA concentration was measured by Qubit dsDNA HS Assay Kit. For barcode enrichment PCR, 25 ng cDNA was used as template. Pool of forward and reverse mix of varying UMI length were mixed and used for PCR. NEBNext® Q5® Hot Start HiFi PCR Master mix was used for PCR as per manufacturers recommendation for 23 cycles. PCR amplicon of size ~170 bp were excised from the gel and cleaned up using NucleoSpin Gel and PCR-Clean-up Kit.

3.1.1.5 Illumina adapter PCR

PCR amplicon concentration was measured by Qubit dsDNA HS Assay Kit. For barcode adapter PCR, 25 ng PCR1 was used as template. For PCR, unique forward and reverse oligonucleotides were used to keep unique sample identity. NEBNext® Q5® Hot Start HiFi PCR Master mix was used for PCR as per manufacturers recommendation for 4 cycles. PCR amplicon of size ~230 bp were excised from the gel and cleaned up using NucleoSpin Gel and PCR-Clean-up Kit.

3.1.1.6 KAPA quantification and pooling

Illumina library concentration was measured using KAPA Library Quant Kits. All steps were followed as per the manufactures protocol. For pooling, Illumina web tool "Pooling Calculator" (https://support.illumina.com/help/pooling-calculator/pooling-calculator.htm) was used. Samples were pooled with different coverage. Samples were pooled such that each sample got 10 million reads each.

3.1.1.7 Data analysis

Samples were pooled at the level Illumina library and for sequencing NextSeq 500/550 High Output Kit v2.5 (150 Cycles) was used with Read1 50 cycles and Read 2 100 cycles. Reads were demultiplexed using a custom bash script.

To trim reads and extract barcodes from Read2 sequences. Barcodes were trimmed by providing adapter sequences as DEC forward and DEC reverse sequences. Other parameters for quality trimming accept a maximum error rate of 0.2, minimum

and maximum length of 35 nucleotides. Finally, the trimmed reads were reported as *.fastq* files. Trimmed reads were mapped to the Index generated in using the *bowtie* tool. For quality alignments, seed length was kept to default of 28 nucleotide with max two mismatches. Alignments with a MAPQ value of 255 were taken further for counting using a custom *awk* command and exported out as *.txt* files.

All *.txt* files were read using custom R scripts. Briefly, I accumulated data from individual files and made a single raw counts data frame. Raw counts were QC verified and upon required data wrangling, raw counts were subjected to *DESeq2* pipeline and an aggregated *dds* object was created. Finally, *results()* function of *DESeq2* was used to where stimulated condition was contrasted always against unstimulated condition. Results were exported to *.txt* files.

Modulators of E-SARE sensor were filtered out by applying a p-value threshold of 0.05 and absolute log2 fold change of more than and equal to 1.

3.1.2 Cloning shRNA-Perturb-seq parent vector

EGFP ORF was PCR amplified from V2597 (50ng) as a template and using custom primers O4187 and O4188, purchased from Integrated DNA Technologies (IDT). The PCR amplicon of length 821 base pairs was excised from the gel and cloned into V1842 at the BamHI and NotI restriction sites replacing GCaMP5G-WPRE ORF. A ligation reaction was set up using T4 DNA Ligase from NEB (New England Biolabs). The ligated product was diluted 1:10 in nuclease-free water and transformed into Endura electrocompetent cells. Transformation mixture, necessary to create a plasmid library with a complexity of 10^6, was inoculated into LB Amp (200 µg/ml) broth. The plasmid was isolated using the NucleoBond Xtra Midi EF Kit, following the manufacturer's protocol.

3.1.3 Cloning individual shRNA to shRNA-Perturb-seq parent vector

Oligonucleotides for each shRNA target were designed such that, upon annealing, they would create sticky ends for AgeI and EcoRI. These oligonucleotides were purchased from Eurofins. Subsequently, the oligonucleotides were annealed and individually ligated to the linearized shRNA-Perturb-seq parent vector. The ligated products were then transformed into chemically competent *Mach1* cells. From each transformation plate, 5-6 clones were selected, and plasmid DNA was purified using the NucleoSpin Plasmid Kit. Sanger sequencing was carried out for each clone to find the association between Pert-BC and the specific shRNA.

3.1.4 Individual plasmid and AAV library preparation

Four clones from each shRNA pooled together in equi-molar concentration. To generate AAVs, 4 µg of each plasmid pools were mixed with 10 µg of pFdelta6 + 3.75

µg of pRV1 + 3.75 µg of pH21. Polyethyleneimine (PEI) transfection protocol was followed to transfect HEK293FT cells. AAV libraries were purified and enriched using Amicon Ultra-15 centrifugal unit. To quantify genomic copies of each AAV library was done by isolating ssDNA genome and AAV ITR oligonucleotides were used to absolute quantification qRT-PCR.

3.1.5 Single nuclei Perturb-seq assay

Cortices were isolated from E15.5 C57BL/6 mice embryos and dissociated using Papain treatment. Three million dissociated cells were mixed with each AAV library separately to a Multiplicity of infection (MOI) of 1000. Cell + AAV suspension was incubated on a rotating shaker (100 rpm) placed inside cell culture incubator. Post-infection 4 hours, cells were centrifuged at 600 rpm for 5 min. Supernatant was discarded without disturbing cell pellet and washed with 2 ml of culture medium (Neurobasal medium + 2% B27 + 1% GlutaMax + 10 % FBS + pH and temperature adjusted). Cell pellet was resuspended in 1 ml culture medium and using P1000 pipette, cell pellet was dissociated to single cell. Cells were seeded on 0.1 mg/ml PDL coated 6 well plates with a cell density of 550-600 cell/mm2. On *DIV1*, spent medium was removed and replaced with culture medium without FBS.

On *DIV11,* cells health and for GFP expression was monitored. One set of culture was treated with TTX cocktail [1 µM TTX + 100 µM D-AP5]. On *DIV12*, second and third set of cultures were treated with 10 µM AMPA and BIC cocktail [50 µM Bicuculline + 100 µM Strychnine + 100 µM Glycine + 1 µM 4- aminopyridine] for four hours, respectively. Post-treatment spent media was aspirated from the cultures and washed with 600 µl of ice-cold 1 x PBS. Cultures were lysed with 600 µl of ice-cold Nuclei isolation buffer (NIB) and placed on ice for 10 min with occasional tapping. Partially lysed cells were further dissociated from the plates using P1000 pipette and transferred to pre-chilled 1.5 ml tubes. Culture wells were washed with additional 400 µl of NIB and gathered in the same 1.5 ml tube. 1 ml of ice-cold sucrose solution is pipetted to a fresh pre-chilled 2 ml tube. ~1000 µl of lysate was transferred onto the sucrose solution as top layer. For sub-cellular fractionation, 2 ml tubes were centrifuged in a pre-chilled centrifuge at 17000 x g for 60 min. Supernatant (Top and interphase) was aspirated out without disturbing the nuclei pellet. Nuclei pellet was gently washed with 400 µl of ice-cold Resuspension buffer (RB). Nuclei pellet was resuspended by adding 500 µl of pre-chilled RB and placed on ice for 30 min. Parallelly, filter unit has been prepared by assembling 1 Miltenyi pre-separation filter on a 15 ml tube and kept on ice. Filter was pre-wet by adding 200 µl of ice-cold RB. Post-incubation 30 min of nuclei with RB, nuclei was resuspended using P200 pipette and passed through the filter unit. 400 µl of additional RB was used to be the filter and collected. Nuclei counting was done using Höest stain (1:1000 dilution) and a cell counter. Finally, this experiment has 4 independent libraries.

Nuclei isolation buffer (NIB)

10 mM Tris-HCl, pH 8; 0.32 M Sucrose; 0.1 mM EDTA, 5 mM $CaCl_2$; 3 mM $Mg(Ac)_2$; 0.1% Triton-X-100; nuclease-free water to balance

Resuspension buffer (RB)

5 mM $CaCl_2$; 3 mM $Mg(Ac)_2$; 1 % BSA; 4 U/ml Protector RNase inhibitor; 1 x PBS to balance

Sucrose solution

10 mM Tris-HCl, pH 8; 6.1g Sucrose; 3mM $Mg(Ac)_2$; 1 x PBS to balance

Chromium Single Cell 3' kit was used to create single-cell RNA-seq libraries, as per manufacturers protocol. Libraries were sequenced using NovaSeq 6000 S1 Reagent Kit v1.5 (100 cycles) for 300 million reads per library.

Pert-BC to cell barcode association was identified directly from the unmapped transcriptomics reads mapped to a Pert-BC custom reference file. Pert-BC were also enriched from the transcriptomics samples by Dial-out PCR using custom primers O3937 and O3938 and sample cDNA as input. PCR amplicon of ~330 bp was excised from the gel and cleaned up using NucleoSpin Gel and PCR-Clean-up Kit. Upon Illumina indexing, enriched Pert-BC were sequenced along with transcriptomics samples with a coverage of 10 million reads per sample.

3.1.6 Data analysis

3.1.6.1 Demultiplexing and mapping transcriptomics reads to *Mm* genome

For this step, *cellranger-7.1.0* software was used. Sample sheet containing sample indices were passed to *cellranger mkfastq* pipeline. Using *cellranger count* pipeline, *FASTQ* files for transcriptomics reads were mapped to *Mus musculus* reference, *mm10* with "include-introns" mode.

3.1.6.2 Extracting Pert-BC reads from transcriptomics reads

To extract Pert-BC reads from transcriptomics reads, *possorted_genome_bam.bam* files were used. To begin with unmapped reads were filtered from the reads. Further reads have cell barcode and Pert-BC flanking sequence, either "GGTGACAC" or "CCTATAGT" were filtered using *samtools 1.12* and saved as "unmapped.bam" file. Next using *bedtools v2.26.0,* BAM file was converted to FASTQ file for further use.

3.1.6.3 Generating custom reference genome and mapping Pert-BC reads

Using *STAR aligner v2.7.10a,* custom reference file was generated. Further the Pert-BC reads extracted in Section 3.1.6.2 were mapped to the custom reference file to identify perturbation identity to cell barcodes. Read alignments, which were position matched and mapping quality of 655 were filtered and used further.

3.1.6.4 Demultiplexing and processing dial-out PCR reads

Dial-out PCR reads were demultiplexed along with transcriptomics reads (Section 3.1.6.1). Individual demultiplexed files contain reads which were trimmed according to sequences flanking Pert-BC. *UMI-tools version: 1.1.2* was used for this step. After required reads data processing, Read1 and Read2 files were merged according to common read identifiers. Finally, the output of this step is a count file containing trimmed reads (Pert-BC- CBC) and their respective read counts.

3.1.6.5 Creating Seurat object and adding perturbation identity to CBC

To begin with, counts files from Section 3.1.6.4 were processed using modified script from (Dixit et al., 2016). Briefly, the Pert-BC and CBC were filtered for read counts more than "2" followed by correcting CBC according to respective *barcodes.tsv* file for a Levenstein distance of "2".

Next, the barcode corrected files were processed with a custom R function, *wrapper_dialout().* Briefly, the function computes the PCR chimera ratio and reads-to-cell proportions for each CBC and Pert-BC combination. Then it collapses read counts for each CBC, calculating the number of Pert-BC per CBC and perturbation fraction.

Finally, the output of the analysis is a .rds file. Finally, *wrapper_Seurat_integration()* function was used to create a Seurat object using UMI count data. Perturbation data were added to metadate. To determine single or multiple perturbation for a cell if one perturbation is 1.3 times higher UMI count to the second perturbation, then it will be considered single perturbation, otherwise that cell will be assigned as multiple perturbations (Jin et al., 2020).

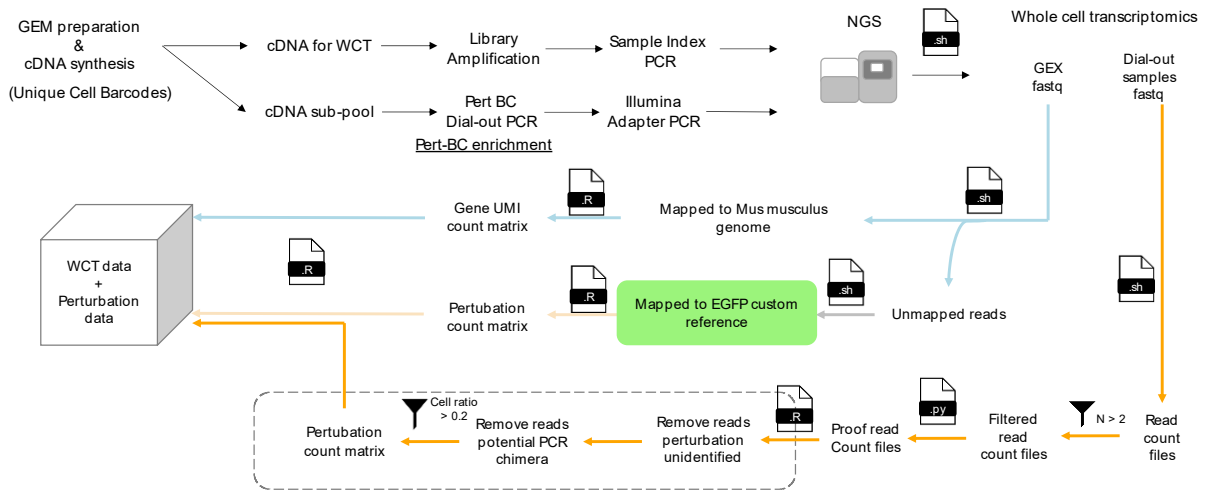

Figure 11 Schematic of Data Analysis Pipeline for Perturbation Identification

3.1.6.6 Dimensionality reduction, clustering and cell type annotation

Seurat object from the previous section were loaded and cells with number of genes less that 450 were discarded. Next, UMI count data underwent SCTransform normalization (Butler et al., 2018) with a parameter setting of vst.flavor = "v2". This normalization method corrects for technical noise inherent in scRNA-seq data, ensuring robust downstream analysis.

To harmonize technical variability across experiments and enable comparative analysis, four datasets were integrated. To identify robust features for integration, the *SelectIntegrationFeatures()* function was applied to all 4 datasets. Features highly variable across datasets were selected, with 2000 features retained for subsequent integration. The datasets were preprocessed for integration using the *PrepSCTIntegration()* function, which prepares the datasets for integration by specifying anchor features identified in the previous step (anchor.features). Integration anchors, representing shared cellular states across datasets, were identified using the *FindIntegrationAnchors()* function. Integration anchors serve as reference points for aligning datasets, accounting for batch effects and technical variability. Normalization was performed using the SCT method (normalization.method = "SCT"). The integrated dataset (integrated.sct) was generated by aligning the individual datasets based on the identified integration anchors. This step ensures that the combined dataset retains biological variability while minimizing technical variation introduced by experimental differences.

Subsequently, principal component analysis (PCA) was performed on the normalized data using the *RunPCA* function with npcs = 50. PCA reduces the data's

dimensionality while preserving most of the variance, facilitating further analysis and visualization.

To visualize the high-dimensional data in a lower-dimensional space, uniform manifold approximation and projection (UMAP) and t-distributed stochastic neighbor embedding (t-SNE) algorithms were employed. UMAP and t-SNE transformations were computed using the *RunUMAP* and *RunTSNE* functions, respectively, retaining the top 10 principal components.

To identify nearest neighbors for each cell, the *FindNeighbors()* function was utilized with the PCA-reduced data (reduction = "pca") and considering the first 10 principal components (dims = 1:10). Next, *FindClusters()* function was utilized for clustering analysis which allows for the construction of a neighborhood graph based on transcriptional similarity, enabling the identification of cellular subpopulations across integrated datasets.

Clustering analysis was performed to group cells based on transcriptional similarity. The *FindClusters()* function was employed with a resolution parameter of 0.3 and the Louvain algorithm (algorithm = 1). This step partitions the cells into distinct clusters based on their expression profiles, enabling the identification of cellular subpopulations. Clusters were assigned to a specific cell type label based on known marker genes. Cell types included "Glutamatergic Neuron", "Astrocytes", "ODCs", "GABAergic Neurons", "*Sst*+ Neurons" and "Unclassified1" for cells not fitting into the defined categories.

New marker genes for each cell type were identified using the *FindAllMarkers()* function. This function computes differential expression between cell clusters based on a Wilcoxon rank sum test (test.use = "wilcox") and filters genes based on a log fold change threshold of 0 (logfc.threshold = 0). To ensure robust marker identification, genes associated with ribosomal proteins (*Rps, Rpl*) and mitochondrial genes (*mt*) were excluded from the analysis using regular expression filtering. From the identified marker genes, the top 20 genes with the highest average log fold change (avg_log2FC) within each cell cluster were selected. Marker gene expression patterns were visualized using the *DoHeatmap()* function from Seurat.

3.1.6.7 Differential gene expression analysis

Differential gene expression analysis was performed to identify genes differentially expressed between treatment conditions (AMPA, BIC, TTX) and the untreated control condition (Unt). The *FindMarkers()* function from the Seurat package was utilized for this analysis. Genes with a log fold change threshold of 0 (logfc.threshold = 0) were considered differentially expressed. For each treatment condition (AMPA, BIC, TTX), differential expression analysis was conducted comparing the treatment group to the untreated control group. Differential expression results were

grouped by the original sample identity (group.by = "orig.ident") and analyzed at the single-cell transcriptomic (SCT) level (assay="SCT"). Differentially expressed genes were selected based on their log fold change values. Genes with an absolute log fold change greater than or equal to 0.585 (FC_thres) and a significant p-value less than 0.05 (pVal_thres) were considered as differentially expressed.

To map activity-regulated genes, external data from the study by (Tyssowski et al., 2018) was imported. Based on the stimulus response type, genes were annotated as activity-regulated genes. Genes associated with different response types were assigned as follows: "rPRG" (rapid primary response genes), "dPRG" (delayed primary response genes), "SRG" (secondary response genes) and "Missing" for unannotated genes.

Additional external datasets were obtained from the study by (Schaukowitch et al., 2017) and unpublished data from Dr. Xiao Ma/Dr. Michael Wehr were used to evaluate gene expression changes in response BIC/TTX stimuli and AMPA stimulus, respectively.

3.1.6.8 Linear discriminant analysis for perturbations predictions

To ensure that perturbed cells are accurately represented and free from any technical artifacts or confounding factors, *mod.detectPerturbations()* function was employed (Santinha et al., 2023). This function first isolates the cells belonging to that cell type and performs DE analysis between each perturbation and the control condition. DE analysis is conducted using the *FindMarkers()* function from the Seurat package, considering the specified log-fold change threshold and minimum percentage of cells expressing a gene. DE genes are identified based on the adjusted p-value threshold of 0.05. The LDA model is trained using gene expression data, and predictions are made for each cell. Cells are labeled as perturbed if they belong to the perturbation group and are predicted to be distinct from the control group. Otherwise, they are labeled as non-perturbed.

3.1.6.9 Pseudo-bulk analysis

Pseudo-bulk analysis provides a more interpretable representation of gene expression patterns at the population level, making it easier to identify biologically meaningful changes associated with experimental conditions, cell types, or perturbations. Moreover, by aggregating expression data from multiple cells into pseudo-bulk profiles, it increases the number of reads per gene, thereby improving the statistical power for detecting differentially expressed genes (DEGs) between conditions or groups. This increased power can be particularly beneficial when dealing with sparse or low-count data inherent in scRNA-seq.

To begin with, the average expression across genes in the control condition (stimulus specific "Scr" for perturbation effect and "Unt_Scr" for treatment + perturbation effect). In order to reduce false positives, genes with an average expression log1p(umi count) below the threshold of 0.25 were filtered out. Further, *mod.pseudoBulk_screen()* function was employed to create pseudo-bulk profiles and genes average expression data is added to the profiles after filtering genes with low umi count (Santinha et al., 2023).

Raw count data obtained from previous step were processed using the *DGEList()* function from the *edgeR* package (version 3.36.0) in R (version 4.1.1). This step involved organizing the count data into a DGEList object, incorporating sample group information for subsequent analysis. Normalization factors were computed to adjust for differences in sequencing depth between samples. The *calcNormFactors()* function was applied to calculate normalization factors using the trimmed mean of M values (TMM) method, a standard approach in RNA-seq analysis for library size normalization. Dispersion values were estimated to model the variability in count data across genes. The *estimateDisp()* function was utilized to calculate gene-specific dispersions, considering the experimental design factors encoded in a design matrix. This step facilitated the accurate modeling of gene expression variability across conditions. Differential expression analysis was performed to identify genes exhibiting significant expression changes between experimental conditions. Two differential expression tests were conducted based on the specified de_subtest parameter:

Quasi-Likelihood F-test (QLF): Conducted using the glmQLFTest function, fitting a quasi-likelihood negative binomial generalized linear model (GLM) with glmQLFit.

Likelihood Ratio Test (LRT): Performed using the glmLRT function, fitting a negative binomial GLM with glmFit.

Differential expression results were post-processed to prioritize significant genes and visualize expression patterns. Genes with adjusted p-values less than 0.05 were considered significant. Heatmaps, volcano plots, and gene expression profiles were generated to visualize differential expression patterns and aid in biological interpretation.

3.1.6.10 Gene Set Enrichment Analysis (GSEA)

The DEGs data were obtained from Section 3.1.6.10. A term-to-gene mapping (*term2gene*) was created using gene symbols for mouse species and various pathway databases (e.g., GO, KEGG, Reactome). GSEA was performed using the *clusterProfiler* R package (Wu et al., 2021; Yu et al., 2012). For each contrast, gene sets from each *term2gene* were tested for enrichment using the Kolmogorov-Smirnov statistic. Gene sets with a minimum size of 10 and a maximum size of 300 were considered. The final GSEA results, including running score plots and heatmaps, were exported as tab-

delimited text files for further analysis and visualization. Additionally, *RDS* files containing processed data frames were saved to ensure reproducibility and facilitate downstream analyses.

3.2 Chapter 2

3.2.1 Creating three potential BDNF sensor TargetFinder libraries

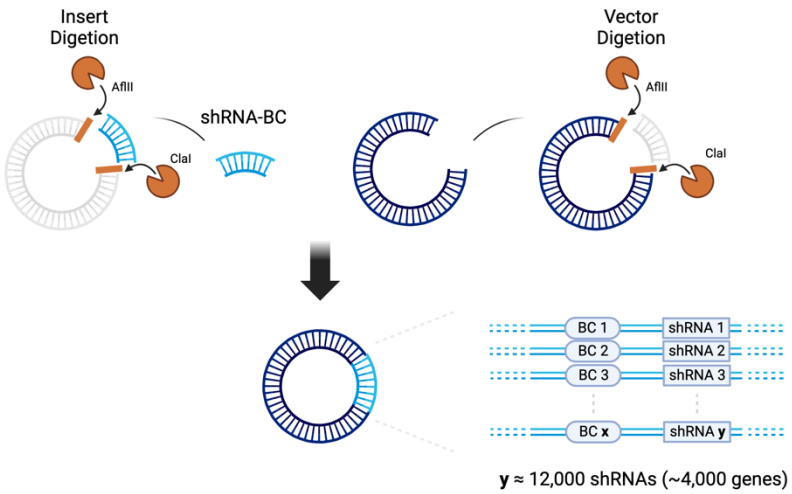

Figure 12 Schematic of cloning strategy for TargetFinder libraries

3.2.1.1 Molecular Cloning

To generate the V3589 (rBDNF-pI), V3590 (rBDNF-pIV), and V3591 (mBDNF-E840) TargetFinder libraries, a 573 bp shRNA cassette was excised from V1338 and subsequently cloned into V1301-rBDNF-pI, V1301-rBDNF-pIV, and V1301-mBDNF-E840 vectors, respectively, at the ClaI and AflII restriction sites (Figure 12). The procedure for plasmid library construction involved DNA digestion and ligation, conducted in accordance with the methodology outlined in Section 3.3.5.1. Following ligation, the transformed material was introduced into electro-competent bacterial cells, employing the techniques delineated in Section 3.3.5.2.

To attain the desired library complexity, the optimal volume of transformation mix was inoculated into 100 ml LB-Amp (200 µg/ml) broth. Subsequently, the efficiency of the library was assessed through restriction digestion, and the sequence validation of 10 randomly selected clones from each library was performed using Sanger sequencing methodology.

3.2.1.2 AAV production and genomics copies (GC) titer

To generate three adeno-associated virus (AAV) libraries, the standard protocol outlined in Section 3.3.2 was meticulously followed. The genomic copy (GC) titer of each library was quantified using hU6 oligos O1459 and O1460.

3.2.2 Evaluation of sensor activity of three potential BDNF sensors

3.2.2.1 Cell Culture

To assess the efficacy of three potential *brain-derived neurotrophic factor* (*Bdnf*) sensors, an online Luciferase assay was conducted. Primary cortical cultures were established from E15.5 C57BL/6 mouse embryos, following the protocol outlined in Section 3.3.3. Subsequently, 0.5 million cells were seeded onto 3.5 cm culture dishes. Each culture was individually infected with one of the three adeno-associated virus (AAV) libraries on *Day-in-vitro* 1 (*DIV1*), with a multiplicity of infection (MOI) of 1000.

On *Day-in-vitro* 7 (*DIV7*), all cultures were subjected to silencing using a TTX cocktail ([1 µM TTX; 100 µM D-AP5]), followed by the addition of 2 µM Luciferin. Cultures were then placed inside the Lumicycler incubator, with specific positional identification, and the software was initialized to commence measurements. After 24 hours of post-silencing, cultures were removed from the incubator, and either a Vehicle (culture medium), KCl solution (culture medium + 25 mM KCl for a final volume of 2 ml), or BDNF solution (culture medium + 50 ng/ml for a final volume of 2 ml) was added.

Following stimulation, cultures were returned to the Lumicycler incubator in their respective positional identifiers. For each AAV + stimulation condition, three replicates were measured to ensure the reliability of the results.

3.2.2.2 Raw Result Acquisition and Data Analysis

Raw data were acquired from the instrument, preprocessed using LumiCycle Analysis, and exported as *.csv* files. Subsequently, a custom R script was employed for data analysis. The script reads data from individual *.csv* files and consolidates them into a single data frame. After necessary data wrangling, the script generates line plots for each AAV library, with each stimulation condition represented by distinct color lines.

3.2.3 Determining optimal time for *mE840 BDNF* sensor maximum activity

3.2.3.1 Cell Culture

To ascertain the time-point at which the *mE840 BDNF* sensor exhibits maximum activity, quantitative real-time polymerase chain reaction (qRT-PCR) was conducted. Primary cortical cultures were established from E15.5 C57BL/6 mouse embryos, following the protocol outlined in Section 3.3.3. Subsequently, 0.5 million cells were seeded onto 6-well plates. Each well was individually infected with A452 on *Day-in-vitro 1 (DIV1)*, at a multiplicity of infection (MOI) of 1000.

On *Day-in-vitro 7 (DIV7)*, all wells were subjected to silencing using a TTX cocktail ([1 µM TTX; 100 µM D-AP5]). After 24 hours of post-silencing, cultures were removed from the incubator, and either a Vehicle (culture medium), KCl solution (culture medium + 25 mM KCl for a final volume of 2 ml), or BDNF solution (culture medium + 50 ng/ml for a final volume of 2 ml) was added. Post-stimulation, cells were lysed at different time points (2, 4, 6, 8, 10, 12 hours) using Qiagen RLT buffer. For the 0^{th} hour control, lysates were collected during stimulation to other wells. All lysates were stored at -80°C until further processing.

3.2.3.2 RNA Harvest, cDNA Synthesis, qRT-PCR, and Data Analysis

Upon thawing at room temperature, all lysates underwent RNA harvest, cDNA synthesis, and qRT-PCR, following the procedures outlined in Sections 3.3.6 and 3.3.7, respectively. Oligonucleotides targeting *Npas4*, *BDNF exon IV*, and *Rpl13* (housekeeping) were utilized.

3.2.3.3 Data Analysis

Raw data were obtained from the instrument, pre-processed, and exported as *.xls* files. Subsequently, a custom R script was employed for data analysis. The script read data from individual *.xls* files and calculated delta Cq values relative to corresponding *Rpl13*, as well as delta delta Cq values relative to the 0^{th} hour sample. After appropriate data wrangling and plotting, a single data frame was created. Finally, the script generated boxplots and stimulation line plots for each stimulation, with different targets represented by distinct color lines.

3.2.4 Creating shRNA-BC library for A452

3.2.4.1 AAV genome isolation from AAV library

Isolation of the AAV ssDNA genome from three AAV libraries was carried out using the following protocol. Initially, 20 µl aliquots of each AAV library were thawed on ice. To eliminate any residual ambient DNA from the AAV production process, the samples underwent DNase treatment. Specifically, the TURBO DNase kit was employed for this purpose, with a reaction volume of 100 µl. Incubation was performed for 30 minutes at 37°C, followed by heat inactivation of enzymatic activity at 95°C for 10 minutes. Subsequently, 20 µl of Proteinase K was added to each sample, and incubation proceeded at 50°C for 60 minutes. After enzymatic treatment, the samples were subjected to cleanup using the M & N Gel and PCR kit, with elution conducted using 52 µl of elution buffer.

3.2.4.2 Enrichment and Illumina adapter PCR

Following isolation, an enrichment step was performed to amplify the shRNA to barcode (BC) combination. Custom oligos O3935 and O3936 were designed and obtained from IDT for this purpose. An optimization PCR was initially conducted to determine the appropriate number of cycles required for sufficient amplification. Upon optimization, the enrichment PCR was carried out for 10 cycles using the NEBNext Q5 HotStart HiFi kit, with reaction volume and composition set according to the manufacturer's protocol. The resulting PCR amplicon, typically a 350 bp band, was excised from a 1.2% agarose gel and purified using the NucleoSpin Gel and PCR-Clean-up Kit, with elution performed using 36 µl of elution buffer.

For Illumina index PCR, custom oligos were selected with consideration for color balance. However, undesired higher order bands were observed alongside the desired PCR amplicon. Despite attempts to mitigate this issue by adjusting PCR conditions such as melting temperature, extension temperature, DNA polymerase, template amount, and primer concentration, the problem persisted. Ultimately, PCR cycling was extended to 12 cycles, and approximately 400 bp fragments were excised from a 1.2% gel. The resulting PCR amplicon was again purified using the NucleoSpin Gel and PCR-Clean-up Kit, with elution carried out using 32 µl of elution buffer.

3.2.4.3 Sample pooling and NGS

Following library preparation, the concentration of the Illumina library was quantified using the KAPA Library Quant Kits, adhering strictly to the manufacturer's protocol.

For the pooling of samples prior to next-generation sequencing (NGS), the Illumina web tool "Pooling Calculator" was employed (https://support.illumina.com/help/pooling-calculator/pooling-calculator.htm). Samples were pooled with varying coverage levels, with Batch 1 samples specifically pooled to ensure that each sample received an equal allocation of 10 million reads. This pooling strategy aimed to maintain consistency and balance in sequencing coverage across the samples, facilitating accurate and comprehensive data analysis during subsequent NGS.

3.2.4.4 Data analysis

Samples were combined at the Illumina library level alongside the BDNF TargetFinder samples. Sequencing was performed using the NextSeq 500/550 High Output Kit v2.5 (150 Cycles), with Read 1 consisting of 50 cycles and Read 2 of 100 cycles. After sequencing, the reads were demultiplexed using a custom bash script. This involved utilizing the *bcl2fastq* command and providing a sample sheet containing sample indices, following all arguments as per the Illumina *bcl2fastq* user guide.

To trim the reads and extract the relevant sequences, the *cutadapt* tool was employed. For Read 1 sequences, which contained the 3' arm of the shRNA, trimming was performed by specifying adapter sequences corresponding to the 3' sequences of the hU6 promoter and a portion of the shRNA loop sequence. Quality trimming parameters allowed for a maximum error rate of 0.2, with minimum and maximum lengths set at 21 nucleotides. The trimmed reads were then saved as *.fastq* files.

For Read 2 sequences, which contained the barcodes, trimming was conducted by providing adapter sequences corresponding to DEC forward and DEC reverse sequences. Similar quality trimming parameters were applied, with a maximum error rate of 0.2 and minimum and maximum lengths set at 35 nucleotides. The resulting trimmed reads were saved as *.fastq* files.

Subsequently, the *seqtk* and *fasta_formatter* tools were utilized for file conversion from *.fastq* to *.fasta* and *.fasta* to *.txt* formats. Read identifiers from both Read 1 and Read 2 were shortened using the sed command. Finally, through necessary data manipulation using *awk* commands, Read 1 and Read 2 files were merged into a single .txt file based on the same read identifier. A bowtie index was generated using the *bowtie-build* tool, which was later used to map TargetFinder samples in Section 3.2.5.7.

3.2.5 Identifying neuronal modulators of mBDNF E840 sensor

3.2.5.1 Cell culture

To identify modulators of mBDNF E840, TargetFinder assay was performed in two batches. Primary cortical cultures were prepared from E15.5 C57BL/6 mice embryo as described in Section 3.3.3 and 10 million cells were seeded on 15 cm dishes. Cultures were separately infected with A452 on *DIV1* with an MOI of 1000. On *DIV7* all wells were silenced by using TTX cocktail [1 µM TTX; 100 µM D-AP5]. For Batch1 , post-silencing 24 hours cultures were taken out of the incubator and either Vehicle [Culture medium] or KCl solution [Culture medium + 25 mM KCl for a final volume of 2 ml] or BDNF solution [Culture medium + 50 ng/ml for a final volume of 2 ml] was added so that I have 3 replicates for each condition. For Batch2, post-silencing 24 hours cultures were taken out of the incubator and either Vehicle [Culture medium] or KCl solution [Culture medium + 25 mM KCl for a final volume of 2 ml] was added so that I have 4 replicates for each condition. BDNF stimulated samples were lysed 2 hours post stimulation whereas KCl stimulated samples were lysed 4 hours post stimulation. Unstimulated samples are always collected along with KCl stimulated samples.

3.2.5.2 RNA harvest, cDNA synthesis

First spent media containing TTX were collected for safe disposal and the cells were washed with 10 ml ice-cold 1 x PBS. To lyse the cells, 2.4 ml of RLT buffer was added. Cells were scrapped from the plate using cell scrapper. Lysates were homogenized using a 19-gauge needle and a syringe. RNA was harvested using RNA Easy Mini Kit as per manufactures protocol. Considering the binding capacity of columns, three columns were used per lysate. RNA concentration was measured using a spectrophotometer. To remove genomic DNA, TURBO DNase kit was used as per manufactures protocol. Each sample was cleaned again using NucleoSpin Gel and PCR-Clean-up Kit as per manufactures protocol. As the RNA concentration before DNase digest step was ~60µg, one column was used at this step.

cDNA synthesis was done using High-Capacity c-DNA Reverse Transcription Kit and as per manufactures protocol. However, the reaction was scaled up considering per reaction limit was 2 µg RNA to cDNA.

3.2.5.3 Quality control for stimulation by qRT-PCR

qRT-PCR was performed as described in Section 3.3.7. Oligonucleotides are used for targets *Luc*, *BDNF* exon IV and *Hprt1* (housekeeping). Sequences are available in Table 2.

3.2.5.4 Barcode enrichment PCR (PCR1)

cDNA concentration was measured by Qubit kit. For barcode enrichment PCR, 25 ng cDNA was used as template. Pool of forward and reverse mix of varying UMI length were mixed and used for PCR. NEBNext® Q5® Hot Start HiFi PCR Master mix was used for PCR as per manufacturers recommendation for 23 cycles. PCR amplicon of size ~170 bp were excised from the gel and cleaned up using NucleoSpin Gel and PCR-Clean-up Kit.

3.2.5.5 Illumina adapter PCR

PCR amplicon concentration was measured by Qubit kit. For barcode adapter PCR, 25 ng PCR1 was used as template. For PCR, unique forward and reverse oligonucleotides were used to keep unique sample identity. NEBNext® Q5® Hot Start HiFi PCR Master mix was used for PCR as per manufacturers recommendation for 4 cycles. PCR amplicon of size ~230 bp were excised from the gel and cleaned up using NucleoSpin Gel and PCR-Clean-up Kit.

3.2.5.6 KAPA quantification and pooling

Illumina library concentration was measured using KAPA Library Quant Kits. All steps were followed as per the manufactures protocol.

For pooling, Illumina web tool "Pooling Calculator" (https://support.illumina.com/help/pooling-calculator/pooling-calculator.htm) was used. Samples were pooled with different coverage. Batch1 samples were pooled such that each sample got 10 million reads whereas Batch2 each sample got 20 million reads each.

3.2.5.7 Data analysis

Samples were pooled at the level Illumina library and for sequencing NextSeq 500/550 High Output Kit v2.5 (150 Cycles) was used with Read1 50 cycles anf Read 2 100 cycles. Reads were demultiplexed using a custom bash script.

To trim reads and extract barcodes from Read2 sequences. Barcodes were trimmed by providing adapter sequences as DEC forward and DEC reverse sequences. Other parameters for quality trimming accept a maximum error rate of 0.2, minimum and maximum length of 35 nucleotides. Finally, the trimmed reads were reported as *.fastq* files. Trimmed reads were mapped to the Index generated using the *bowtie* tool. For quality alignments, seed length was kept to default of 28 nucleotide with max two mismatches. Alignments with a MAPQ value of 255 were taken further for counting using a custom awk command and exported out as *.txt* files.

All .txt files were read using custom R scripts. Briefly, I accumulate data from individual files and make a single raw counts data frame. Raw counts were QC verified and upon required data wrangling, raw counts were subjected to *DESeq2* pipeline and an aggregated dds object was created. Finally, *results()* function of *DESeq2* was used to where stimulated condition was contrasted always against unstimulated condition. Results were exported to *.txt* files.

Modulators of BDNF sensor were filtered out by applying a p-value threshold of 0.05 and log2 fold change of more than and equal to 1.

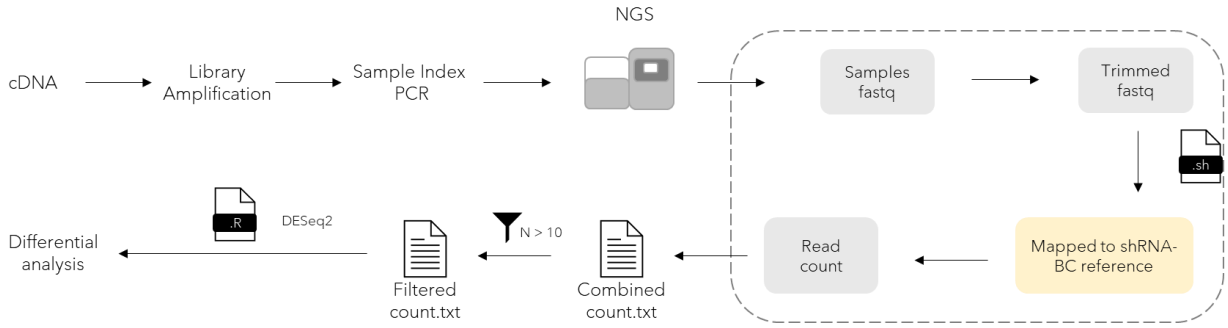

Figure 13 Schematic of Data Analysis Pipeline for the TargetFinder assay

Pathway analysis was done using a functional enrichment analysis web tool WebGestalt (WEB-based Gene SeT AnaLysis Toolkit) (Liao et al., 2019; Wang et al., 2017).

3.3 General Methods

These are some generalized methods I have used in this study except specifically mentioned otherwise.

3.3.1 Cell culture and maintenance

HEK293FT cells (ATCC cat. no. SD-3515) were exclusively utilized in this study for the production of AAV or Lentivirus. The HEK293FT cells employed in this investigation were maintained within passages 7 to 15. Throughout the study, cells were cultured in suitable growth medium at 37°C in a 5% CO2 humidified atmosphere. Cultures were routinely monitored every 2-3 days during maintenance to assess cell health, morphology, confluency, and particularly for contamination, as antibiotics were not utilized at any stage. Upon reaching 80-90% confluency, cell cultures were sub-cultured using a standard trypsin-dissociation protocol.

During subculturing, spent cell culture media was aspirated, and cultures were gently washed with temperature-adjusted 1x PBS to remove any residual media. Cells were then detached from the dish by incubation at 37°C for 2 minutes with a Trypsin/Vernese enzyme mix. The enzymatic reaction was halted by adding an appropriate volume of temperature-adjusted culture medium containing 10% FBS. The resulting cell suspension was collected in a fresh sterile 15 ml tube and centrifuged at 1000 x g for 5 minutes. The cell pellet was resuspended in an appropriate volume of temperature-adjusted growth medium and subsequently seeded according to experimental requirements.

The maintenance of cell stocks and periodic testing for Mycoplasma contamination were conducted by Beate Kauschat and Nadia Gabellini from the Molecular Neurobiology Department of Psychiatry, LMU Munich.

3.3.2 AAV production and genomic copies (GC) titer

3.3.2.1 Transfection

HEK293FT cells were cultured and maintained according to the procedure described in Section 2.1.1. For the preparation of a single AAV, a 15 cm dish was utilized. Prior to transfection, cell culture dishes were coated with Poly-L-lysine (PLL, 0.02 mg/ml) for 120 minutes, followed by three washes with sterile water. Transfection commenced when cultures reached 80-90% confluency. Approximately 60 minutes before transfection, spent media was replaced with 15 ml of temperature-adjusted maintenance media (DMEM + 10% FBS + 1% GlutMax). The transfection mix was prepared by combining 500 µl of OptiMEM medium with the following plasmids: 10 µg

of pFdelta6, 3.75 µg of pRV1, 3.75 µg of pH21, and 4 µg of p-AAV-genome. Polyethyleneimine (PEI) served as the main transfection agent and was mixed with the transfection mix to achieve a final ratio of PEI:DNA::4:1. After vortex mixing, the final transfection mix was incubated at room temperature. Following a 10-minute incubation period, the transfection mix was added to the cells drop-wise with gentle swirling to ensure homogenous distribution. After 4 hours of transfection, an additional 15 ml of temperature-adjusted maintenance medium was added.

3.3.2.2 AAV harvest

At 72 hours post-transfection, cells were scraped from the dish and collected in a sterile 50 ml falcon tube. The cell suspension was centrifuged at 1000 rpm for 10 minutes, and after removing the supernatant, the cell pellet was resuspended in 5 ml of AAV lysis buffer. Subsequently, three freeze-thaw cycles (20 minutes at –80°C followed by 20 minutes at 37°C) were performed to lyse the cells. Ambient genomic DNA was digested by incubating the lysate with 50 U/ml of Benzonase at 37°C for 30 minutes. Cell debris was removed by centrifugation, and the supernatant was clarified using a 0.45 µm filter and enriched using an Amicon Ultra-15 centrifugal unit. During enrichment, the clarified supernatant was diluted with 10 ml of cold sterile PBS and centrifuged until the volume reduced to 250-500 µl. The enriched AAVs were aliquoted in 20 µl aliquots and stored at -80°C until further use.

3.3.2.3 Genomic copies (GC) titer, absolute quantification

Ambient DNA was digested using TURBO DNase, with 5 µl of enriched AAV aliquot, 10 µl of 10X TURBO DNase buffer, 1 µl of TURBO DNase, and 84 µl of water per reaction. After incubation at 37°C for 30 minutes, DNase activity was heat-inactivated at 95°C for 10 minutes. Subsequently, 5 µl of Proteinase K (20 mg/ml) was added to the reaction and incubated at 50°C for 60 minutes to remove capsid. Single-stranded DNA (ssDNA) was cleaned using the NucleoSpin Gel and PCR-Clean-up Kit, and the AAV genome was eluted in 200 µl elution buffer.

For absolute quantification, DNA standards were prepared by serial dilution of plasmid DNA from 10^8 molecules to 10^3 molecules in water. AAV genomic DNA was diluted 1:100, 1:500, and 1:1000 and used as a template. The qPCR mastermix was prepared according to the manufacturer's protocol from primaQUANT SYBRGreen Master Mix, sufficient for 3 technical replicates. Primers targeting AAV ITRs were used for absolute quantification.

3.3.3 Primary culture of Mouse cortical neurons

In this study, primary cortical cultures were meticulously prepared from E15.5 C57BL/6 mouse embryos to establish a robust neuronal model system. The process involved several precise steps to ensure the successful isolation and cultivation of cortical neurons. Firstly, culture dishes were meticulously coated with poly-D-lysine (PDL) solution (0.1 mg/ml in dH2O) and left to incubate for 8-12 hours. This coating facilitated cell attachment and growth on the culture surface. Following incubation, the dishes were thoroughly washed three times with sterile water to remove any excess PDL. Next, an optimal volume of plating medium, comprising Neurobasal medium supplemented with 5% FBS, 2% B27, and 1% GlutaMax, was added to the coated dishes. This medium provided essential nutrients and growth factors necessary for the survival and proliferation of cortical neurons. The mouse embryos, obtained from E15.5 C57BL/6 mice, were humanely sacrificed by cervical dislocation, and their cortices were carefully dissected out using standard dissection protocols. The dissected cortices were then transferred to ice-cold HBSS/5mM HEPES solution to maintain tissue viability until further processing.

Up to 16 cortices were dissociated in a solution of activated papain, a proteolytic enzyme, to facilitate tissue digestion. The papain solution, prepared in DMEM and supplemented with DNase and L-cysteine, was incubated at 37°C for precisely 30 minutes to ensure optimal enzymatic activity. Following digestion, the enzymatic reaction was stopped by adding temperature- and pH-adjusted DMEM supplemented with 10% FBS. The dissociated cortical tissue was then gently triturated to obtain a single-cell suspension using a P1000 pipette. Undissociated tissue debris was removed by passing the cell suspension through a 10 µm cell strainer, resulting in a homogenous population of cortical neurons.

Cell counts were performed using Trypan blue staining and a cell counting chamber to assess cell viability and determine cell density accurately. Finally, the cortical neurons were seeded onto the pre-coated culture dishes at the desired density to initiate cell attachment and growth.

On *Day-in-vitro 1 (DIV1)*, the plating medium was completely replaced with temperature- and pH-adjusted culture medium, consisting of Neurobasal medium supplemented with 2% B27 and 1% GlutaMax. This medium exchange ensured the transition from a growth-supportive environment to a maintenance medium optimized for neuronal maturation and function.

For routine maintenance, the cultured neurons were fed every 3-4 days by removing 30% of the spent medium and replacing it with fresh, temperature- and pH-adjusted culture medium. This regimen provided continuous support for neuronal health and viability throughout the experimental period.

3.3.4 In-suspension transduction protocol for primary CNs

Following the isolation of primary mouse cortical neurons as described in Section 3.3.3, the required cells were aliquoted into a fresh 50 ml tube based on cell counting results. The adeno-associated virus (AAV) was diluted according to experimental requirements and added directly to the aliquoted cell suspension. The cell suspension containing the AAV was then incubated by placing it on a horizontal shaker set to gentle swirling at 100 rpm, inside the cell culture incubator. This incubation period allowed for efficient viral transduction of the primary cortical neurons.

After 4 hours of incubation, the cells were centrifuged at 600 rpm for 5 minutes at room temperature to facilitate the removal of the supernatant without disturbing the cell pellet. Subsequently, 2 ml of temperature- and pH-adjusted culture medium was added to resuspend the cells.

Using a P1000 pipette, the cell pellet was gently triturated to achieve a single-cell suspension. Following cell counting to determine the appropriate cell density, the required number of cells was seeded onto culture plates pre-coated with poly-D-lysine (PDL) at a concentration of 0.1 mg/ml.

This in-suspension AAV transduction method ensured efficient and uniform viral delivery to the primary cortical neurons, facilitating subsequent experimental manipulations and analyses.

3.3.5 Molecular cloning

3.3.5.1 Restriction cloning

For the construction of insert DNA, multiple approaches were employed, including Polymerase Chain Reaction (PCR), gene block synthesis, or isolation from existing vectors utilizing restriction enzymes.

In cases where PCR was utilized for insert DNA generation, oligonucleotides were custom-designed and ordered from Eurofins. The PCR reactions were performed using NEBNext Q5 Hot Start HiFi PCR Master Mix following the manufacturer's protocol to ensure high-fidelity amplification.

Alternatively, if gene blocks were required, they were sourced from IDT to ensure accurate and reliable synthesis.

For the isolation of insert DNA from existing vectors, restriction enzymes obtained from NEB were employed.

Later, ligation of the insert DNA into the desired vector backbone was done using T4 DNA ligase. Depending on the specific requirements of the experiment, different strains of chemically competent cells were employed. Chemically competent Mach1 cells were used for other plasmid constructs.

3.3.5.2 Library cloning

The ligation product, resulting from the molecular joining of DNA fragments, underwent a 1:2 dilution in nuclease-free water to optimize its concentration for subsequent transformation steps. Subsequently, 30 µl of Endura Electrocompetent cells were carefully introduced into a pre-chilled 1.5 ml tube, followed by the addition of 2 µl of the diluted ligation product. This amalgamation was gently mixed via tapping to ensure homogeneous distribution of the DNA construct among the electrocompetent cells.

The transformation mix, consisting of the cell-DNA mixture, was then introduced into a pre-chilled electroporation cuvette. Electroporation, a method of introducing DNA into cells using electrical impulses, was executed using the Eporator at a voltage of 1800 V for a duration of 4-5 ms, effectively facilitating the uptake of the exogenous DNA by the electrocompetent cells.

Post-electroporation, 1 ml of pre-warmed Recovery medium was promptly added to the cuvette, and the transformed cell-DNA mixture was transferred to a sterile bacterial culture tube. Any residual transformation mix adhering to the cuvette was carefully washed out by the addition of an additional 1 ml of Recovery medium, which was then combined with the collected mixture in the bacterial culture tube.

The culture tube, now containing the transformed cells, was incubated at 37°C for 60 minutes with gentle agitation at 180 rpm, allowing for the recovery and expression of the transformed cells.

To assess the efficiency of the transformation process, the transformation mix was diluted at varying ratios (1:10, 1:100, and 1:1000) and plated onto LB Agar plates. Simultaneously, the remaining transformation mix was stored at 4°C for subsequent analyses.

Following an incubation period of 14-16 hours, the number of colonies forming units (CFU) on the plated samples was enumerated to gauge the success of the transformation process. Depending on the desired complexity of the library, the stored transformation mix was further inoculated into LB broth supplemented with antibiotics to propagate the transformed cells.

Lastly, plasmids harboring the desired DNA inserts were isolated from the transformed cells using the M and N midi prep kit in accordance with the manufacturer's protocol, enabling downstream applications.

3.3.6 RNA isolation and cDNA synthesis

RNA isolation and cDNA synthesis were conducted using rigorous protocols to ensure high-quality nucleic acid samples for downstream applications. Specifically, Qiagen RNeasy kits were employed for RNA extraction, while the High-capacity cDNA kit was utilized for cDNA synthesis. All procedures were meticulously executed in accordance with the manufacturers' instructions to maintain consistency and reliability.

During RNA isolation, the Qiagen RNeasy kits facilitated efficient purification of total RNA from the samples. Notably, an on-column DNase treatment step was incorporated into the protocol using the RNase-Free DNase Set (Qiagen), ensuring the removal of genomic DNA contaminants and enhancing the purity of the isolated RNA. This step is crucial for eliminating any potential interference from genomic DNA during subsequent analyses.

Following RNA isolation, cDNA synthesis was carried out using the High-capacity cDNA kit. The kit provided "Random primers" were utilized for the initiation of cDNA synthesis, ensuring unbiased representation of the mRNA transcripts present in the sample. However, it is worth noting that specific sections, denoted as Section 3.1.1.2 and 3.2.3.2 deviated from the standard protocol provided by the manufacturer, implying the utilization of alternative or customized procedures for these steps.

Throughout the entire process, strict adherence to the manufacturers' protocols was maintained to minimize variability and ensure reproducibility of the results. By employing these standardized methodologies, high-quality RNA and cDNA samples were obtained, laying a solid foundation for subsequent molecular analyses and experimental investigations.

3.3.7 Quantitative real-time PCR (qRT-PCR)

Quantitative real-time PCR (qRT-PCR) was performed utilizing the primaQuant 2x qPCR CYBR Mix, adhering strictly to the manufacturer's protocol to ensure accuracy and reliability of results. Gene-specific target sequences were meticulously designed using NCBI Primer-BLAST or sourced from literature reviews and subsequently ordered from Eurofins.

For optimal qRT-PCR performance, the cDNA template input was carefully controlled within the range of 10-20 ng, a decision informed by the Ct values obtained from experimental Section 3.3.8. This ensures consistent and reliable amplification across samples, facilitating accurate quantification of gene expression levels.

Housekeeping genes utilized in this study, critical for normalization and ensuring data integrity, are listed in Table 2, serving as internal controls to account for variations in RNA input and reverse transcription efficiency. Their stable expression levels make

them suitable reference genes for comparative analysis of target gene expression across experimental conditions.

By meticulously adhering to standardized protocols and utilizing appropriate quality controls, the qRT-PCR experiments were conducted with precision, enabling robust and accurate quantification of gene expression levels in the experimental samples.

3.3.8 qRT-PCR, primer efficiency testing

For primer efficiency testing in qRT-PCR, a cDNA dilution series was meticulously prepared in sterile water, spanning concentrations from 2 ng/µl down to 0.0032 ng/µl. These dilutions were then utilized as templates for PCR amplification to assess the efficiency of the primers across a range of template concentrations.

Primers exhibiting efficiency values falling within the range of 0.95 to 1.05, indicative of optimal amplification dynamics, and featuring a single melting temperature (Tm) peak were exclusively selected for inclusion in this study. These criteria ensure the accuracy and reliability of the qRT-PCR results by minimizing the potential for non-specific amplification or primer dimer formation.

The amplification reactions were performed using the primaQuant 2x qPCR CYBR Mix, a high-performance reagent specifically formulated for absolute quantification applications. Throughout the experiment, all steps were meticulously executed in strict accordance with the manufacturer's protocol to ensure consistency and reproducibility of results.

By adhering to stringent selection criteria and employing standardized protocols, the qRT-PCR experiments for primer efficiency testing were conducted with precision, enabling accurate quantification of gene expression levels across the cDNA dilution series.

3.4 Materials

3.4.1 Reagents, Kits, Equipment's and Software

Table 1 List of Reagents, kits, equipment's and software's

Reagent or Resource	Source	Identifier
Cell culture		
15 cm dish	BD Falcon	353025
3,5 cm dish	BD Falcon	353001
40 µm Cell Strainer	BD Falcon	352340
6 cm dish	BD Falcon	353004
6-well plate	BD Falcon	353046
Amicon Ultra-15 Centrifugal Filter Units; 15 ml; 100kDa	Millipore	UFC910024
B27 (50x)	ThermoFisher Scientific	17504044
Benzonase	Sigma	E1014
Cell Scraper	BD Falcon	3010
Cell strainer 40µm (blue)	BD Falcon	352340
D-Luciferin, free acid	PJK	102112
DMEM, 4,5 g/L Glucose	ThermoFisher Scientific	21969035
Fetal Bovine Serum (FBS), heat-inactivated	ThermoFisher Scientific	10500064
Glutamax (100x)	ThermoFisher Scientific	35050038
HEPES	Sigma-Aldrich	
Hoechst 33342	Invitrogen	H3570
L-Cystein	Sigma-Aldrich	C - 7880
Millex HA-Filter, 0.45µm, 33mm	Millipore	SLHA033SS
Neurobasal Medium	ThermoFisher Scientific	21103049
Opti-MEM, with GlutaMAX	ThermoFisher Scientific	51985026
Papain		LS 003126
PEG-it Virus Precipitation Solution	SBI	LV810A-1
Poly-D-lysine	Sigma-Aldrich	P7886
Polyethylenimin (PEI),linear, MW 25,000	Polyscience	23966-2
Trypan blue (0,4%)	ThermoFisher Scientific	15250-061
Trypsin (2,5%, 10X), no Phenol Red	ThermoFisher Scientific	15090046
Versene Solution	ThermoFisher Scientific	15040-033
Drugs and chemicals		

(-)-Bicuculline methiodide	Abcam	ab120108
4-Aminopyridine (4-AP)	Abcam	ab120122
Ampicilin	Sigma-Aldrich	A9518-5G
Bacto Trypton	BD Bioscience	211705
Bacto Yeast	BD Bioscience	212750
Bacto-Agar	BD Bioscience	214010
D-AP5	R&D Systems	0106
DNase I	Sigma-Aldrich	DN25
Glycine	Abcam	ab120050
Recombinant Human BDNF	PeproTech	AF-450-02-10
Strychnine hydrochloride	Abcam	ab120416
Tetrodotoxin citrate	R&D Systems	1069

Molecular biology		
1.5 ml LoBind Tubes	Eppendorf	30108051
5.0 ml LoBind Tubes	Eppendorf	30108310
Electroporation cuvettes 100 µl	Carl Roth	PP38.1
Ethidium bromide solution 1 %, 10 ml	Carl Roth	2218.1
GeneRuler 1 kb DNA Ladder	ThermoFisher Scientific	SM0312
GeneRuler 100 bp DNA Ladder	ThermoFisher Scientific	SM0242
LE Agarose	Biozym	840004
MicroAmp Fast Optical 96-Well-Reaction Plate	ThermoFisher Scientific	4346907
MicroAmp Optical Adhesive Film	ThermoFisher Scientific	4311971
NEBNext Q5 Hot Start HiFi PCR Master Mix	NEB	M0543 L
PCR SingleCap 8er-SoftStrips 0.2 ml, farblos	Biozym	710970
Petri dish, 150 x 20 mm, transparent, with ventilation cams	Sarstedt	82.1184.500
Proteinase K 20mg/ml, RNA grade	ThermoFisher Scientific	25530049
T4 ligase	NEB	M0202L
Turbo DNase	ThermoFisher Scientific	AM2239
UV-Cuvettes, micro	Brand	759200

Commercial kits		
Chromium Next GEM Single Cell 3' Reagent Kits v3.1	10X Genomics	PN-1000269
High-Capacity c-DNA Reverse Transcription Kit	ThermoFisher Scientific	4368814
KAPA Library Quant Kits (Illumina/ABI)	Roche	7960204001
NextSeq 500/550 High Output Kit v2.5 (150 Cycles)	Illumina	20024904
NovaSeq 6000 S1 Reagent Kit v1.5 (100 cycles)	Illumina	20028319
NucleoBond Xtra Midi EF	Macherey & Nagel	740.420.50

NucleoSpin Gel and PCR-Clean-up (250)	Macherey & Nagel	740609.250
NucleoSpin Plasmid	Macherey&Nagel	740588.250
primaQuant 2xqPCR CYBR Mix	Steinbrenner	SL-9902HR-20ML
Qubit dsDNA HS Assay Kit	ThermoFisher Scientific	Q32854
RNA Easy Mini Kit + Shredder	Qiagen	GR8RNA
Equipment		
32-Channel Luminometer	ActiMetrics	LumiCycle 32
BioPhotometer	Eppendorf	6131
Cell culture incubator	Thermo Scientific	Cytoperm 2
Centrifuge 5810/5810 R	Eppendorf	VB-2185
Chromium X Series (X/iX)	10x Genomics	1000326
Eporator	Eppendorf	4309 000.019
Incubator Shaker	Multitron Pro	INFORS HT
Inverted fluroscence microscope	Zeiss	Observer Z1
Microcentrifuge, Refrigerated	Thermo Scientific	75002423
Molecular Imager, Gel Doc XR+ System	BIO-RAD	1708195EDU
Phase Contrast Microscope	Zeiss	Axiovert 40C
Qubit® 2.0 Fluorometer	Invitrogen	Q32866
StepOnePlus™ Real-Time PCR System	Applied Biosystems	4376600
Stereo microscope	Zeiss	Stemi-2000C
Thermal Cycler	Thermo Scientific	N11467
Thermomixer	Eppendorf	5355 000.011
Software		
2100 Expert	Agilent	B.02.11.SI824 (SR1)
BioRender		
ChatGPT	OpenAI	GPT-3.5
Image Lab 6.0		6
LumiCycle Analysis	ActiMetrics	2.5
Python		3.11.0
R (x86_64-pc-linux-gnu (64-bit))	R	version 4.3.2
Rstudio (Cherry Blossom)	Rstudio	2023.03.0+386
SnapGene	SnapGene	4.1.9
Ubuntu 22.04.3 LTS (jammy)	Ubuntu	22.04.3
ZEN 2012	Ziess	1.1.2.0
Zotero	Zotero	6.0.36

3.4.2 Oligonucleotide

Table 2 List of oligonucleotides used.

OF ID	Name	Sequence (5' to 3')
O1459	hU6_as	tttcaagttacggtaagcatatgatagt

O1460	hU6_s	caaggctgttagagagataattggaat
O1489	AFA_qDec1.2	ccgagtagaattaaccctcactaaa
O1490	AFA_qDec2.2	cgcgtctactaatacgactcac
O1582	Mm Camk2d	ttacagtgaagctgatgccagt
O1583	Mm Camk2d	ttaggtcccgatggactacg
O2949	Mm Sharp1_s	aaaccacagaaggaatagtctagca
O2950	Mm Sharp1_as	caaactgggtctacaatgaacg
O3117	P7_i7_read2	caagcagaagacggcatacgagattaaggcgagtgactggagttcagacg
O3120	P7_i7-N702_read2	caagcagaagacggcatacgagatcgtactaggtgactggagttcagacg
O3121	P7_i7-N703_read2	caagcagaagacggcatacgagataggcagaagtgactggagttcagacg
O3122	P7_i7-N704_read2	caagcagaagacggcatacgagattcctgagcgtgactggagttcagacg
O3123	P7_i7-N705_read2	caagcagaagacggcatacgagatggactcctgtgactggagttcagacg
O3303	Dec_UMI_read1_fwd(25bp)	tctttccctacacgacgctcttccgatctnnnnnnnnnnnnnnnnnnnnnnnctactaatacgactcactatagg
O3304	P7_i7-N706_read2	caagcagaagacggcatacgagattaggcatggtgactggagttcagacg
O3316	Luc_s	cgccattctacccactcgaa
O3317	Luc_as	tgtccacctcgatatgtgcg
O3341	P5_i5-S505_read1	aatgatacggcgaccaccgagatctacacgtaaggagacactctttccctacacgacgc
O3342	P5_i5-S506_read1	aatgatacggcgaccaccgagatctacacactgcataacactctttccctacacgacgc
O3370	Camk2d_s_2	ccccacagtacccatcaact
O3371	Camk2d_as_2	ttcatgcactcagaaacatgc
O3372	Vegfa_s	acatctgcaagtacgttcgtt
O3373	Vegfa_as	cttgttcagagcggagaaagc
O3374	Camkk2_s	aggacgagaactgcacactg
O3375	Camkk2_as	ctgccttgcttcgtgagc
O3376	Map3k12_s	tatcggaggagggcttccat
O3377	Map3k12_as	actggcatcagcttcactgt
O3384	Fgf5_s	agaaaacctggtgcacccta
O3385	Fgf5_as	tcacattcccgaattaagctc
O3386	Vegfa_shRNA_s	ccggcgtcactgttgacagaatagtgttaatattcatagcactgttctgtcaacggtgacgtttt
O3387	Vegfa_shRNA_as	aattaaaacgtcaccgttgacagaacagtgctatgaatattaacactattctgtcaacagtgacg
O3388	Camkk2_shRNA_s	ccggcctgcgtttctatagcagtatgttaatattcatagcatgctgctatggaaacgcaggtttt
O3389	Camkk2_shRNA_as	aattaaaacctgcgtttccatagcagcatgctatgaatattaacatactgctatagaaacgcagg
O3390	Map3k12_shRNA_s	ccggcctaaattagatgcagccttagttaatattcatagctagggctgcatctagtttaggtttt

O3391	Map3k12_shRNA_as	aattaaaacctaaactagatgcagccctagctatgaatattaactaaggctgcatctaatttagg
O3396	Erbb2_shRNA_s	ccgggcttcaatcttgagtggttaagttaatattcatagcttaaccactcaggattgaagctttt
O3397	Erbb2_shRNA_as	aattaaaagcttcaatcctgagtggttaagctatgaatattaacttaaccactcaagattgaagc
O3456	Dec_read2_frame2_rev	gtgactggagttcagacgtgtgctcttccgatctcactaaagggtaggtgacact
O3457	Dec_read2_frame3_rev	gtgactggagttcagacgtgtgctcttccgatctgcactaaagggtaggtgacact
O3458	Dec_read2_frame4_rev	gtgactggagttcagacgtgtgctcttccgatcttgcactaaagggtaggtgacact
O3516	Fgf5_shRNA_s	ccggcccagtgaagtatagattgaagttaatattcatagcttcagtctgtacttcactgggtttt
O3517	Fgf5_shRNA_as	aattaaaacccagtgaagtacagactgaagctatgaatattaacttcaatctatacttcactggg
O3520	Nrg1_shRNA_s	ccgggccacaaacaacagaaattaagttaatattcatagcttagtttctgttgtttgtggctttt
O3521	Nrg1_shRNA_as	aattaaaagccacaaacaacagaaactaagctatgaatattaacttaatttctgttgtttgtggc
O3522	Synj2_shRNA_s	ccggcccacctataagtatgatgttgttaatattcatagcaacgtcatacttgtaggtgggtttt
O3523	Synj2_shRNA_as	aattaaaacccacctacaagtatgacgttgctatgaatattaacaacatcatacttataggtggg
O3526	Nrg1_s_mouse	acccaagtcaggaactcagc
O3527	Nrg1_as_mouse	ggtcccagtcgtggatgtag
O3551	Dec_UMI23_read1_fwd	tctttccctacacgacgctcttccgatctnnnnnnnnnnnnnnnnnnnnnnctactaatacgactcactatagg
O3552	Dec_UMI21_read1_fwd	tctttccctacacgacgctcttccgatctnnnnnnnnnnnnnnnnnnnnctactaatacgactcactatagg
O3553	Dec_UMI27_read1_fwd	tctttccctacacgacgctcttccgatctnnnnnnnnnnnnnnnnnnnnnnnnnnctactaatacgactcactatagg
O3839	P7_i7-N707_read2	caagcagaagacggcatacgagatctctctacgtgactggagttcagacg
O3840	P7_i7-N708_read2	caagcagaagacggcatacgagatcagagagggtgactggagttcagacg
O3855	MmBdnf_exon IV_s	gct gcc ttg atg ttt act ttg a
O3856	MmBdnf_exon IV_as	gca acc gaa gta tga aat aac c
O3857	Synj2_FP	ccaagggttcccactatgaa
O3858	Synj2_RP	gagatgcccgagtacacctt
O3866	AAV2 ITR_s	ggaacccctagtgatggagtt
O3867	AAV2 ITR_as	cggcctcagtgagcga
O3868	Hprt1(Mm and Rr/Rn)_s	cagtcccagcgtcgtgatta
O3869	Hprt1(Mm and Rr/Rn)_as	agcaagtctttcagtcctgtc

O3870	mBDNF exon I_s	aac aag aca cat tac ctt cct gca t
O3871	mBDNF exon I_as	ctc ttc tca cct ggt gga aca tt
O3872	oligodT(18)	ttttttttttttttttt
O3935	shRNA_pathSCREENER_hU6_read2	tctttccctacacgacgctcttccgatctggaaaggacgaaacaccgg
O3936	Dec_UMI23_read2_rev	gtgactggagttcagacgtgtgctcttccgatctnnnnnnnnnnnnnnnnnnnnnncactaaagggtaggtgacact
O3937	Partial Read 1_shRNA_scPerturb-seq	ctacacgacgctcttccgatct
O3938	Partial Read 2_shRNA_scPerturb-seq	gtgactggagttcagacgtgtgctcttccgatctttcactaaagggtaggtgacac
O4004	Npas4_s	gctatactcagaaggtccagaaggc
O4005	Npas4_as	tcagagaatgagggtagcacagc
O4187	BamHI-EGFP_s	cgaaggatccacccgccaccatggtgagcaaggg
O4188	shRNA_scRNA_Perturb2_as	ccgaagcggccgctactaatacgactcactataggnnnnnnnnnnnnnnnnnnnngtgtcacctaccctttagtgaagcttttacttgtacagctcgtccatgccg
O626	erbB2_s	cgctttgtggtcatccaga
O627	erbB2_as	cggtagaaggtgctgtccat
O854	rpl13_s	atccctccaccctatgacaa
O855	rpl13_as	gccccaggtaagcaaactt
	Bhlhe40_s	ccgggtcagcacaattaagtaagaagttaatattcatagcttcttgcttaattgtgctgacttttt
	Bhlhe40_as	aattaaaagtcagcacaattaagcaagaagctatgaatattaacttcttacttaattgtgctgac

3.4.3 Plasmids

Table 3 List of plasmids used.

OF ID	Plasmid name
V2909	pAAV_4xSARE-ArcMin-luc2_hU6_shRNA-Vegfa
V2910	pAAV_4xSARE-ArcMin-luc2_hU6_shRNA-Map3k12
V2918	pAAV_4xSARE-ArcMin-luc2_hU6_shRNA-Erbb2
V2915	pAAV_4xSARE-ArcMin-luc2_hU6_shRNA-Camkk2
V3011	pAAV_4xSARE-ArcMin-luc2_hU6_shRNA-Nrg1
V3013	pAAV_4xSARE-ArcMin-luc2_hU6_shRNA-Fgf5
V3014	pAAV_4xSARE-ArcMin-luc2_hU6_shRNA-Synj2
V3576	VS007_pAAV-hSynP-EGFP_DECr-shRNABC-DECf_SV40pA_shRNAstuff-hU6
V3577	VS008_ pAAV-hSynP-EGFP_DECr-shRNABC-DECf_SV40pA_shRNA_Scr1-hU6
V3578	VS009_pAAV-hSynP-EGFP_DECr-shRNABC-DECf_SV40pA_shRNA_Scr2-hU6
V3579	VS010_pAAV-hSynP-EGFP_DECr-shRNABC-DECf_SV40pA_shRNA_Vegfa-hU6
V3580	VS011_pAAV-hSynP-EGFP_DECr-shRNABC-DECf_SV40pA_shRNA_Map3k12-hU6
V3581	VS012_pAAV-hSynP-EGFP_DECr-shRNABC-DECf_SV40pA_shRNA_Erbb2-hU6
V3582	VS013_pAAV-hSynP-EGFP_DECr-shRNABC-DECf_SV40pA_shRNA_Fgf5-hU6
V3583	VS014_pAAV-hSynP-EGFP_DECr-shRNABC-DECf_SV40pA_shRNA_Nrg1-hU6
V3584	VS015_pAAV-hSynP-EGFP_DECr-shRNABC-DECf_SV40pA_shRNA_Synj2-hU6
V3585	VS016_pAAV-hSynP-EGFP_DECr-shRNABC-DECf_SV40pA_shRNA_Camk2d-hU6
V3586	VS017_pAAV-hSynP-EGFP_DECr-shRNABC-DECf_SV40pA_shRNA_Bhlhe40-hU6
V3587	VS023_pAAV-hSynP-EGFP_DECr-shRNABC-DECf_SV40pA_shRNA_Camkk2-hU6
V3589	pAAV-rBDNF-pI-fireLuc-BC-pA_shRNA-hU6
V3590	pAAV-rBDNF-pIV-fireLuc-BC-pA_shRNA-hU6
V3591	pAAV-mBDNF-E840-fireLuc-BC-pA_shRNA-hU6
V1301	pAAV_4xSARE-ArcMin-luc2_hU6
V1301_Vegfa	pAAV_4xSARE-ArcMin-luc2_Vegfa-hU6
V1301_Map3k12	pAAV_4xSARE-ArcMin-luc2_Map3k12-hU6
V1301_Erbb2	pAAV_4xSARE-ArcMin-luc2_Erbb2-hU6
V1301_Fgf5	pAAV_4xSARE-ArcMin-luc2_Fgf5-hU6
V1301_Nrg1	pAAV_4xSARE-ArcMin-luc2_Nrg1-hU6
V1301_Synj2	pAAV_4xSARE-ArcMin-luc2_Synj2-hU6

V1301_Camk2d	pAAV_4xSARE-ArcMin-luc2_Camk2d-hU6
V1301_Bhlhe40	pAAV_4xSARE-ArcMin-luc2_Bhlhe40-hU6
V1301_Camkk2	pAAV_4xSARE-ArcMin-luc2_Camkk2-hU6

3.4.4 AAV

Table 4 List of Adeno-associated virus (AAV) used.

OF ID	Name
A125-7	pAAV_Syn1p_tRFP_V1909
A387	AAV_SARE-luc2_hU6-shVegfa
A388	AAV_SARE-luc2_hU6-shMap3k12
A391	AAV_SARE-luc2_hU6-shCamkk2
A392	AAV_SARE-luc2_hU6-shErbb2
A397	pAAV_4xSARE-ArcMin-luc2_hU6
A449	VS008_pAAV-hSynP-EGFP_DECr-shRNABC-DECf_SV40pA_shRNA_Scr1-hU6
A450	V3589_pAAV-rBDNF-pI-fireLuc-BC-pA_shRNA-hU6
A451	V3590_pAAV-rBDNF-pIV-fireLuc-BC-pA_shRNA-hU6
A452	V3591_pAAV-rBDNF-E840-fireLuc-BC-pA_shRNA-hU6
A486	AAV_SARE-luc2_hU6-shScr1
A487	AAV_SARE-luc2_hU6-shScr2
A488	AAV_SARE-luc2_hU6-shFgf5
A489	AAV_SARE-luc2_hU6-shNrg1
A490	AAV_SARE-luc2_hU6-shSynj2
A72-1	AAV_SARE-luc2_hU6-shCamk2d.1
A74-1	AAV_SARE-luc2_hU6-shBhlhe40.1
VS008_3_Scr	pAAV-hSynP-EGFP_DECr-shRNABC-DECf_SV40pA_Scr_hU6
VS010_Vegf4a	pAAV-hSynP-EGFP_DECr-shRNABC-DECf_SV40pA_Vegf4a_hU6
VS011_Map3k12	pAAV-hSynP-EGFP_DECr-shRNABC-DECf_SV40pA_Map3k12_hU6
VS012_Erbb2	pAAV-hSynP-EGFP_DECr-shRNABC-DECf_SV40pA_Erbb2_hU6
VS013_Fgf5	pAAV-hSynP-EGFP_DECr-shRNABC-DECf_SV40pA_Fgf5_hU6
VS014_Nrg1	pAAV-hSynP-EGFP_DECr-shRNABC-DECf_SV40pA_Nrg1_hU6
VS015_Synj2	pAAV-hSynP-EGFP_DECr-shRNABC-DECf_SV40pA_Synj2_hU6
VS016_Camk2d	pAAV-hSynP-EGFP_DECr-shRNABC-DECf_SV40pA_Camk2d_hU6
VS017_Bhlhe40	pAAV-hSynP-EGFP_DECr-shRNABC-DECf_SV40pA_Bhlhe40_hU6
VS023_3_Camkk2	pAAV-hSynP-EGFP_DECr-shRNABC-DECf_SV40pA_Camkk2_hU6

3.4.5 Perturb-seq barcodes

Table 5 List of PeruturbSeq shRNA-bc to target gene association using Sanger sequencing.

Target_ID	shRNAbc
VS008_06_Scr1	ACTTCCCATAACAGAACCTA
VS008_07_Scr1	GTTATCTCGAACACAGAACA
VS009_09_Scr2	TAGCATGATATTCAACAAGC
VS009_10_Scr2	CAAACAATATTGATGGAGTC
VS010_12_Vegf4a	TTGAATAATCTGTAGTTGAA
VS010_B_Vegf4a	GGATAAGGCACATCACTTTT
VS010_C_Vegf4a	TAGTCCATTGTGTTACGAAC
VS010_D_Vegf4a	TGGGTCATCCTAATGGTTAT
VS011_19_Map3k12	GTGTTACACACAGTCTATAC
VS011_A_Map3k12	AACTCCTAGGTCCGTCCTTA
VS011_B_Map3k12	CTCGAGAGGCACCAAATGGA
VS012_23_Erbb2	ACCCGATTGCGACATCGCTC
VS012_E_Erbb2	CGTTAGGCCGAGAAAACGTG
VS012_G_Erbb2	AAACGGAGCAGAGATAAAGT
VS012_H_Erbb2	GGTTCCGGGACACCTAAAAT
VS013_25_Fgf5	AAATCGCACACACTCGAATG
VS013_F_Fgf5	CAATATTCCGAGCCCATTGG
VS013_G_Fgf5	GGAATACATCGACCATTCGC
VS014_27_Nrg1	GTTACGTGCTCACAACAAAG
VS014_28_Nrg1	CGATCAGCTCTTGTACACAC
VS014_R_Nrg1	CTCCCGGGCGAGCGCGCATA
VS014_S_Nrg1	CAGATTCCAGCCGCACCAAT
VS015_31_Synj2	TGTGGCCTCAGATGCTAACA
VS015_32_Synj2	GCGTGAAGCCCCGACTCCGA
VS015_J_Synj2	CACTCCCTTACATTGGTTAT
VS016_T_Camk2d	GACAGCTCTTAGCGGGCAAC
VS016_U_Camk2d	TAGACCACACTCGATTCTGT
VS016_V_Camk2d	TCGCAAACTCCCCTAGTCCC
VS016_W_Camk2d	GCACATCTGAAGGCACTCAA
VS017_33_Bhlhe40	CAAACACAGATTGAATGTCT
VS017_34_Bhlhe40	TTTATCCTCCCGTCCACAAT
VS017_N_Bhlhe40	AATGATTGTCTGGTGCCGGA
VS017_P_Bhlhe40	ATAACAGCAACCCGACGCGC
VS023_2_Camkk2	TCCGCACTCTACTGCAAATC
VS023_3_Camkk2	ATTATAATCGGCTGATGATA
VS023_5_Camkk2	GATTAGAATCCTAGCGACCC
VS023_6_Camkk2	TGAGGCTCATATGGCTCAAG

4 Results

4.1 Chapter 1

4.1.1 Identification of modulators of the E-SARE sensor.

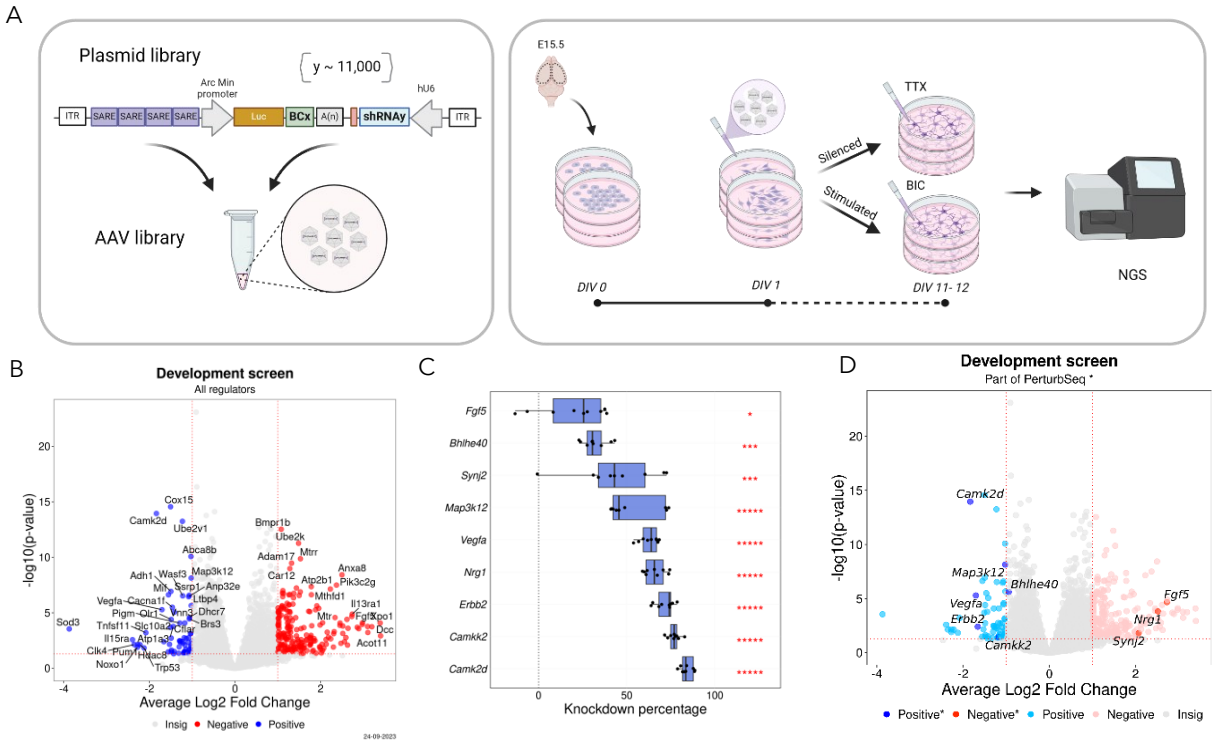

Figure 14 TargetFinder assay identifies developmental modulators of synaptic activity.

(A) Left panel shows schematics of the plasmid library. Plasmid library comprises of sensor and effector cassette as described in Figure 7. 4-times SARE followed by *Arc* minimal promoter was used as the genetic sensor driving expression of a transcript that codes for *Luciferase* (*Luc*) and a shRNA specific molecular barcode (BCx). Each BCx is uniquely coupled to transcript specific shRNA (shRNAy). Plasmid library was created which comprises of approximately 11,000 shRNA targeting approximately 3,500 mRNA transcripts. AAV library was created from plasmid library. Right panel shows schematics of cell culture setup. Primary cortical neurons were harvested from E15.5 wild-type mouse embryos and plated in many cell culture dishes. AAV libraries were transduced to all cultures on *DIV1* and separated onto 2 groups where each group contains 3 replicates. One group was silenced for 24 hours using TTX cocktail and other group was stimulated using BIC cocktail for 4 hours. RNA was harvested and after barcode amplification and adapter PCR, samples were pooled and sequenced.

(B) Volcano plots showing results of differential analysis. Vertical and horizontal dotted lines indicate the average log2 fold change threshold and p-value threshold, respectively. Negative and positive modulators were depicted with red and blue dots, respectively.

(C) The boxplot depicts the distribution of knockdown percentages across different modulators, with the dotted line indicating the baseline (no knockdown). "*" denotes significance levels (p-value < 0.05 and so on) derived from Wilcoxon rank sum test statistics, reflecting the differences observed between knock-down and scramble control.

(D) Position of selected modulators whose knockdown efficiency was validated and will be part of shRNA-Perturb-seq.

To identify genetic modulators of E-SARE sensor, TargetFinder assay was conducted using primary cortical neuron cultures derived from E15.5 wild-type mouse. Cultures were transduced with the AAV library on *DIV1* and divided into two groups.

Each group consisted of three independent dishes, which were subsequently either silenced using TTX cocktail on *DIV11* or stimulated using BIC cocktail on *DIV12*.

Silenced cultures were lysed after 24 hours and stimulated cultures were lysed after 4 hours. RNA harvest, cDNA synthesis, barcode enrichment PCR, indexing PCR and Next-generation sequencing (NGS) was performed.

Differential expression analysis was conducted utilizing the *DESeq2* package with default parameters. To identify Differentially Sensor Modulators (DSMs), a volcano plot was employed, highlighting variations in fold change in sensor activity indicative of the type of modulator affecting the E-SARE sensor. DSMs meeting the criteria of an absolute average fold change of >= 1 and a p-value <= 0.05 were considered significant. Based on the directionality of average fold change, DSMs were categorized as either "up" or "down," denoting negative or positive regulators of the E-SARE sensor, respectively.

Top and interesting DSMs were selected manually, and shRNA knock-down efficiency was evaluated using relative quantification. DSMs which show significant knockdown efficiency were selected for shRNA-Perturb-seq experiment.

4.1.2 Establishment of shRNA-Perturb-seq

4.1.2.1 Evaluating Pert-BC expression in primary mouse cortical neurons

To check the expression of *hSyn1* promoter driven BC cassette in primary cortical neurons, a scramble short hairpin RNA (shRNA) construct was employed, and the corresponding adeno-associated virus (AAV) was generated and transduced into neuron cultures on *DIV1* at a MOI of 500. The expression was evaluated on *DIV9* through live-cell imaging, focusing on enhanced green fluorescent protein (*EGFP*) expression. Robust whole-cell localization of GFP was observed, indicating successful expression of the *hSyn1* promoter-driven BC cassette in primary cortical neurons.

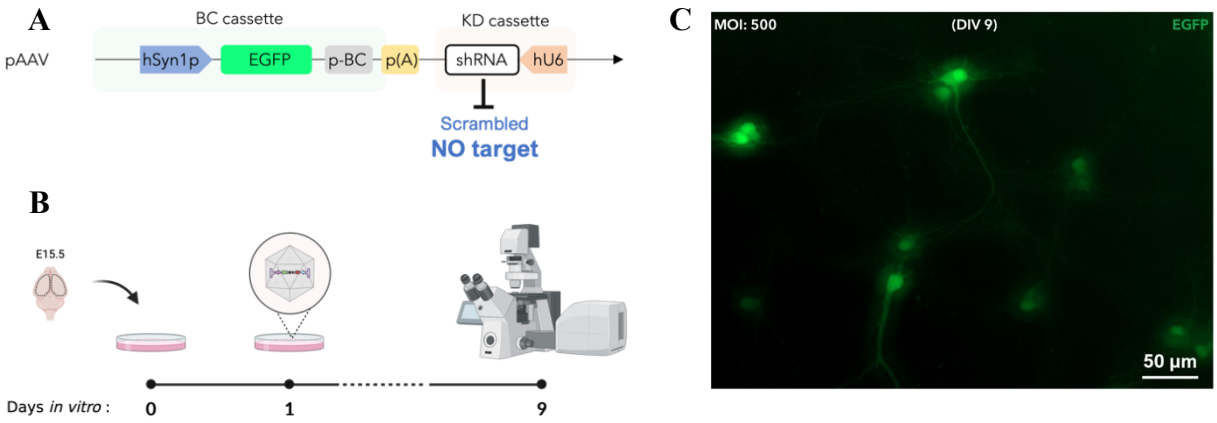

Figure 15 Functional testing of shRNA-Perturb-seq vector in primary mouse cortical neurons.

(A) Diagram depicting the shRNA-Perturb-seq assay plasmid structure, highlighting the Barcode (BC) and Knockdown (KD) cassette along with their components. KD cassette comprises of a constitutive Pol III promotor, *hU6* driving the expression of shRNA targeting specific transcript. BC cassette comprises of a human *Synapsin* 1 promoter driving the expression of EGFP-shRNA-BC transcript. Entire construct is flanked by AAV ITRs.

(B) Schematic representation of the experiment. Primary cortical neurons were harvested from E15.5 wild-type embryos and plated onto culture dishes. Cultures were transduced to all cultures on *DIV1* with an MOI of 500 and live cell was performed on *DIV9*.

(C) Representative live cell image of cultures at *DIV9*.

4.1.2.2 Evaluation of transduction efficiency of AAV in neuronal cultures

To determine the functional genomic copy (GC) titer of adeno-associated virus (AAV) and assess infection efficiency in neuronal cultures. Serial dilutions of AAV, ranging from 2000 to 63 (62.5) with a dilution factor of 1:2, were transduced into different neuron cultures on *DIV1*. The number of EGFP positive cells and fluorescence intensity were evaluated on *DIV14*. Remarkably, robust *EGFP* expression was observed even with a reduced MOI of 63, indicating robust transduction efficiency. Additionally, increased fluorescence intensity was noted with higher MOIs, suggesting multiple infections.

Figure 16 Quantification of functional genomics copies

(A) Schematic representation of the experiment. Primary cortical neurons were harvested from E15.5 wild-type embryos and cultured in dishes. On *DIV1*, the cultures were transduced starting with an MOI of 2000 and subjected to serial dilutions up to 63 with a 1:2 dilution factor.

(B) Representative live cell image of cultures at *DIV14*. Increase in GFP localization is correlating with increasing MOI value, suggesting multiple infection.

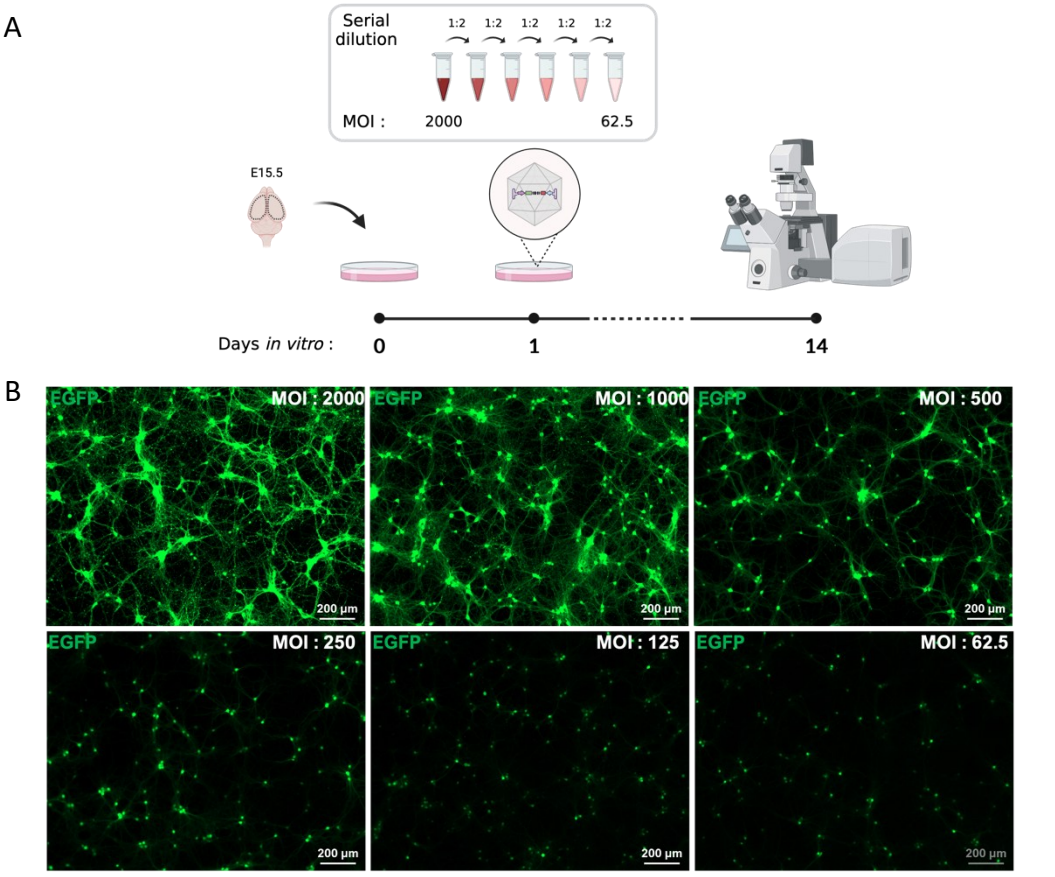

4.1.2.3 In-suspension transduction and cell pooling assay

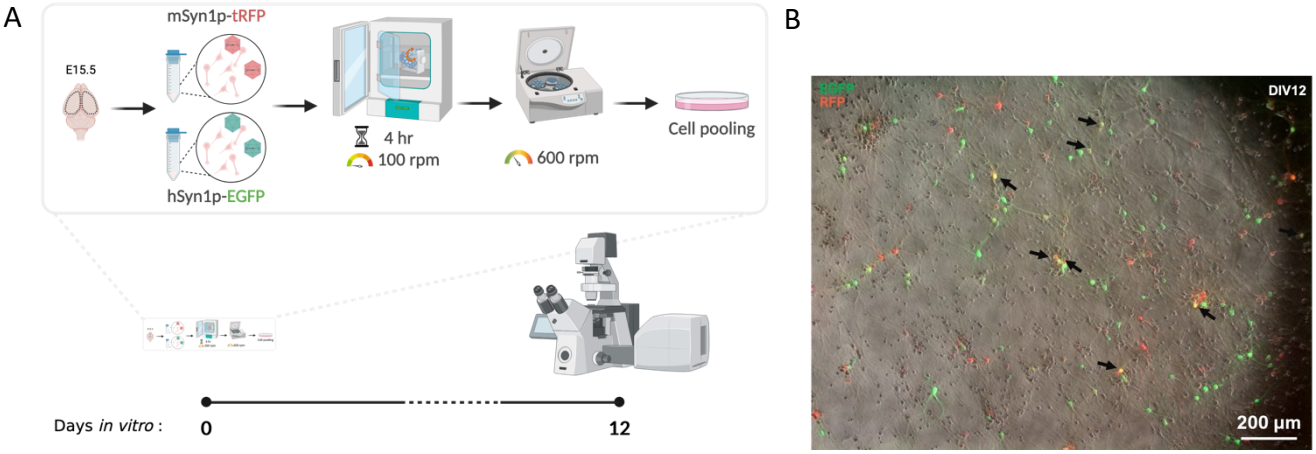

Figure 17 In-suspension transduction and optimization of cell pooling

(A) Schematic representation of the experiment. Primary cortical neurons were harvested from E15.5 wild-type embryos and "in-suspension transduction protocol" was followed as discussed in Section 3.3.4. On *DIV1*, the cultures were split onto two groups. Group 1 was transduced by AAV-mSyn1p-tRFP and Group2 was transduced by AAV-hSyn1p-EGFP with a MOI of 1000. Cells were transduced for 4 hr, followed by washing and pooling in ratio of 1:1.

(B) Live cell fluorescence imaging of cells at days in vitro 12 (DIV12). Cells exhibiting colocalization for GFP and RFP were indicated with arrows.

To mitigate the potential confounding effects of cross-transduction in AAV pooled cell cultures, in-suspension transduction and cell pooling assay was developed. In this assay, cells were transduced separately with either pAAV-hSyn1p-EGFP or pAAV-mSyn1p-tRFP. Following transduction, cultures along with AAV mixtures were incubated on a shaking platform inside the incubator for 4 hours. Subsequently, cells were pelleted and resuspended in fresh medium, followed by trituration. Equi-numbered cells were pooled and plated on culture plates. Live cell imaging conducted on *DIV12* for GFP and RFP revealed that colocalized cells constituted less than 10% of the culture, indicating successful reduction of residual cross-transduction.

4.1.3 shRNA-Perturb-seq experiment

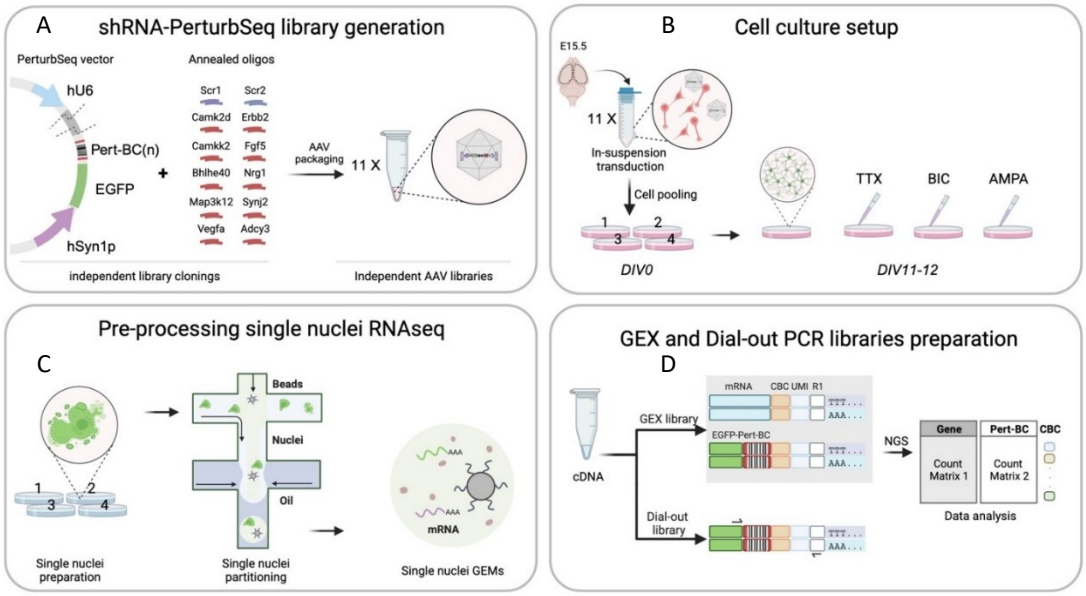

Figure 18 shRNA-Perturb-seq experiment.

(A) Schematics of shRNA-Perturb-seq libraries cloning. Individual shRNA oligos were annealed. Perturb-seq vector was linearized and annealed oligos were ligated and cloned separately. 4-5 clones from individual cloning were pooled equi-molarly and AAV was prepared.

(B) Schematic of cell culture. Primary cortical neurons were harvested and separated into 11 tubes and in-suspension transduction and cell-pooling protocol discussed in section 4.1.2.3 was performed and cells were pooled equi-number. Cultures were treated either with Vehicle or TTX cocktail (12 hr) or BIC cocktail (4 hr) or AMPA (4 hr) on *DIV* 11-12.

(C) Overview of the pre-processing steps involved in single-nuclei RNAseq using the 10X Genomics kit. Briefly, upon adequate treatment time single nuclei were prepared as discussed in section 3.1.5. Subsequently,10X Genomics protocol was followed for partitioning and GEMs preparation.

(D) Diagram depicting the generation of gene expression and Dial-out PCR libraries from cDNA. Each library was pooled and sequenced. Count matrix was prepared for gene expression and Pert-BC for downstream analysis steps.

4.1.3.1 Demultiplexing and mapping of Next-Generation Sequencing (NGS) reads

Cell culture and data analysis has been described in Section 3.1.6. Transcriptomics data yielded approximately 300 million reads, while Dial-out PCR

generated approximately 13 million reads. For transcriptomics data, approximately 95% of the reads were successfully mapped to the *Mus musculus* genome for each sample. The remaining ~5% of unmapped reads were aligned to a custom *EGFP-Pert-BC* reference, designed to capture perturbation-specific sequences. Of the unmapped transcriptomics reads aligned to the *EGFP-Pert-BC* reference, approximately 45% were successfully mapped. These mapped reads constitute the basis for generating the Perturbation Count Matrix, referred to as the "10X method."

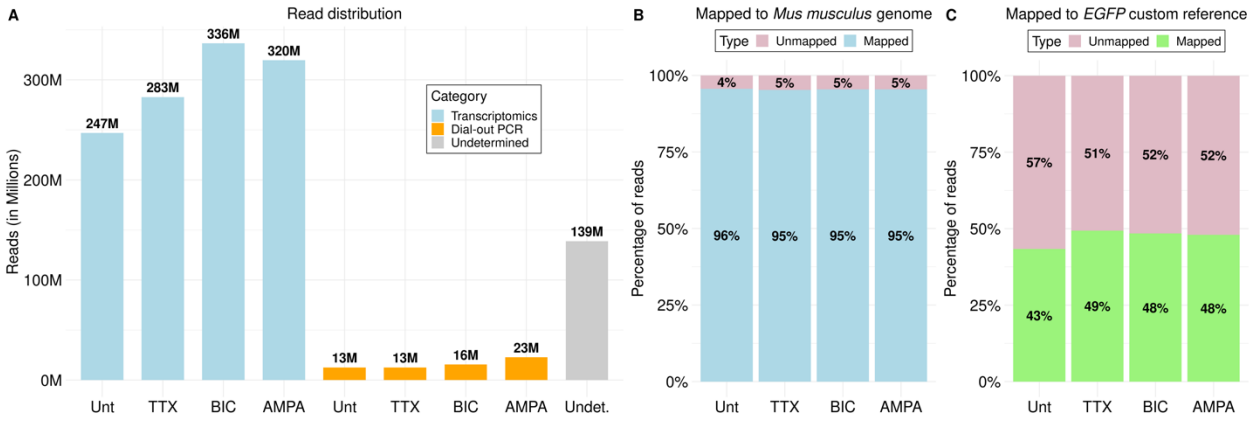

Figure 19 NGS read analysis

(A) Read distribution of libraries after demultiplexing. For gene expression library (Transcriptomics) reads have on average 300 million reads and dial-out PCR libraires (Pert-BC) have on average 15 million reads.

(B) Approximately 95 % transcriptomics reads mapped to *Mus musculus* genome.

(C) 5% of unmapped transcriptomics reads was mapped to custom *EGFP-Pert-BC* reference. Approximately 47% of the reads mapped to custom *EGFP-Pert-BC* reference.

4.1.3.2 Methods for identifying cellular perturbations.

Perturbation of cell identity was accomplished through two distinct methods: the "10X method" directly from transcriptomic reads Section 3.1.6.2 and the "Dial-out method" employing enrichment dial-out PCR followed by independent sequencing. The processing of Dial-out reads was detailed in Sections 3.1.6.4.

Following the respective methods, perturbations were assigned to individual cells. Notably, both methods contributed to assigning perturbations for approximately 25% of cells. Approximately 5% of cells were exclusively attributed to the 10X method and approximately 17% of cells were solely assigned perturbations through the Dial-out method. Approximately 15% of cells exhibited multiple perturbations and

approximately 7% of cells displayed conflicts in perturbation identity between the two methods. Finally, approximately 30% of cells had unidentifiable perturbation identities.

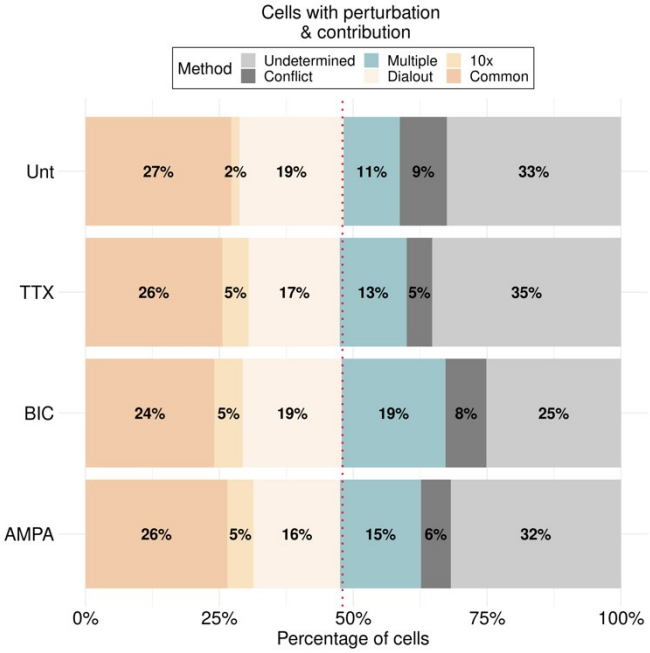

Figure 20 Relative distribution of perturbation identity contributed by two methods

Perturbation identity (Pert-BC), a cell was carrying identified using two methods. Contribution by either method is shown using stacked barplot. Approximately 25% of cell barcode (CBC) to Pert-BC were identified by either method. Additional 5% and 17% CBC to Pert-BC was identified by 10X and Dial-out method, respectively. Approximately 15% CBC has identified to have multiple Pert-BC and 7% CBC have conflicted Pert-BC identity from both methods. Approximately 30% CBC's no Pert-BC has been identified.

4.1.3.3 Standard pre-processing of snRNA-seq data

Cells were evaluated based on standard quality metrics. Samples exhibited less than 2% mitochondrial genes and 15 % of ribosomal genes, which also adheres to the recommended thresholds by 10X Genomics. The median number of genes detected per cell was approximately 550 across all samples. Cells were filtered to retain those

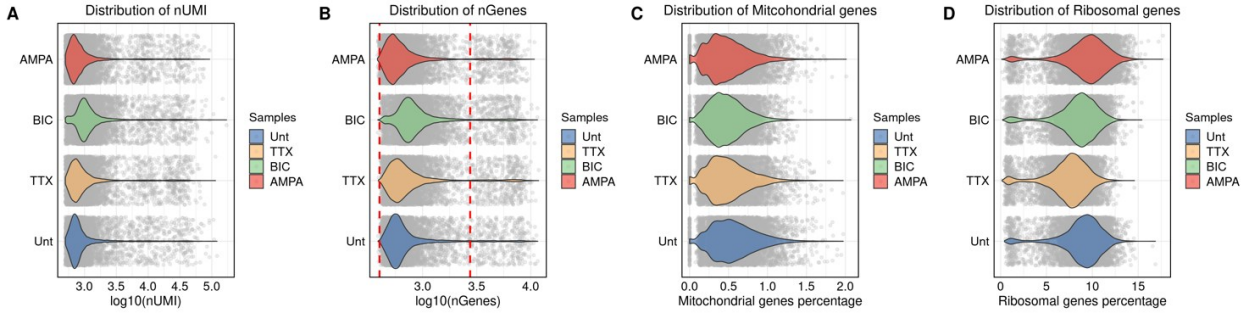

Figure 21 Visualizing QC metrics of snRNA-seq data

(A-D) Violin plots showing distribution of different features.

(A) Distribution of number of transcripts (nUMI) in log10 scale. Median nUMI for all samples is around 2000.

(B) Distribution of number of genes (nGene) in log10 scale. Median nGene for all samples is around 550. Red dotted lines signify filter criteria.

(C-D) Distribution of percentage mitochondrial and ribosomal genes. Samples have less than 2% mitochondrial genes and less than 15% ribosomal genes.

with a gene count falling within the range of 450 to 1500 genes. This criterion helps to exclude cells with exceptionally low or high gene counts, which may introduce noise or bias into subsequent analyses.

4.1.3.4 Exploring cellular heterogeneity through transcriptomic analysis

Canonical marker genes were utilized to classify clusters into their respective cell types. This classification included GABAergic neurons, Astrocytes, Oligodendrocytes, and Unclassified cells, which demonstrated distinct clustering patterns. Notably, Sst+ neurons clustered within the Glutamatergic neuron population, as depicted in Figure 3.7.A. Furthermore, Sst+ neurons exhibited expression of canonical markers associated with both GABAergic and Glutamatergic neurons, as illustrated in Figure 22 C,D.

Despite the distinct clustering patterns observed, the Glutamatergic neuron cluster did not exhibit robust expression of canonical marker genes, as depicted in Figure 22 C. To gather additional evidence, the *FindMarker()* function of Seurat was employed to conduct differential expression analysis between clusters. The expression levels of the top 20 genes were examined across clusters, revealing unique marker genes for each cluster. However, for the Glutamatergic neuron cluster, the top 20 genes predominantly comprised pan-neuronal markers, as shown in Figure 22 E.

Given the focus on perturbed cells in this study, the distribution of perturbated cells per cell type was explored. Across samples and perturbations, it was observed that more than 85% of the cells belonged to the Glutamatergic neuron cluster, as depicted in Figure 22 B. Consequently, for further analysis, only the Glutamatergic neuron cluster was considered.

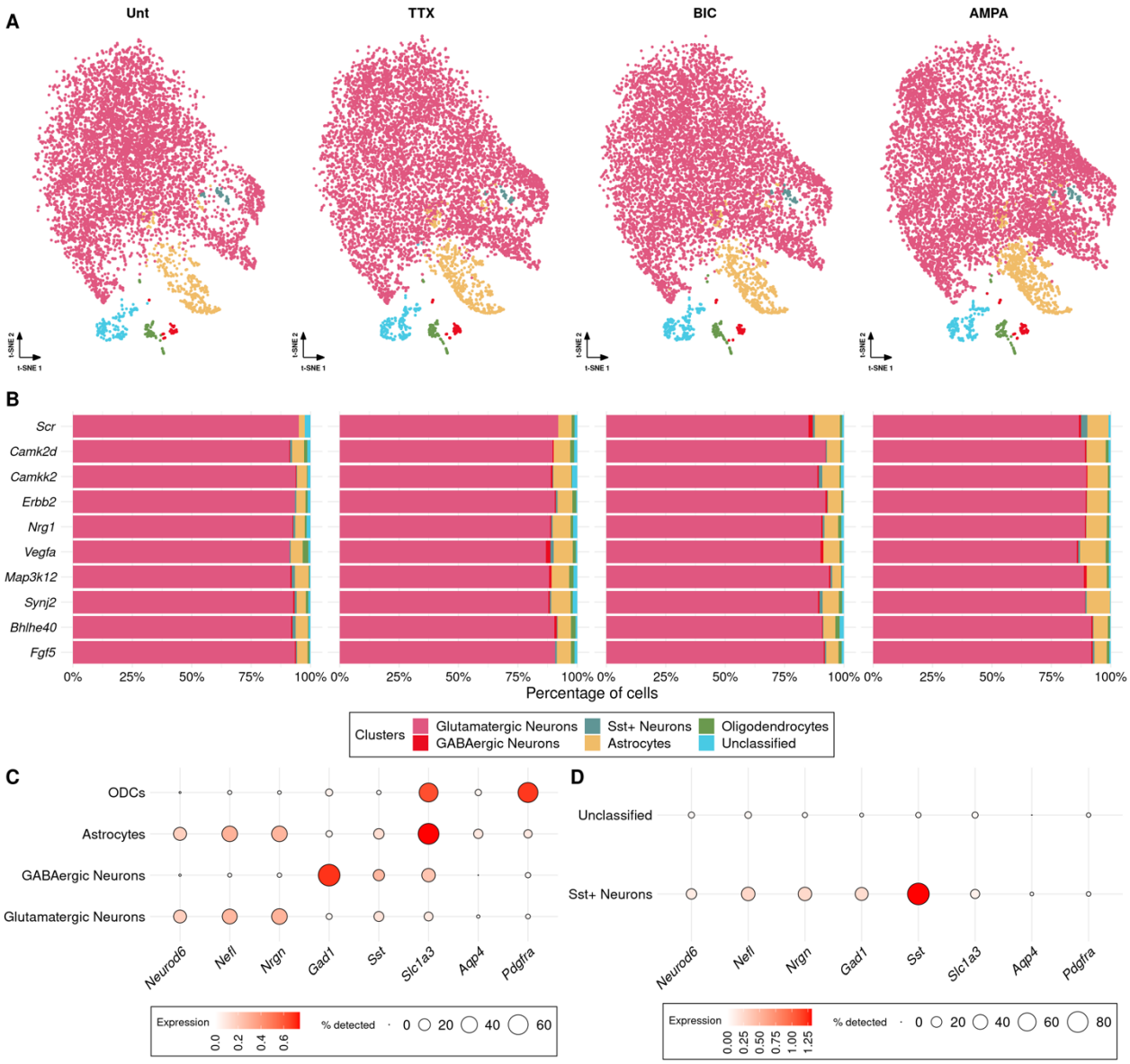
A
Unt
TTX
BIC
AMPA
t-SNE 2
t-SNE 1
B
Scr
Camk2d
Camkk2
Erbb2
Nrg1
Vegfa
Map3k12
Synj2
Bhlhe40
Fgf5
0%
25%
50%
75%
100%
Percentage of cells
Clusters
Glutamatergic Neurons
GABAergic Neurons
Sst+ Neurons
Astrocytes
Oligodendrocytes
Unclassified
C
ODCs
Astrocytes
GABAergic Neurons
Glutamatergic Neurons
Neurod6
Nefl
Nrgn
Gad1
Sst
Slc1a3
Aqp4
Pdgfra
Expression
0.0
0.2
0.4
0.6
% detected
0
20
40
60
D
Unclassified
Sst+ Neurons
Neurod6
Nefl
Nrgn
Gad1
Sst
Slc1a3
Aqp4
Pdgfra
Expression
0.00
0.25
0.50
0.75
1.00
1.25
% detected
0
20
40
60
80

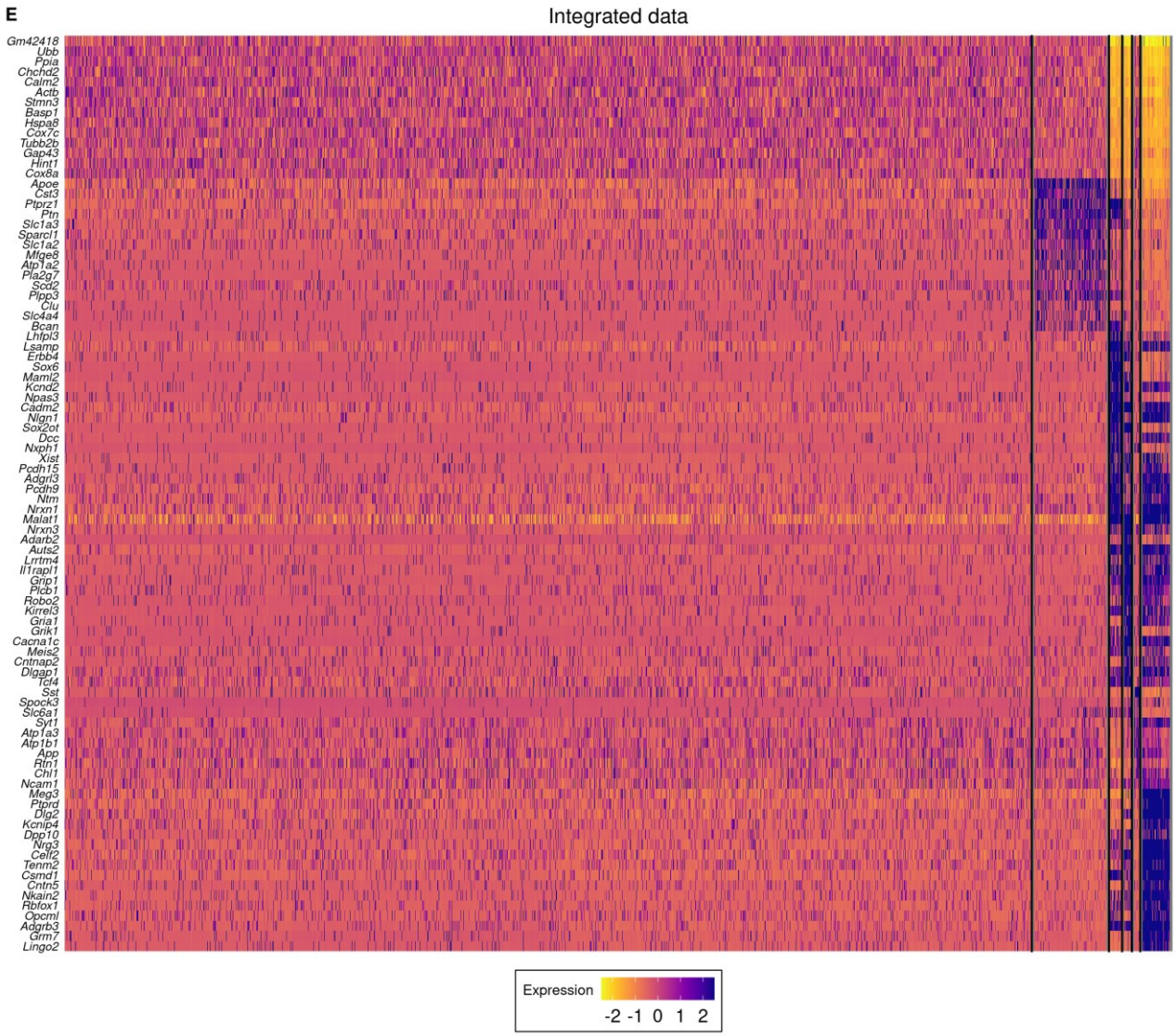

Figure 22 shRNA-Perturb-seq identifies neuronal cell types.

(A) tSNE plots showing clustering of different neuronal cells in the assay. 6 clusters were identified based on marker gene expression.

(B) Distribution of perturbed cells per cell type cluster. Approximately 95% of the cells carrying Pert-BC belongs to Glutamatergic cluster.

(C, D) Dotplot showing the expression levels of canonical marker genes for each cell-type cluster.

(E) Heatmap showing the expression levels of top20 marker genes for each cell-type cluster. Black lines showing the demarcation of distinct marker per cell-type cluster.

4.1.3.5 Differential gene expression analysis identifies treatment specific transcriptional responses

Differential gene expression analysis was conducted to identify transcriptional response for each treatment group (TTX, BIC, and AMPA) and the control group (Unt). A substantial number of genes exhibited differential expression patterns across the treatment groups, indicating distinct transcriptional responses to each treatment condition (Figure 23 A, B, C). External RNA-seq dataset (Schaukowitch et al., 2017) containing transcripts differentially expressed in response to the same treatments was overlaid onto the snRNA-seq dataset. The comparison revealed a consistent trend in the direction of gene expression changes between the snRNA-seq and external RNA-

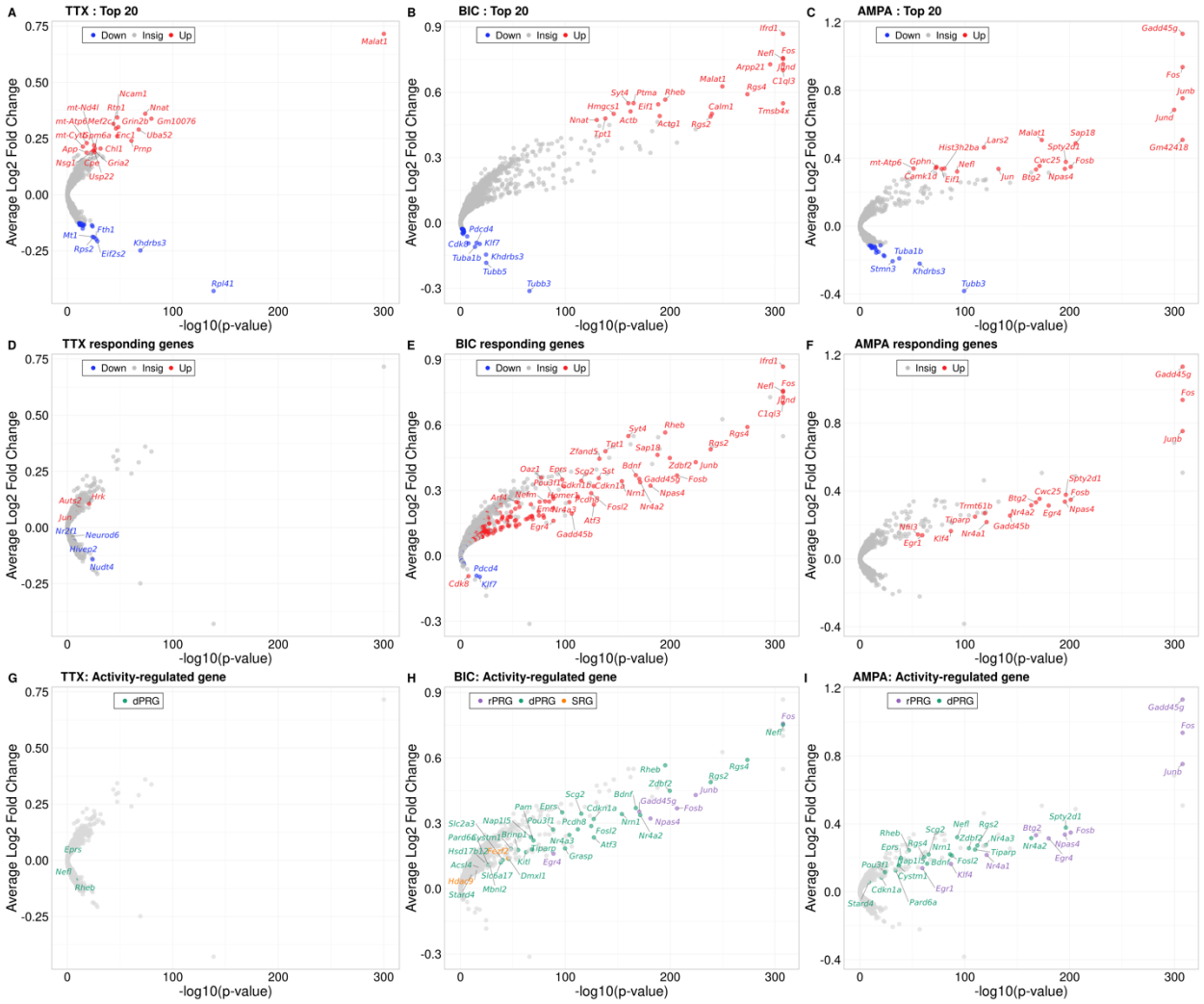

Figure 23 Differential gene expression analysis identifies treatment specific transcripts in Glutamatergic cluster.

(A, B, C) Volcano plots highlight the differential expression patterns of genes in response to TTX, BIC, and AMPA treatments compared to the control group, with the top 20 genes with the highest average log2 fold change.

(D, E, F) Differential expressed transcripts from external RNA-Seq from respective treatment were overlaid.

(G, H, I) Activity regulated genes (ARGs) from KCl/Bicuculine, reported by Tyssowski et al., 2018 were overlaid to each treatment group. rPRG or dPRG: rapid or delayed Primary Response Gene; SRG: Secondary response gene.

seq datasets (Figure 22 D, E, F). Despite the consistency in trends, the average log2(fold change) values were observed to be relatively low, suggesting potential limitations of single-nuclei RNA-seq in capturing larger fold changes in gene expression. Subsequently, we delved into three distinct kinetically temporal waves of gene induction, as discussed in (Tyssowski et al., 2018). Specifically, we focused on elucidating the gene expression dynamics following BIC and AMPA treatments. We observed two primary types of response genes: delayed and rapid. Delayed primary response genes exhibited a slower onset of induction, suggesting a gradual cellular response to the treatment. In contrast, rapid primary response genes displayed an immediate and robust upregulation in expression levels shortly after treatment initiation. The identification of delayed and rapid primary response genes aligns closely with the experimental paradigm employed in this study. Moreover, BIC and AMPA treatments have distinct kinetic profiles, advocating for specific cellular responses characterized by different treatments.

4.1.3.6 Pseudo-bulk differential expression analysis

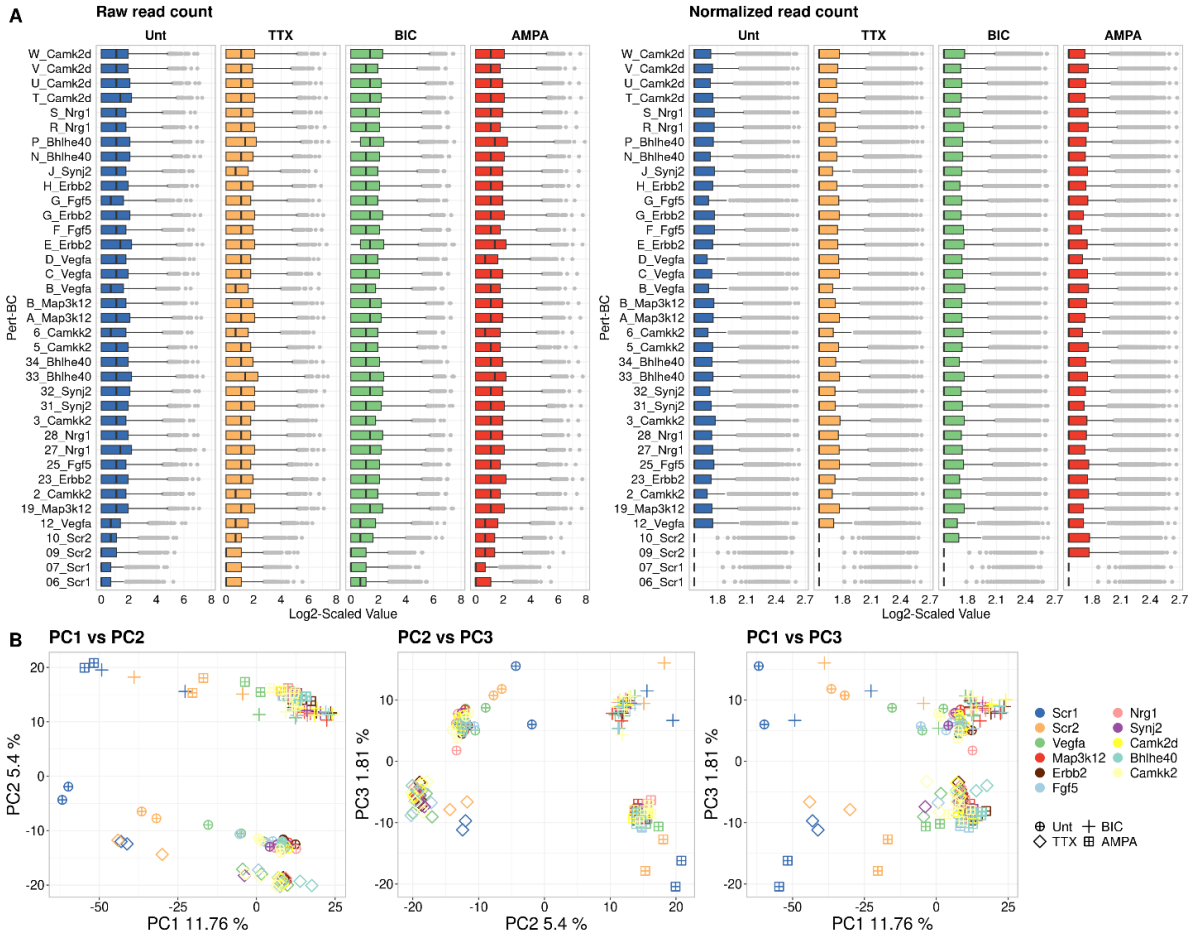

Figure 24 Quality control for pseudo-bulk differential expression analysis.

(A) Box plot depicting the distribution of read counts for individual Pert-BC combinations before and after normalization.

(B) Variance explained by the principal components (PC1, PC2, and PC3) in a Principal Components Analysis (PCA) conducted on the normalized read counts.

Raw read counts were subjected to normalization and log-transformation to address biases stemming from variations in sequencing depth and library composition across different Pert-BC conditions, which were further stratified by treatment groups. This preprocessing step aimed to ensure comparability and robustness in downstream analyses. Principal Component Analysis (PCA) was then conducted to evaluate the variance explained by each principal component, focusing on PC1, PC2, and PC3. The percentage of variance explained by each PC offers valuable insights into the relative significance of various sources of variability within the data, including perturbation effects, treatment effects, or their combined influence. Treatment effects were prominent in the first three PCs, with BIC and AMPA treatment groups showing distinct separation from Unt and TTX groups (Figure 24 B).

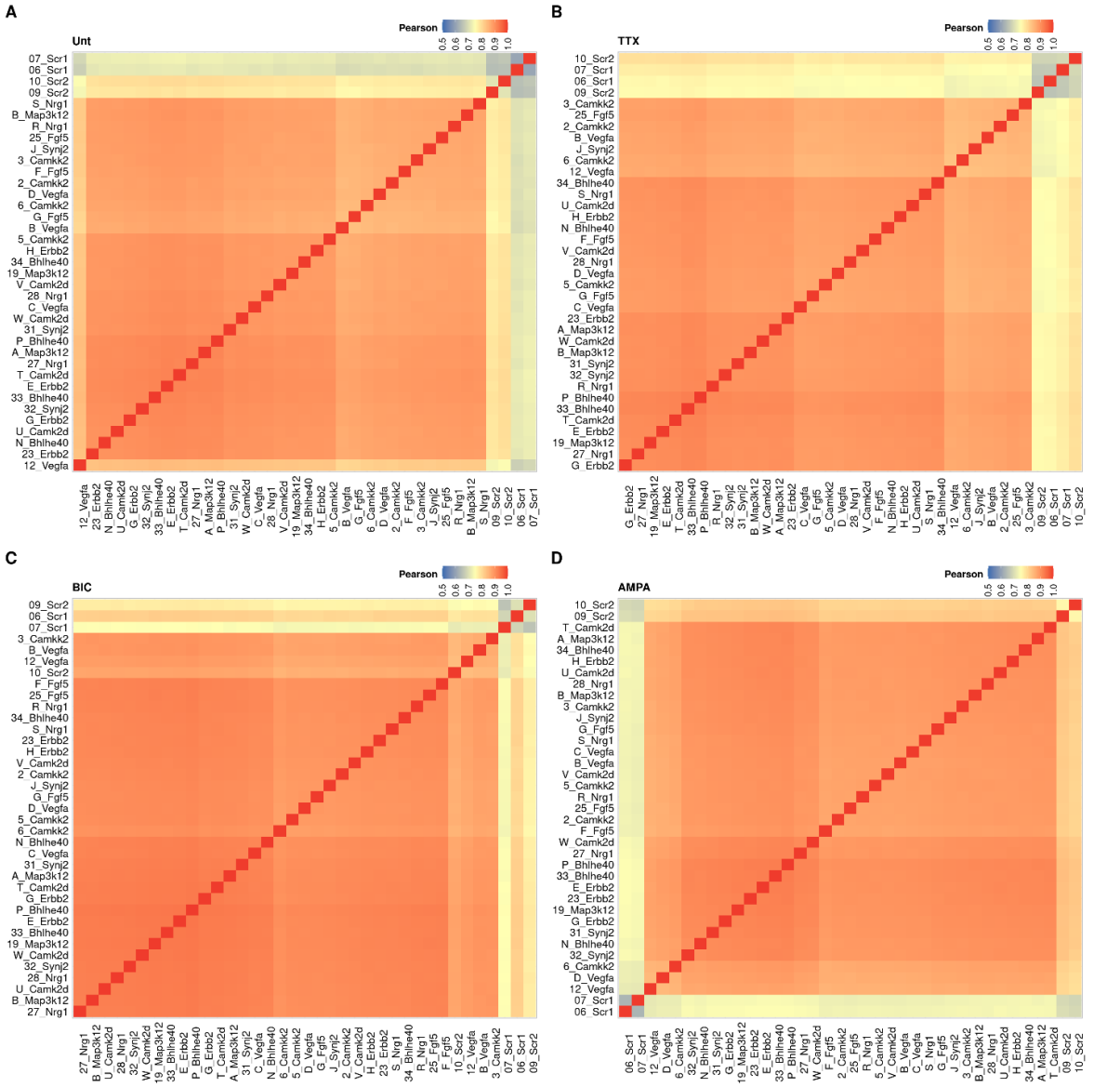

Figure 25 Correlation heatmap per treatment condition.

(A-D) Correlation heatmap represents the Pearson correlation coefficients between gene expression profiles under different treatment conditions.

However, it is noteworthy that despite normalization efforts, low read counts observed in *Scr* samples persisted and were not fully mitigated (Figure 25). This observation underscores the inherent challenges associated with low-count data in single-nuclei RNA sequencing (snRNA-seq) experiments. It emphasizes the necessity for cautious consideration during downstream data analysis, particularly in interpreting and generalizing findings derived from such samples.

4.1.3.7 Differential gene expression analysis identifies perturbation and perturbation + treatment specific transcriptional responses

Differential expression analysis was conducted to identify transcriptional responses across different perturbation and treatment groups. For perturbation only effect, every perturbation from a treatment group is contrasted against respective *"Scr"* control from the same treatment group (Figure 26). Whereas for combined perturbation and treatment effect, every perturbation and treatment group are contrasted against "*Untreated Scr*" control (Figure 27). Volcano plots were generated to visualize the distribution of differentially expressed genes (DEGs) based on their log2 fold change and statistical significance. Each volcano plot represents a specific perturbation, with treatment groups displayed row-wise. Genes meeting the criteria of an absolute average log2 fold change greater than 0.58 (approximately 1.5-fold change) and a p-value less than 0.05 were considered DEGs. These genes were color-coded based on their fold change values, with red indicating upregulation and blue indicating downregulation.

To assess the overlap and uniqueness of differentially expressed genes (DEGs) across perturbation and treatment groups, upset plots were utilized. Upset plots provide a visual representation of set intersections, allowing for the identification of common and distinct elements between multiple sets. Common DEGs refer to genes that are differentially expressed across multiple perturbations and treatment groups. Distinct DEGs are unique to specific perturbations or treatment groups, suggesting context-specific regulatory mechanisms or functional pathways (Figure 28, 29).

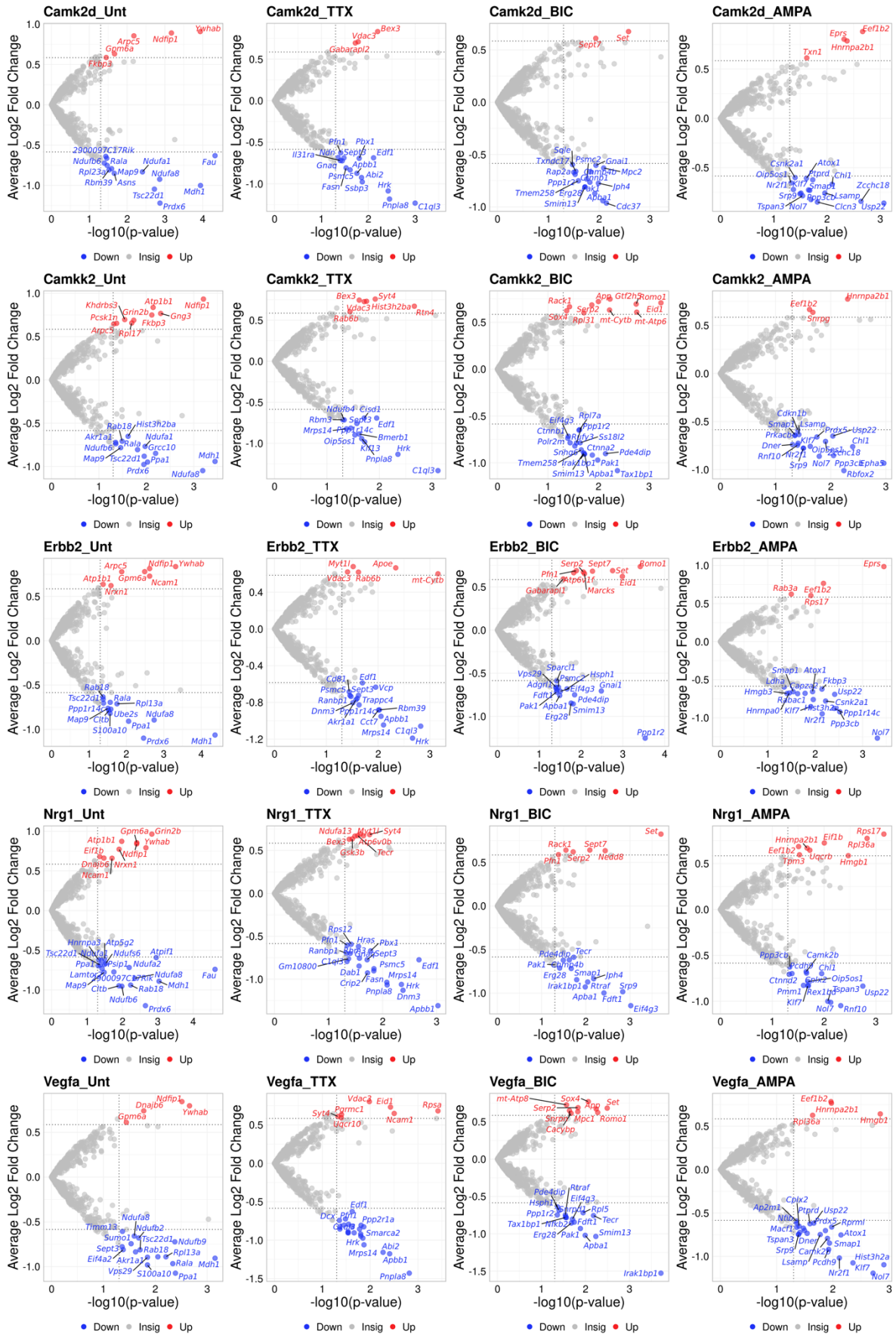
Camk2d_Unt
Camk2d_TTX
Camk2d_BIC
Camk2d_AMPA
Camkk2_Unt
Camkk2_TTX
Camkk2_BIC
Camkk2_AMPA
Erbb2_Unt
Erbb2_TTX
Erbb2_BIC
Erbb2_AMPA
Nrg1_Unt
Nrg1_TTX
Nrg1_BIC
Nrg1_AMPA
Vegfa_Unt
Vegfa_TTX
Vegfa_BIC
Vegfa_AMPA
Average Log2 Fold Change
-log10(p-value)
Down
Insig
Up

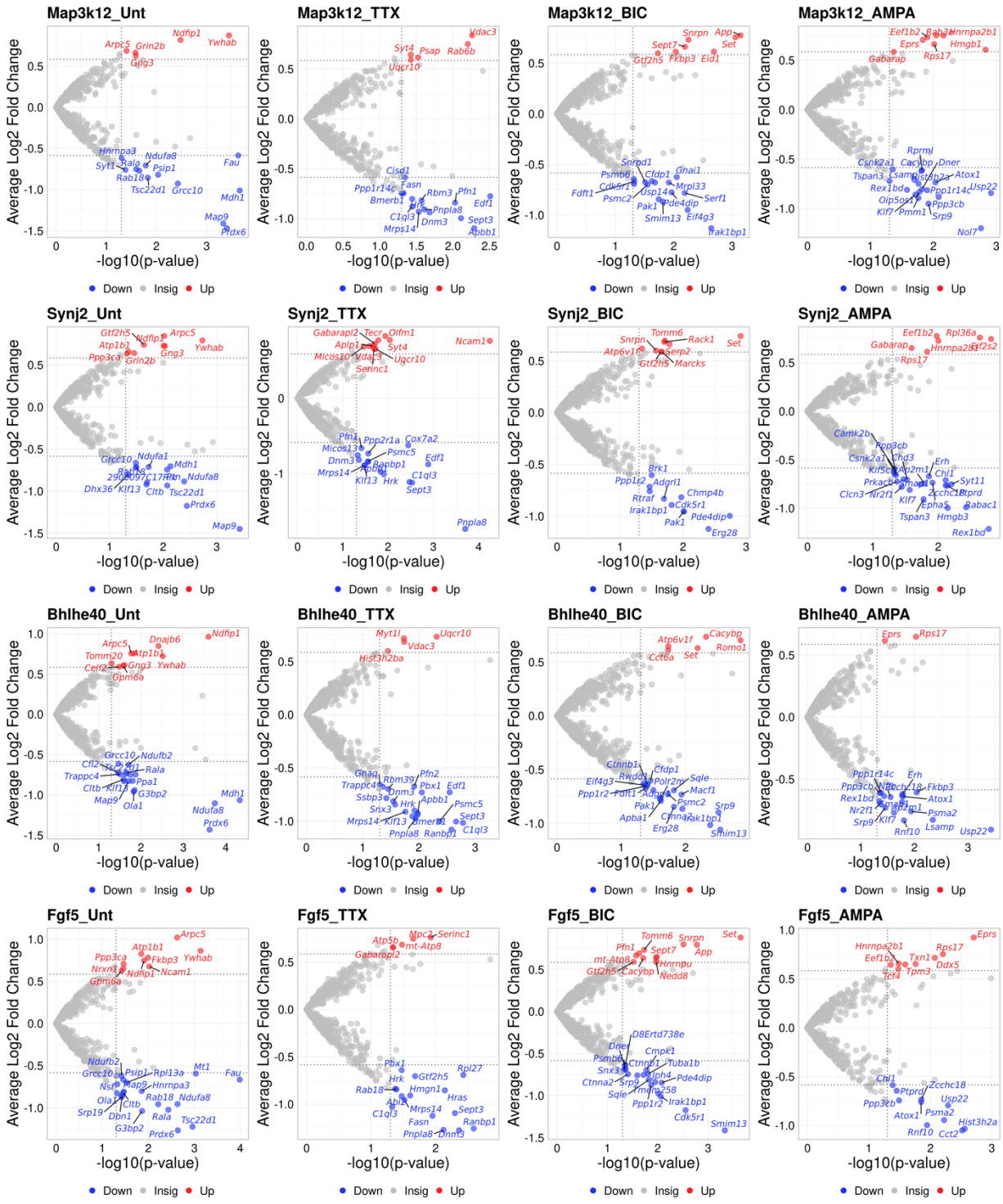

Figure 26 Differential expression of genes from perturbation only effect across various perturbations and treatment groups

Volcano plots illustrating the differential expression of genes (DEGs) from perturbation only effect across various perturbations and treatment groups. Each row corresponds to a specific perturbation, while each column represents a treatment group. DEGs are identified based on an absolute average log2 fold change greater than 0.58 (approximately 1.5-fold change) and a p-value less than 0.05. Genes with higher expression in treated samples compared to controls are denoted in red, while those with lower expression are denoted in blue. Thresholds for fold change and p-value significance are delineated by grey dotted lines.

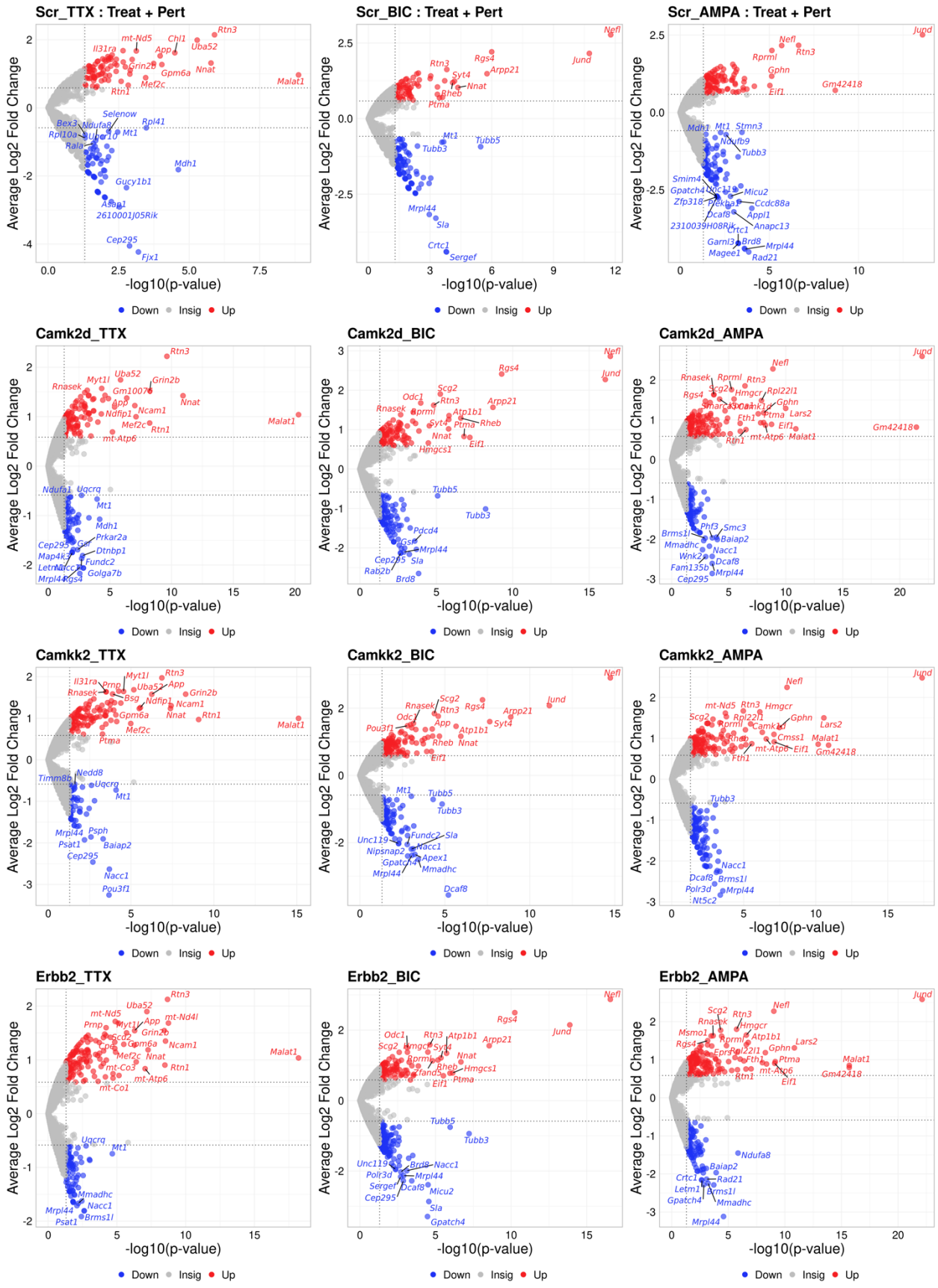
Scr_TTX : Treat + Pert
Scr_BIC : Treat + Pert
Scr_AMPA : Treat + Pert
Camk2d_TTX
Camk2d_BIC
Camk2d_AMPA
Camkk2_TTX
Camkk2_BIC
Camkk2_AMPA
Erbb2_TTX
Erbb2_BIC
Erbb2_AMPA
Average Log2 Fold Change
-log10(p-value)
Down
Insig
Up

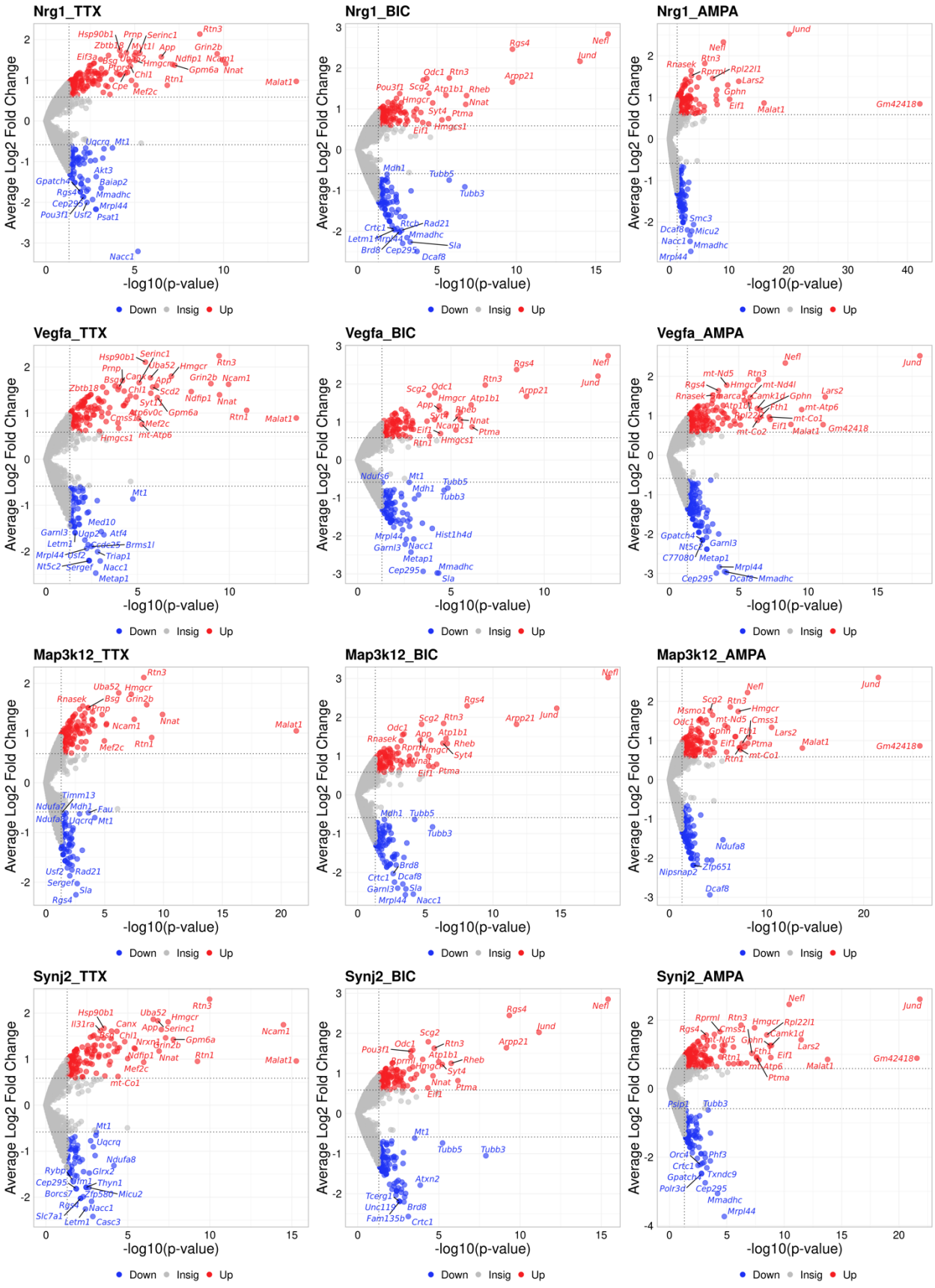
Nrg1_TTX
Nrg1_BIC
Nrg1_AMPA
Vegfa_TTX
Vegfa_BIC
Vegfa_AMPA
Map3k12_TTX
Map3k12_BIC
Map3k12_AMPA
Synj2_TTX
Synj2_BIC
Synj2_AMPA
Average Log2 Fold Change
-log10(p-value)
Down
Insig
Up

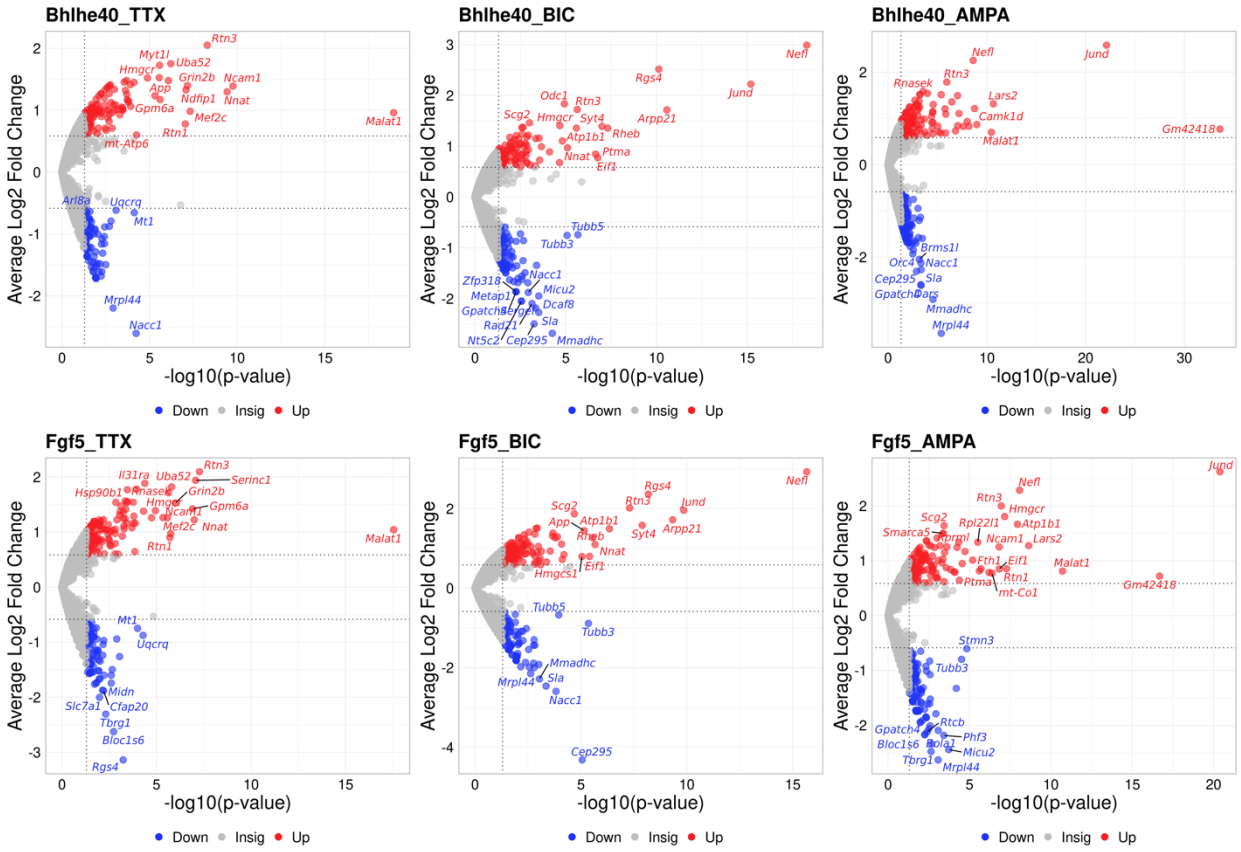

Figure 27 Differential expression of genes from treatment and perturbation combined effect across various perturbations and treatment groups

Volcano plots illustrating the differential expression of genes (DEGs) from treatment and perturbation combined effect across various perturbations and treatment groups. Each row corresponds to a specific perturbation, while each column represents a treatment group. DEGs are identified based on an absolute average log2 fold change greater than 0.58 (approximately 1.5-fold change) and a p-value less than 0.05. Genes with higher expression in treated samples compared to controls are denoted in red, while those with lower expression are denoted in blue. Thresholds for fold change and p-value significance are delineated by grey dotted lines.

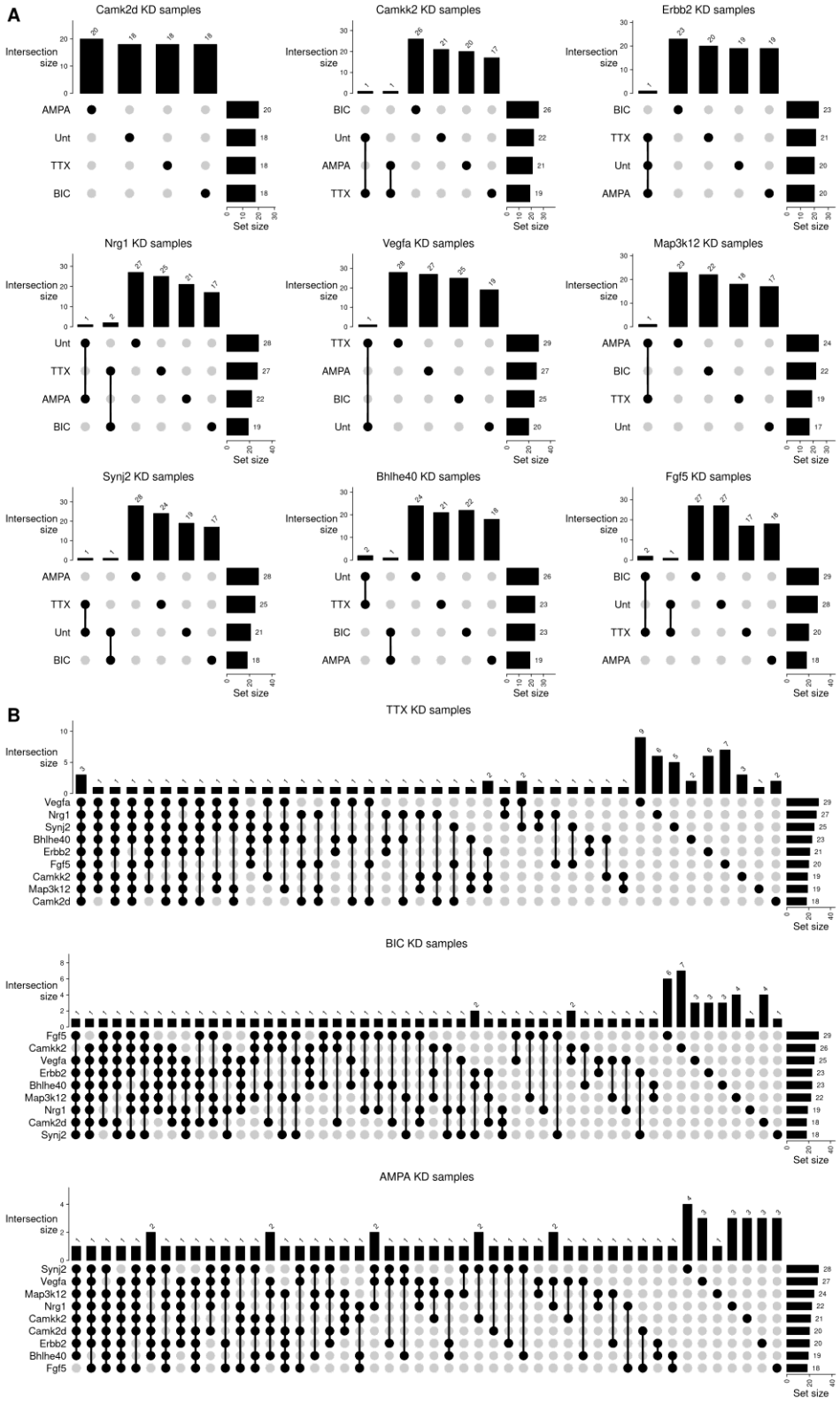

Figure 28 Upset plots comparing DEGs from perturbation only effect between different perturbations and treatment groups.

(A) Overlapping DEGs from perturbation perspective. Common DEGs are few between treatment.

(B) Overlapping DEGs from treatment group perspective. Higher overlap between perturbation withing treatment.

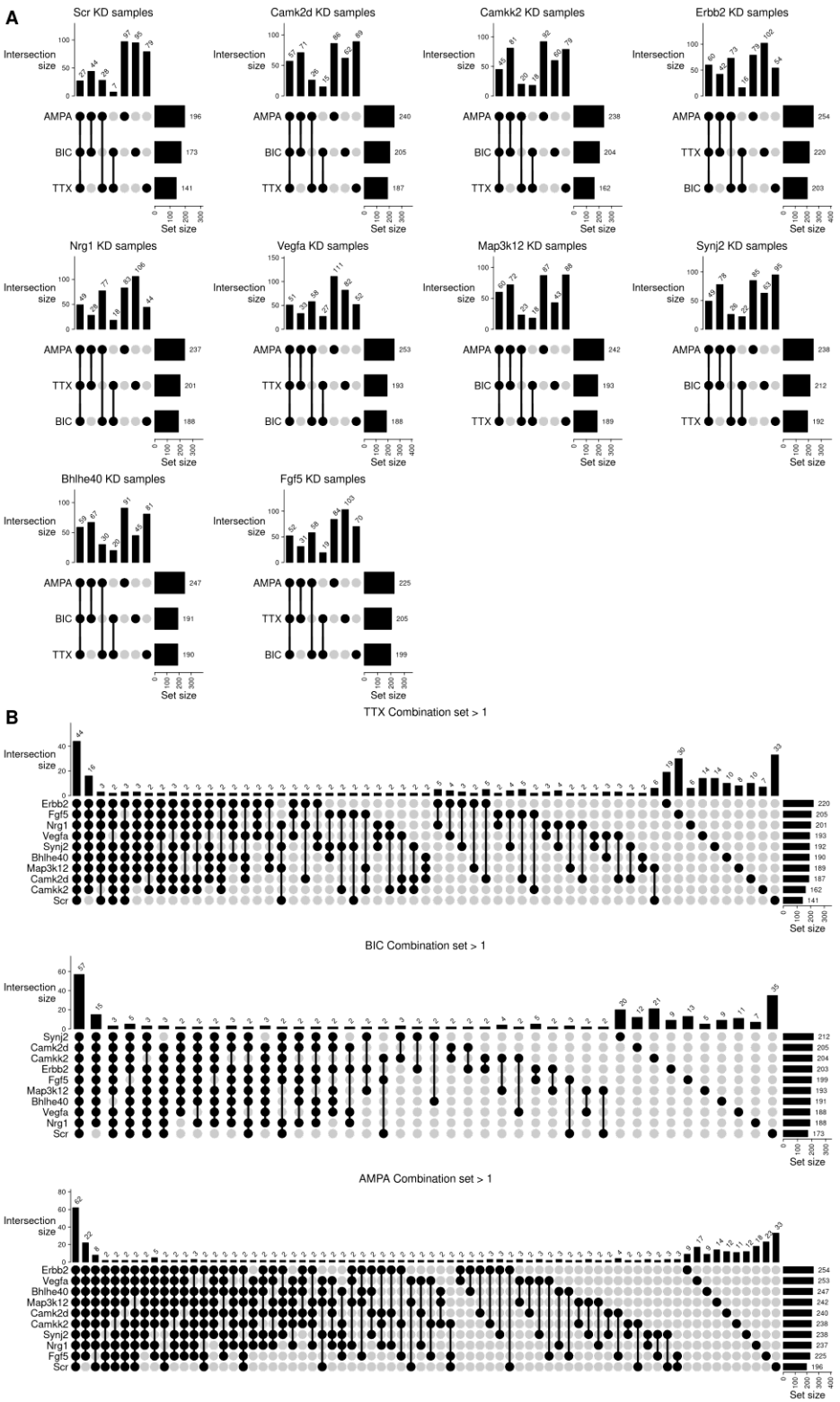

Figure 29 Upset plots comparing DEGs from perturbation and treatment effect between different perturbations and treatment groups.

(A) Overlapping DEGs from perturbation perspective.

(B) Overlapping DEGs from treatment group perspective. Only overlapping genes occurring in more than one group are displayed due to space constraints.

4.1.3.8 Identification of biological pathways altered due to perturbation-only

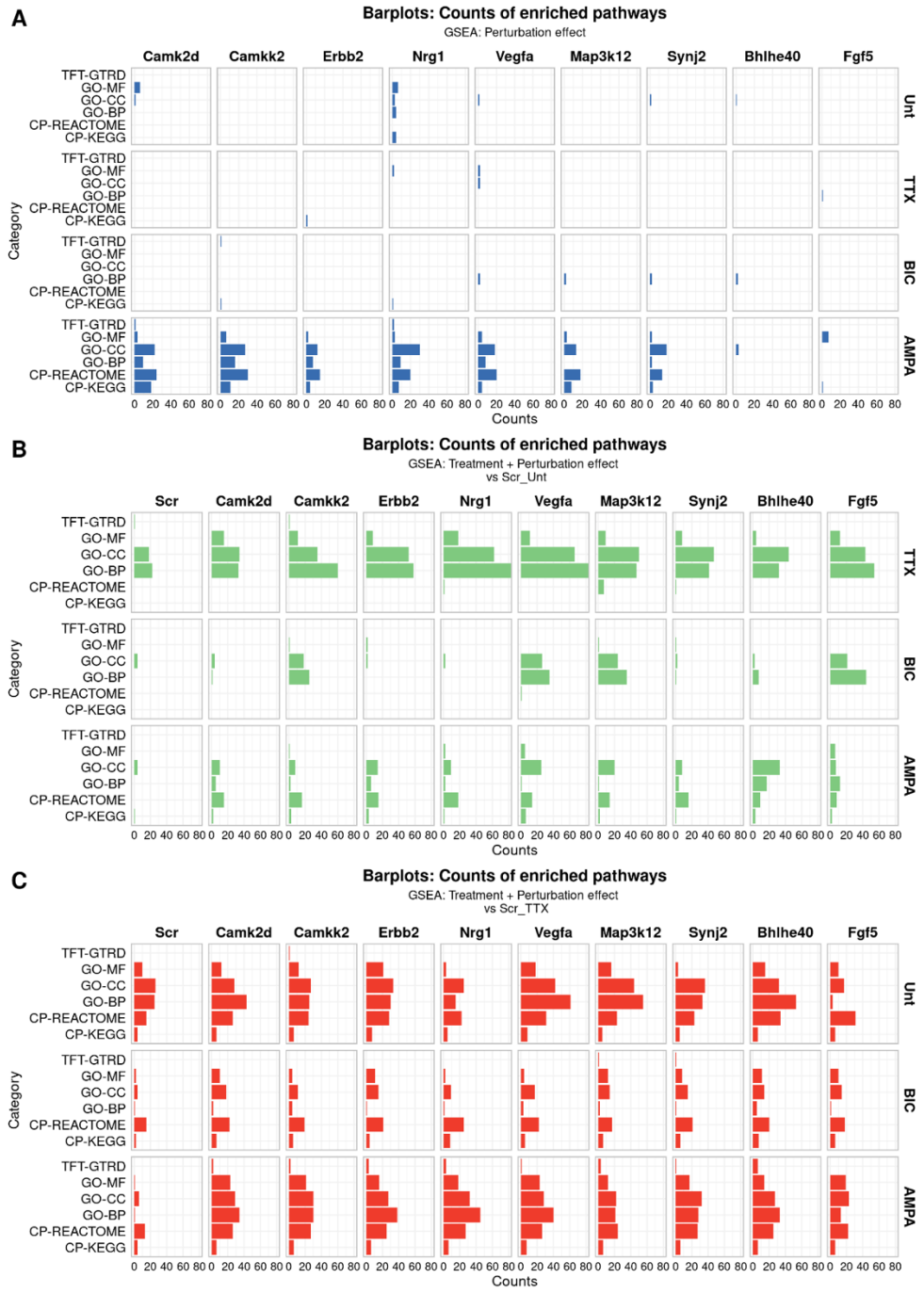

Figure 30 Histogram depicting enriched pathways identified during GSEA

(A) Distribution of enriched pathways based on perturbation effects across different categories.

(B) Distribution of enriched pathways based on treatment and perturbation effects compared to scramble untreated samples, across different categories.

(C) Distribution of enriched pathways based on treatment and perturbation effects compared to scramble samples treated with TTX (Tetrodotoxin), across different categories.

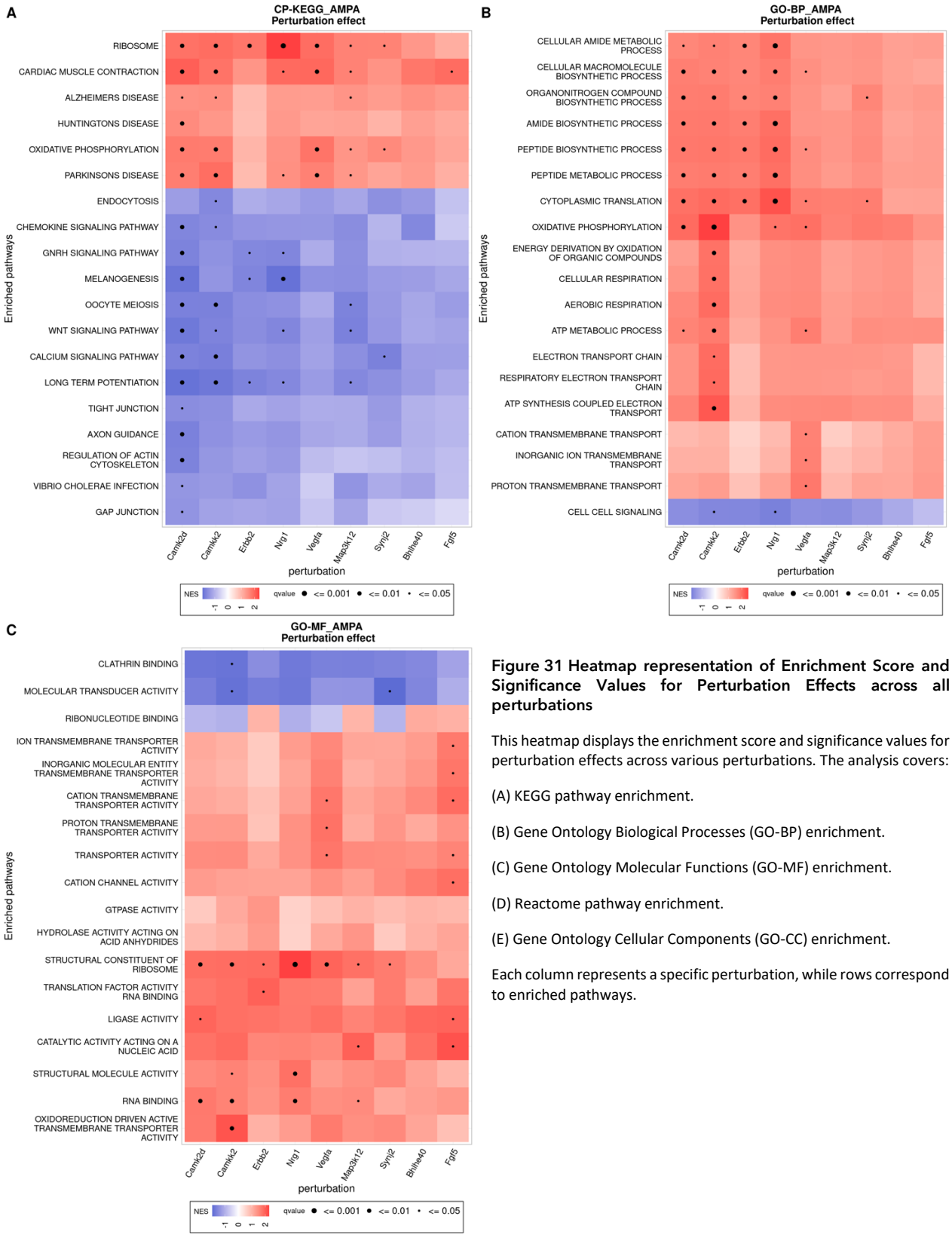

Figure 31 Heatmap representation of Enrichment Score and Significance Values for Perturbation Effects across all perturbations

This heatmap displays the enrichment score and significance values for perturbation effects across various perturbations. The analysis covers:

(A) KEGG pathway enrichment.

(B) Gene Ontology Biological Processes (GO-BP) enrichment.

(C) Gene Ontology Molecular Functions (GO-MF) enrichment.

(D) Reactome pathway enrichment.

(E) Gene Ontology Cellular Components (GO-CC) enrichment.

Each column represents a specific perturbation, while rows correspond to enriched pathways.


D
CP-REACTOME_AMPA
Perturbation effect
SELENOAMINO ACID METABOLISM
TRANSLATION
RRNA PROCESSING
EUKARYOTIC TRANSLATION ELONGATION
INFLUENZA INFECTION
RESPONSE OF EIF2AK4 GCN2 TO AMINO ACID DEFICIENCY
EUKARYOTIC TRANSLATION INITIATION
NONSENSE MEDIATED DECAY NMD
METABOLISM OF RNA
ACTIVATION OF THE MRNA UPON BINDING OF THE CAP BINDING COMPLEX AND EIFS AND SUBSEQUENT BINDING TO 43S
METABOLISM OF AMINO ACIDS AND DERIVATIVES
REGULATION OF EXPRESSION OF SLITS AND ROBOS
SRP DEPENDENT COTRANSLATIONAL PROTEIN TARGETING TO MEMBRANE
CELLULAR RESPONSE TO STARVATION
MITOCHONDRIAL BIOGENESIS
ORGANELLE BIOGENESIS AND MAINTENANCE
CRISTAE FORMATION
FORMATION OF ATP BY CHEMIOSMOTIC COUPLING
PROCESSING OF CAPPED INTRON CONTAINING PRE MRNA
MRNA SPLICING
RESPIRATORY ELECTRON TRANSPORT ATP SYNTHESIS BY CHEMIOSMOTIC COUPLING AND HEAT PRODUCTION BY UNCOUPLING PROTEINS
THE CITRIC ACID TCA CYCLE AND RESPIRATORY ELECTRON TRANSPORT
RESPIRATORY ELECTRON TRANSPORT
RESOLUTION OF SISTER CHROMATID COHESION
RHO GTPASES ACTIVATE FORMINS
AGGREPHAGY
CELLULAR RESPONSES TO STIMULI
SIGNALING BY ROBO RECEPTORS
INFECTIOUS DISEASE
NEUROTRANSMITTER RECEPTORS AND POSTSYNAPTIC SIGNAL TRANSMISSION
NEURONAL SYSTEM
SIGNALING BY GPCR
G ALPHA I SIGNALLING EVENTS
OPIOID SIGNALLING
EPH EPHRIN SIGNALING
ACTIVATION OF NMDA RECEPTORS AND POSTSYNAPTIC EVENTS
TRANSMISSION ACROSS CHEMICAL SYNAPSES
HEMOSTASIS
Enriched pathways
Camk2d
Camkk2
Erbb2
Nrg1
Vegfa
Map3k12
Synj2
Bhlhe40
Fgf5
Perturbation
NES
-2 -1 0 1 2
qvalue
<= 0.001
<= 0.01
<= 0.05
E
GO-CC_AMPA
Perturbation effect
NEURON PROJECTION
AXON
CELL BODY
SOMATODENDRITIC COMPARTMENT
POSTSYNAPTIC MEMBRANE
SYNAPTIC MEMBRANE
PLASMA MEMBRANE REGION
APICAL PART OF CELL
INTRINSIC COMPONENT OF PLASMA MEMBRANE
PERIKARYON
GLUTAMATERGIC SYNAPSE
INTRACELLULAR PROTEIN CONTAINING COMPLEX
SPLICEOSOMAL COMPLEX
CONDENSED CHROMOSOME
PROTON TRANSPORTING ATP SYNTHASE COMPLEX
RIBOSOME
RIBOSOMAL SUBUNIT
CYTOSOLIC RIBOSOME
SMALL RIBOSOMAL SUBUNIT
CYTOSOLIC SMALL RIBOSOMAL SUBUNIT
RIBONUCLEOPROTEIN COMPLEX
ENVELOPE
MITOCHONDRIAL ENVELOPE
CYTOCHROME COMPLEX
MITOCHONDRIAL PROTEIN CONTAINING COMPLEX
INNER MITOCHONDRIAL MEMBRANE PROTEIN COMPLEX
ORGANELLE INNER MEMBRANE
PROTON TRANSPORTING TWO SECTOR ATPASE COMPLEX PROTON TRANSPORTING DOMAIN
PROTON TRANSPORTING ATP SYNTHASE COMPLEX COUPLING FACTOR F O
POLYSOMAL RIBOSOME
POLYSOME
MITOCHONDRION
TRANSPORTER COMPLEX
NUCLEAR PROTEIN CONTAINING COMPLEX
RESPIRASOME
NADH DEHYDROGENASE COMPLEX
LARGE RIBOSOMAL SUBUNIT
CYTOSOLIC LARGE RIBOSOMAL SUBUNIT
RESPIRATORY CHAIN COMPLEX IV
Enriched pathways
Camk2d
Camkk2
Erbb2
Nrg1
Vegfa
Map3k12
Synj2
Bhlhe40
Fgf5
Perturbation
NES
-1 0 1 2
qvalue
<= 0.001
<= 0.01
<= 0.05

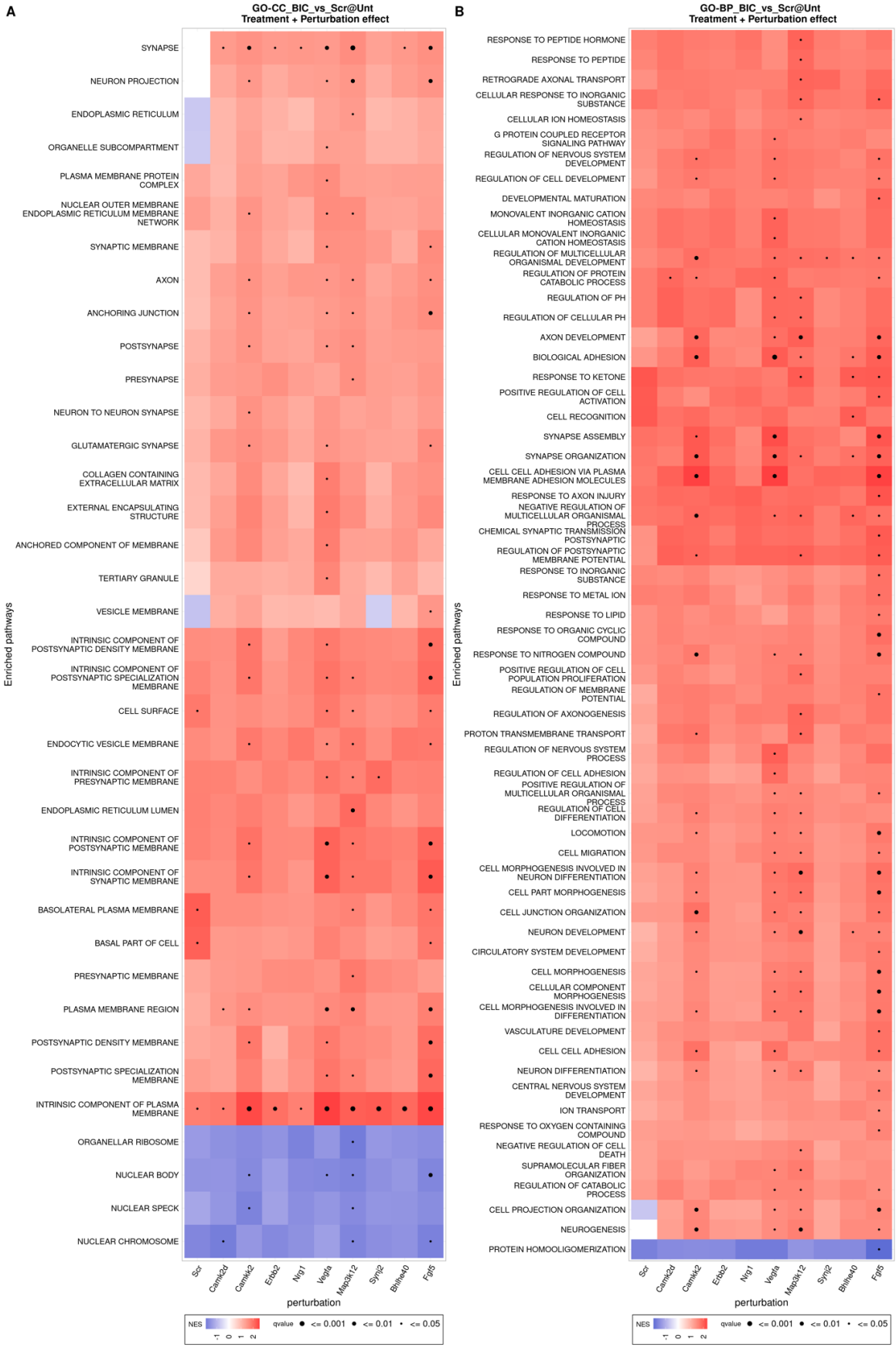
A
GO-CC_BIC_vs_Scr@Unt
Treatment + Perturbation effect
SYNAPSE
NEURON PROJECTION
ENDOPLASMIC RETICULUM
ORGANELLE SUBCOMPARTMENT
PLASMA MEMBRANE PROTEIN COMPLEX
NUCLEAR OUTER MEMBRANE ENDOPLASMIC RETICULUM MEMBRANE NETWORK
SYNAPTIC MEMBRANE
AXON
ANCHORING JUNCTION
POSTSYNAPSE
PRESYNAPSE
NEURON TO NEURON SYNAPSE
GLUTAMATERGIC SYNAPSE
COLLAGEN CONTAINING EXTRACELLULAR MATRIX
EXTERNAL ENCAPSULATING STRUCTURE
ANCHORED COMPONENT OF MEMBRANE
TERTIARY GRANULE
VESICLE MEMBRANE
INTRINSIC COMPONENT OF POSTSYNAPTIC DENSITY MEMBRANE
INTRINSIC COMPONENT OF POSTSYNAPTIC SPECIALIZATION MEMBRANE
CELL SURFACE
ENDOCYTIC VESICLE MEMBRANE
INTRINSIC COMPONENT OF PRESYNAPTIC MEMBRANE
ENDOPLASMIC RETICULUM LUMEN
INTRINSIC COMPONENT OF POSTSYNAPTIC MEMBRANE
INTRINSIC COMPONENT OF SYNAPTIC MEMBRANE
BASOLATERAL PLASMA MEMBRANE
BASAL PART OF CELL
PRESYNAPTIC MEMBRANE
PLASMA MEMBRANE REGION
POSTSYNAPTIC DENSITY MEMBRANE
POSTSYNAPTIC SPECIALIZATION MEMBRANE
INTRINSIC COMPONENT OF PLASMA MEMBRANE
ORGANELLAR RIBOSOME
NUCLEAR BODY
NUCLEAR SPECK
NUCLEAR CHROMOSOME
Enriched pathways
Scr
Camk2d
Camk2
Erbb2
Nrg1
Vegfa
Map3k12
Syngap1
Bhlhe40
Fgf5
perturbation
NES
-1 0 1 2
qvalue
<= 0.001
<= 0.01
<= 0.05
B
GO-BP_BIC_vs_Scr@Unt
Treatment + Perturbation effect
RESPONSE TO PEPTIDE HORMONE
RESPONSE TO PEPTIDE
RETROGRADE AXONAL TRANSPORT
CELLULAR RESPONSE TO INORGANIC SUBSTANCE
CELLULAR ION HOMEOSTASIS
G PROTEIN COUPLED RECEPTOR SIGNALING PATHWAY
REGULATION OF NERVOUS SYSTEM DEVELOPMENT
REGULATION OF CELL DEVELOPMENT
DEVELOPMENTAL MATURATION
MONOVALENT INORGANIC CATION HOMEOSTASIS
CELLULAR MONOVALENT INORGANIC CATION HOMEOSTASIS
REGULATION OF MULTICELLULAR ORGANISMAL DEVELOPMENT
REGULATION OF PROTEIN CATABOLIC PROCESS
REGULATION OF PH
REGULATION OF CELLULAR PH
AXON DEVELOPMENT
BIOLOGICAL ADHESION
RESPONSE TO KETONE
POSITIVE REGULATION OF CELL ACTIVATION
CELL RECOGNITION
SYNAPSE ASSEMBLY
SYNAPSE ORGANIZATION
CELL CELL ADHESION VIA PLASMA MEMBRANE ADHESION MOLECULES
RESPONSE TO AXON INJURY
NEGATIVE REGULATION OF MULTICELLULAR ORGANISMAL PROCESS
CHEMICAL SYNAPTIC TRANSMISSION POSTSYNAPTIC
REGULATION OF POSTSYNAPTIC MEMBRANE POTENTIAL
RESPONSE TO INORGANIC SUBSTANCE
RESPONSE TO METAL ION
RESPONSE TO LIPID
RESPONSE TO ORGANIC CYCLIC COMPOUND
RESPONSE TO NITROGEN COMPOUND
POSITIVE REGULATION OF CELL POPULATION PROLIFERATION
REGULATION OF MEMBRANE POTENTIAL
REGULATION OF AXONOGENESIS
PROTON TRANSMEMBRANE TRANSPORT
REGULATION OF NERVOUS SYSTEM PROCESS
REGULATION OF CELL ADHESION
POSITIVE REGULATION OF MULTICELLULAR ORGANISMAL PROCESS
REGULATION OF CELL DIFFERENTIATION
LOCOMOTION
CELL MIGRATION
CELL MORPHOGENESIS INVOLVED IN NEURON DIFFERENTIATION
CELL PART MORPHOGENESIS
CELL JUNCTION ORGANIZATION
NEURON DEVELOPMENT
CIRCULATORY SYSTEM DEVELOPMENT
CELL MORPHOGENESIS
CELLULAR COMPONENT MORPHOGENESIS
CELL MORPHOGENESIS INVOLVED IN DIFFERENTIATION
VASCULATURE DEVELOPMENT
CELL CELL ADHESION
NEURON DIFFERENTIATION
CENTRAL NERVOUS SYSTEM DEVELOPMENT
ION TRANSPORT
RESPONSE TO OXYGEN CONTAINING COMPOUND
NEGATIVE REGULATION OF CELL DEATH
SUPRAMOLECULAR FIBER ORGANIZATION
REGULATION OF CATABOLIC PROCESS
CELL PROJECTION ORGANIZATION
NEUROGENESIS
PROTEIN HOMOOLIGOMERIZATION
Enriched pathways
Scr
Camk2d
Camk2
Erbb2
Nrg1
Vegfa
Map3k12
Syngap1
Bhlhe40
Fgf5
perturbation
NES
-1 0 1 2
qvalue
<= 0.001
<= 0.01
<= 0.05

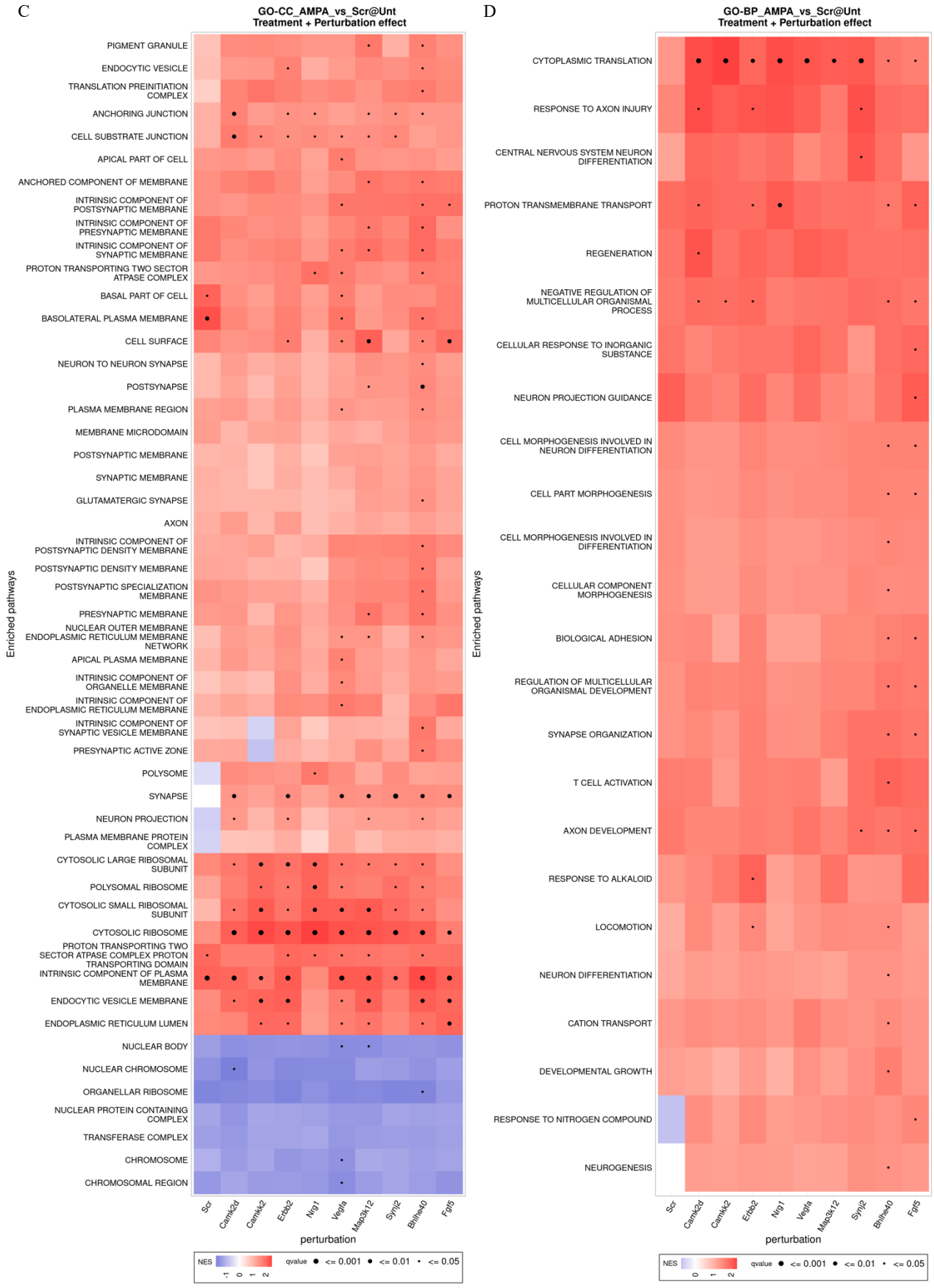
C
GO-CC_AMPA_vs_Scr@Unt
Treatment + Perturbation effect
PIGMENT GRANULE
ENDOCYTIC VESICLE
TRANSLATION PREINITIATION COMPLEX
ANCHORING JUNCTION
CELL SUBSTRATE JUNCTION
APICAL PART OF CELL
ANCHORED COMPONENT OF MEMBRANE
INTRINSIC COMPONENT OF POSTSYNAPTIC MEMBRANE
INTRINSIC COMPONENT OF PRESYNAPTIC MEMBRANE
INTRINSIC COMPONENT OF SYNAPTIC MEMBRANE
PROTON TRANSPORTING TWO SECTOR ATPASE COMPLEX
BASAL PART OF CELL
BASOLATERAL PLASMA MEMBRANE
CELL SURFACE
NEURON TO NEURON SYNAPSE
POSTSYNAPSE
PLASMA MEMBRANE REGION
MEMBRANE MICRODOMAIN
POSTSYNAPTIC MEMBRANE
SYNAPTIC MEMBRANE
GLUTAMATERGIC SYNAPSE
AXON
INTRINSIC COMPONENT OF POSTSYNAPTIC DENSITY MEMBRANE
POSTSYNAPTIC DENSITY MEMBRANE
POSTSYNAPTIC SPECIALIZATION MEMBRANE
PRESYNAPTIC MEMBRANE
NUCLEAR OUTER MEMBRANE ENDOPLASMIC RETICULUM MEMBRANE NETWORK
APICAL PLASMA MEMBRANE
INTRINSIC COMPONENT OF ORGANELLE MEMBRANE
INTRINSIC COMPONENT OF ENDOPLASMIC RETICULUM MEMBRANE
INTRINSIC COMPONENT OF SYNAPTIC VESICLE MEMBRANE
PRESYNAPTIC ACTIVE ZONE
POLYSOME
SYNAPSE
NEURON PROJECTION
PLASMA MEMBRANE PROTEIN COMPLEX
CYTOSOLIC LARGE RIBOSOMAL SUBUNIT
POLYSOMAL RIBOSOME
CYTOSOLIC SMALL RIBOSOMAL SUBUNIT
CYTOSOLIC RIBOSOME
PROTON TRANSPORTING TWO SECTOR ATPASE COMPLEX PROTON TRANSPORTING DOMAIN
INTRINSIC COMPONENT OF PLASMA MEMBRANE
ENDOCYTIC VESICLE MEMBRANE
ENDOPLASMIC RETICULUM LUMEN
NUCLEAR BODY
NUCLEAR CHROMOSOME
ORGANELLAR RIBOSOME
NUCLEAR PROTEIN CONTAINING COMPLEX
TRANSFERASE COMPLEX
CHROMOSOME
CHROMOSOMAL REGION
Enriched pathways
Scr
Camk2d
Camkk2
Erbb2
Nrg1
Vegfa
Map3k12
Synj2
Bhlhe40
Fgf5
perturbation
NES
-1
0
1
2
qvalue
<= 0.001
<= 0.01
<= 0.05
D
GO-BP_AMPA_vs_Scr@Unt
Treatment + Perturbation effect
CYTOPLASMIC TRANSLATION
RESPONSE TO AXON INJURY
CENTRAL NERVOUS SYSTEM NEURON DIFFERENTIATION
PROTON TRANSMEMBRANE TRANSPORT
REGENERATION
NEGATIVE REGULATION OF MULTICELLULAR ORGANISMAL PROCESS
CELLULAR RESPONSE TO INORGANIC SUBSTANCE
NEURON PROJECTION GUIDANCE
CELL MORPHOGENESIS INVOLVED IN NEURON DIFFERENTIATION
CELL PART MORPHOGENESIS
CELL MORPHOGENESIS INVOLVED IN DIFFERENTIATION
CELLULAR COMPONENT MORPHOGENESIS
BIOLOGICAL ADHESION
REGULATION OF MULTICELLULAR ORGANISMAL DEVELOPMENT
SYNAPSE ORGANIZATION
T CELL ACTIVATION
AXON DEVELOPMENT
RESPONSE TO ALKALOID
LOCOMOTION
NEURON DIFFERENTIATION
CATION TRANSPORT
DEVELOPMENTAL GROWTH
RESPONSE TO NITROGEN COMPOUND
NEUROGENESIS
Enriched pathways
Scr
Camk2d
Camkk2
Erbb2
Nrg1
Vegfa
Map3k12
Synj2
Bhlhe40
Fgf5
perturbation
NES
0
1
2
qvalue
<= 0.001
<= 0.01
<= 0.05

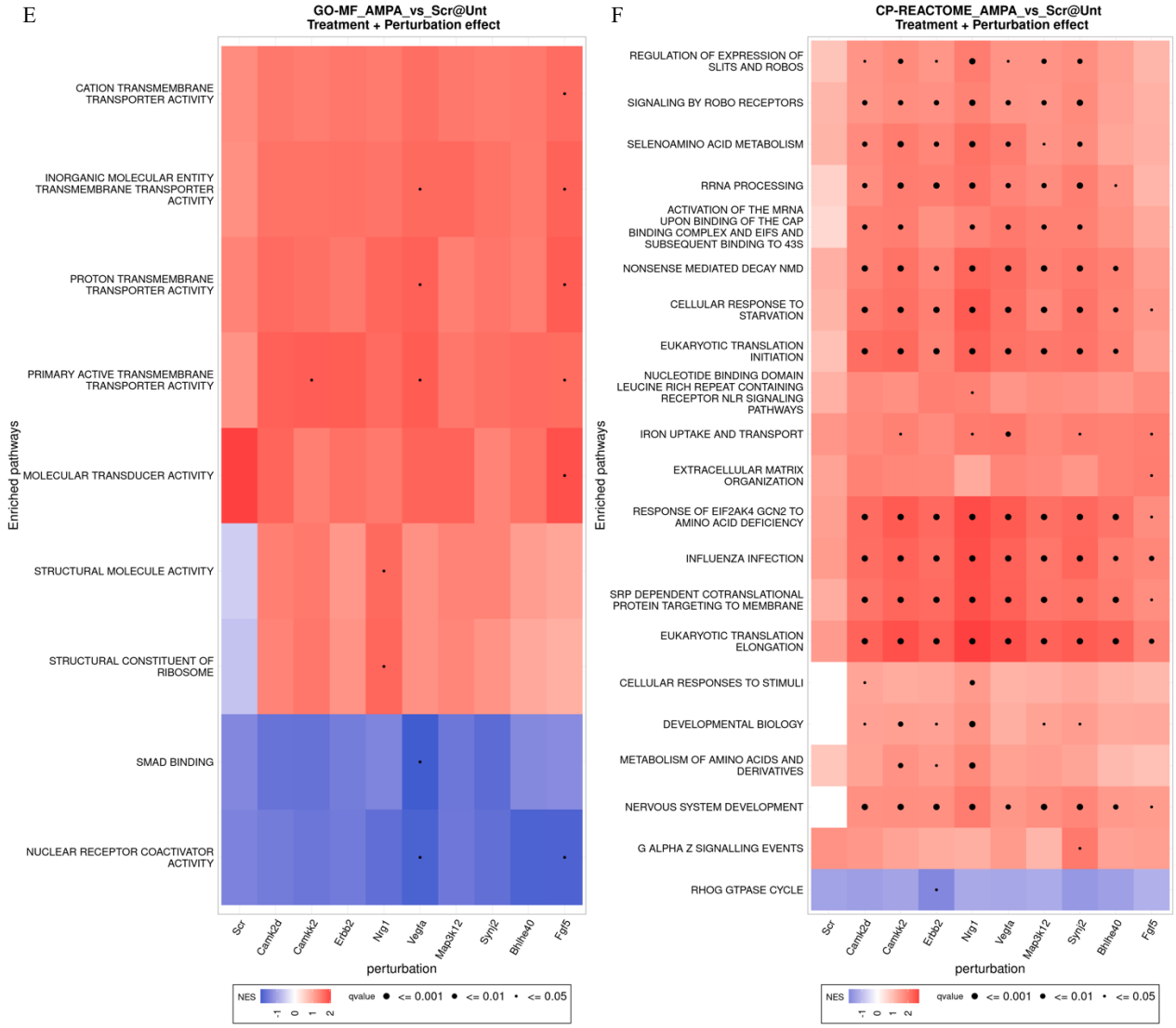

Figure 32 Heatmap representation of Enrichment Score and Significance Values for Treatment and Perturbation combined effects compared to Scramble Untreated Samples across all perturbations

Heatmaps illustrate the enrichment score and significance values for treatment and perturbation effects compared to scramble untreated samples across various perturbations. The analysis includes:

(A) Gene Ontology Cellular Components (GO-CC) enrichment for DEGs (Differentially Expressed Genes) in BIC samples.

(B) Gene Ontology Biological Processes (GO-BP) enrichment for DEGs in BIC samples.

(C) Gene Ontology Cellular Components (GO-CC) enrichment for DEGs in AMPA samples.

(D) Gene Ontology Biological Processes (GO-BP) enrichment for DEGs in AMPA samples.

(E) Gene Ontology Molecular Functions (GO-MF) enrichment for DEGs in AMPA samples.

(F) Reactome pathway enrichment for DEGs in AMPA samples.

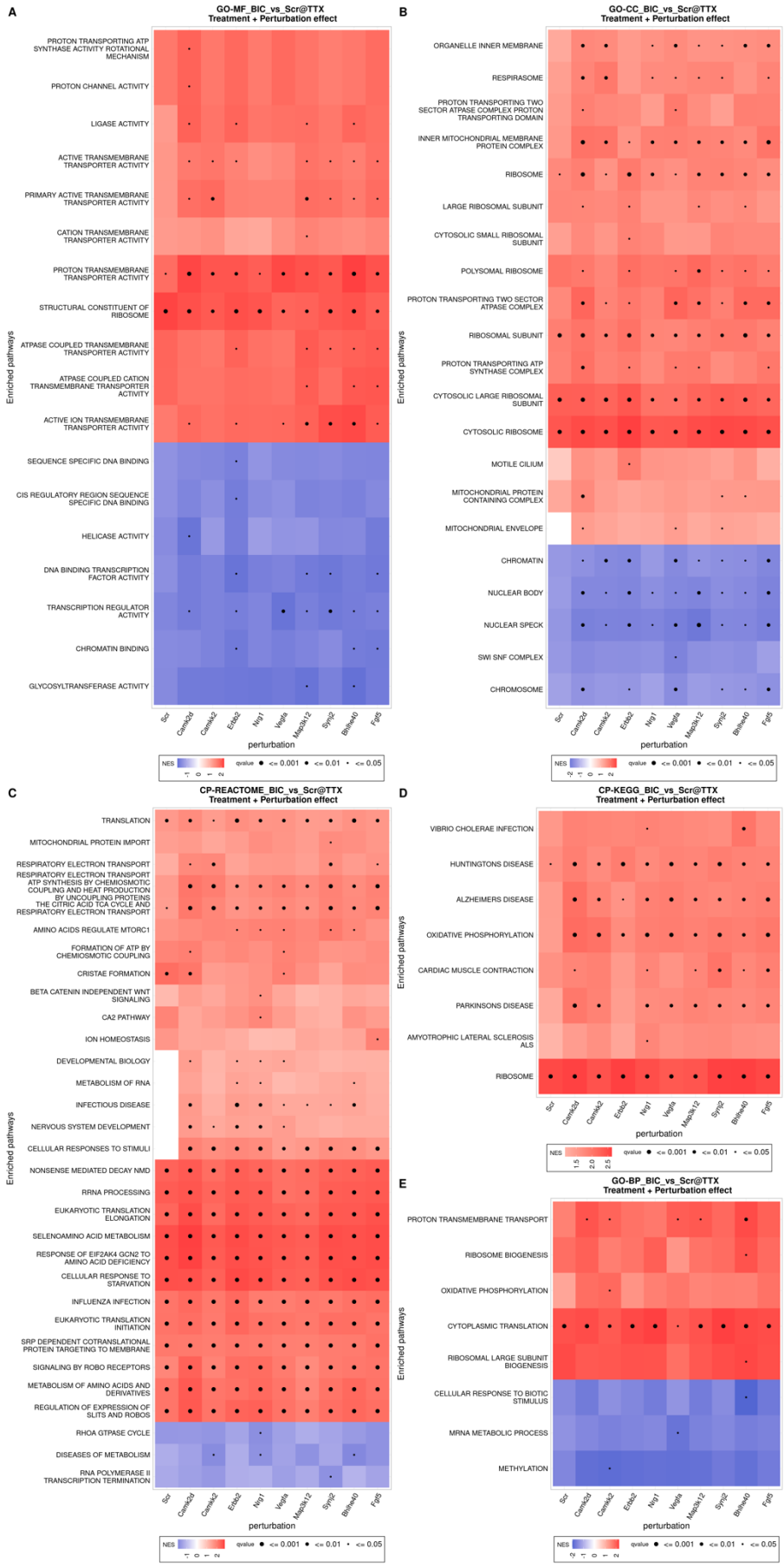
A
GO-MF_BIC_vs_Scr@TTX
Treatment + Perturbation effect
PROTON TRANSPORTING ATP SYNTHASE ACTIVITY ROTATIONAL MECHANISM
PROTON CHANNEL ACTIVITY
LIGASE ACTIVITY
ACTIVE TRANSMEMBRANE TRANSPORTER ACTIVITY
PRIMARY ACTIVE TRANSMEMBRANE TRANSPORTER ACTIVITY
CATION TRANSMEMBRANE TRANSPORTER ACTIVITY
PROTON TRANSMEMBRANE TRANSPORTER ACTIVITY
STRUCTURAL CONSTITUENT OF RIBOSOME
ATPASE COUPLED TRANSMEMBRANE TRANSPORTER ACTIVITY
ATPASE COUPLED CATION TRANSMEMBRANE TRANSPORTER ACTIVITY
ACTIVE ION TRANSMEMBRANE TRANSPORTER ACTIVITY
SEQUENCE SPECIFIC DNA BINDING
CIS REGULATORY REGION SEQUENCE SPECIFIC DNA BINDING
HELICASE ACTIVITY
DNA BINDING TRANSCRIPTION FACTOR ACTIVITY
TRANSCRIPTION REGULATOR ACTIVITY
CHROMATIN BINDING
GLYCOSYLTRANSFERASE ACTIVITY
Enriched pathways
Scr
Camk2d
Camk2a
Ebf2
Nrg1
Vegfa
Mapk12
Syngr2
Bhlhe40
Fgf5
perturbation
NES
qvalue
<= 0.001
<= 0.01
<= 0.05
B
GO-CC_BIC_vs_Scr@TTX
Treatment + Perturbation effect
ORGANELLE INNER MEMBRANE
RESPIRASOME
PROTON TRANSPORTING TWO SECTOR ATPASE COMPLEX PROTON TRANSPORTING DOMAIN
INNER MITOCHONDRIAL MEMBRANE PROTEIN COMPLEX
RIBOSOME
LARGE RIBOSOMAL SUBUNIT
CYTOSOLIC SMALL RIBOSOMAL SUBUNIT
POLYSOMAL RIBOSOME
PROTON TRANSPORTING TWO SECTOR ATPASE COMPLEX
RIBOSOMAL SUBUNIT
PROTON TRANSPORTING ATP SYNTHASE COMPLEX
CYTOSOLIC LARGE RIBOSOMAL SUBUNIT
CYTOSOLIC RIBOSOME
MOTILE CILIUM
MITOCHONDRIAL PROTEIN CONTAINING COMPLEX
MITOCHONDRIAL ENVELOPE
CHROMATIN
NUCLEAR BODY
NUCLEAR SPECK
SWI SNF COMPLEX
CHROMOSOME
C
CP-REACTOME_BIC_vs_Scr@TTX
Treatment + Perturbation effect
TRANSLATION
MITOCHONDRIAL PROTEIN IMPORT
RESPIRATORY ELECTRON TRANSPORT
RESPIRATORY ELECTRON TRANSPORT ATP SYNTHESIS BY CHEMIOSMOTIC COUPLING AND HEAT PRODUCTION BY UNCOUPLING PROTEINS THE CITRIC ACID TCA CYCLE AND RESPIRATORY ELECTRON TRANSPORT
AMINO ACIDS REGULATE MTORC1
FORMATION OF ATP BY CHEMIOSMOTIC COUPLING
CRISTAE FORMATION
BETA CATENIN INDEPENDENT WNT SIGNALING
CA2 PATHWAY
ION HOMEOSTASIS
DEVELOPMENTAL BIOLOGY
METABOLISM OF RNA
INFECTIOUS DISEASE
NERVOUS SYSTEM DEVELOPMENT
CELLULAR RESPONSES TO STIMULI
NONSENSE MEDIATED DECAY NMD
RRNA PROCESSING
EUKARYOTIC TRANSLATION ELONGATION
SELENOAMINO ACID METABOLISM
RESPONSE OF EIF2AK4 GCN2 TO AMINO ACID DEFICIENCY
CELLULAR RESPONSE TO STARVATION
INFLUENZA INFECTION
EUKARYOTIC TRANSLATION INITIATION
SRP DEPENDENT COTRANSLATIONAL PROTEIN TARGETING TO MEMBRANE
SIGNALING BY ROBO RECEPTORS
METABOLISM OF AMINO ACIDS AND DERIVATIVES
REGULATION OF EXPRESSION OF SLITS AND ROBOS
RHOA GTPASE CYCLE
DISEASES OF METABOLISM
RNA POLYMERASE II TRANSCRIPTION TERMINATION
D
CP-KEGG_BIC_vs_Scr@TTX
Treatment + Perturbation effect
VIBRIO CHOLERAE INFECTION
HUNTINGTONS DISEASE
ALZHEIMERS DISEASE
OXIDATIVE PHOSPHORYLATION
CARDIAC MUSCLE CONTRACTION
PARKINSONS DISEASE
AMYOTROPHIC LATERAL SCLEROSIS ALS
RIBOSOME
E
GO-BP_BIC_vs_Scr@TTX
Treatment + Perturbation effect
PROTON TRANSMEMBRANE TRANSPORT
RIBOSOME BIOGENESIS
OXIDATIVE PHOSPHORYLATION
CYTOPLASMIC TRANSLATION
RIBOSOMAL LARGE SUBUNIT BIOGENESIS
CELLULAR RESPONSE TO BIOTIC STIMULUS
MRNA METABOLIC PROCESS
METHYLATION

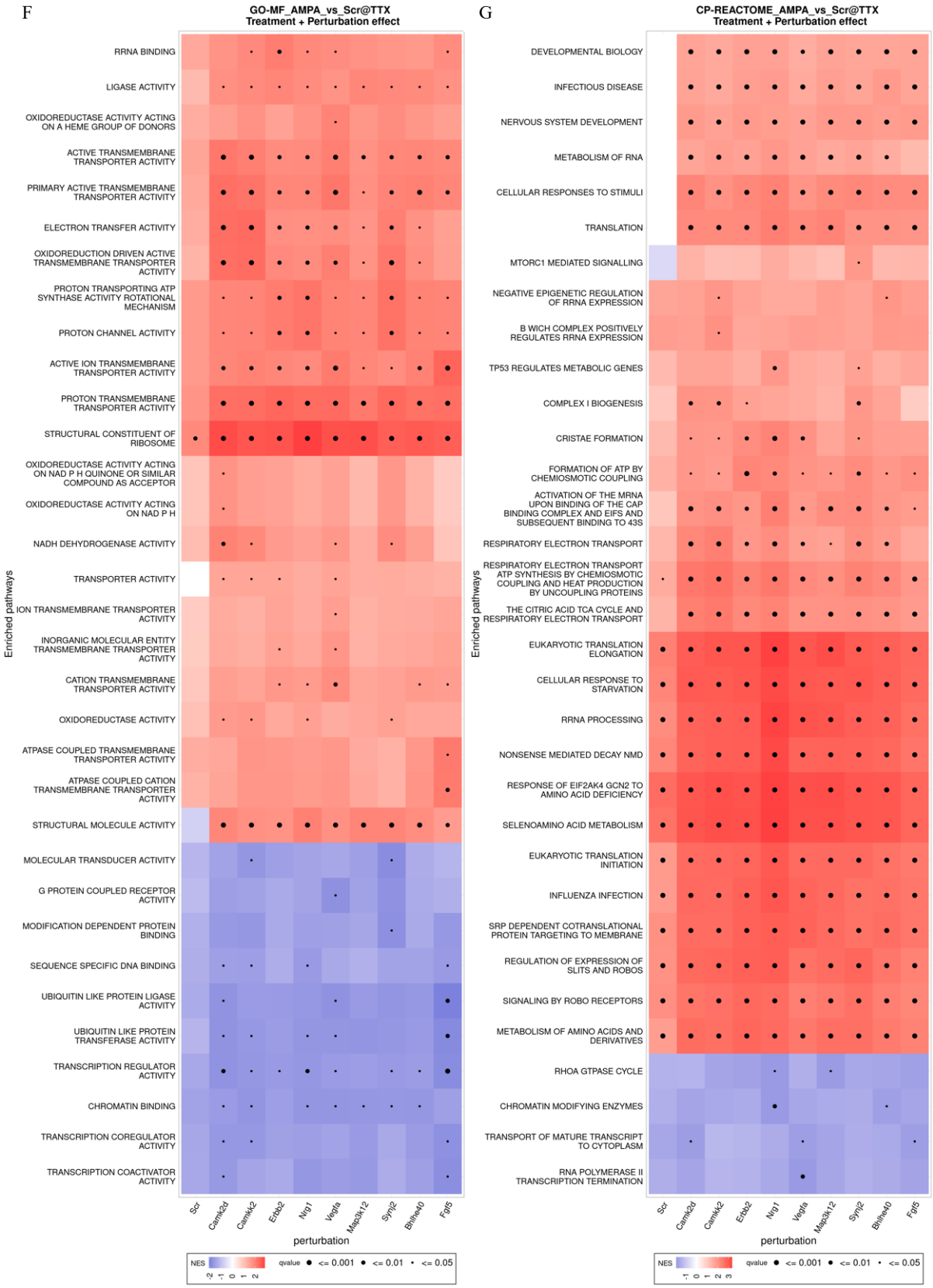
F
GO-MF_AMPA_vs_Scr@TTX
Treatment + Perturbation effect
RRNA BINDING
LIGASE ACTIVITY
OXIDOREDUCTASE ACTIVITY ACTING ON A HEME GROUP OF DONORS
ACTIVE TRANSMEMBRANE TRANSPORTER ACTIVITY
PRIMARY ACTIVE TRANSMEMBRANE TRANSPORTER ACTIVITY
ELECTRON TRANSFER ACTIVITY
OXIDOREDUCTION DRIVEN ACTIVE TRANSMEMBRANE TRANSPORTER ACTIVITY
PROTON TRANSPORTING ATP SYNTHASE ACTIVITY ROTATIONAL MECHANISM
PROTON CHANNEL ACTIVITY
ACTIVE ION TRANSMEMBRANE TRANSPORTER ACTIVITY
PROTON TRANSMEMBRANE TRANSPORTER ACTIVITY
STRUCTURAL CONSTITUENT OF RIBOSOME
OXIDOREDUCTASE ACTIVITY ACTING ON NAD P H QUINONE OR SIMILAR COMPOUND AS ACCEPTOR
OXIDOREDUCTASE ACTIVITY ACTING ON NAD P H
NADH DEHYDROGENASE ACTIVITY
TRANSPORTER ACTIVITY
ION TRANSMEMBRANE TRANSPORTER ACTIVITY
INORGANIC MOLECULAR ENTITY TRANSMEMBRANE TRANSPORTER ACTIVITY
CATION TRANSMEMBRANE TRANSPORTER ACTIVITY
OXIDOREDUCTASE ACTIVITY
ATPASE COUPLED TRANSMEMBRANE TRANSPORTER ACTIVITY
ATPASE COUPLED CATION TRANSMEMBRANE TRANSPORTER ACTIVITY
STRUCTURAL MOLECULE ACTIVITY
MOLECULAR TRANSDUCER ACTIVITY
G PROTEIN COUPLED RECEPTOR ACTIVITY
MODIFICATION DEPENDENT PROTEIN BINDING
SEQUENCE SPECIFIC DNA BINDING
UBIQUITIN LIKE PROTEIN LIGASE ACTIVITY
UBIQUITIN LIKE PROTEIN TRANSFERASE ACTIVITY
TRANSCRIPTION REGULATOR ACTIVITY
CHROMATIN BINDING
TRANSCRIPTION COREGULATOR ACTIVITY
TRANSCRIPTION COACTIVATOR ACTIVITY
Enriched pathways
Scr
Camkk2d
Camkk2
Erbb2
Nrg1
Vegfa
Map3k12
Synj2
Bhlhe40
Fgf5
perturbation
NES
-2 -1 0 1 2
qvalue
<= 0.001
<= 0.01
<= 0.05
G
CP-REACTOME_AMPA_vs_Scr@TTX
Treatment + Perturbation effect
DEVELOPMENTAL BIOLOGY
INFECTIOUS DISEASE
NERVOUS SYSTEM DEVELOPMENT
METABOLISM OF RNA
CELLULAR RESPONSES TO STIMULI
TRANSLATION
MTORC1 MEDIATED SIGNALLING
NEGATIVE EPIGENETIC REGULATION OF RRNA EXPRESSION
B WICH COMPLEX POSITIVELY REGULATES RRNA EXPRESSION
TP53 REGULATES METABOLIC GENES
COMPLEX I BIOGENESIS
CRISTAE FORMATION
FORMATION OF ATP BY CHEMIOSMOTIC COUPLING
ACTIVATION OF THE MRNA UPON BINDING OF THE CAP BINDING COMPLEX AND EIFS AND SUBSEQUENT BINDING TO 43S
RESPIRATORY ELECTRON TRANSPORT
RESPIRATORY ELECTRON TRANSPORT ATP SYNTHESIS BY CHEMIOSMOTIC COUPLING AND HEAT PRODUCTION BY UNCOUPLING PROTEINS
THE CITRIC ACID TCA CYCLE AND RESPIRATORY ELECTRON TRANSPORT
EUKARYOTIC TRANSLATION ELONGATION
CELLULAR RESPONSE TO STARVATION
RRNA PROCESSING
NONSENSE MEDIATED DECAY NMD
RESPONSE OF EIF2AK4 GCN2 TO AMINO ACID DEFICIENCY
SELENOAMINO ACID METABOLISM
EUKARYOTIC TRANSLATION INITIATION
INFLUENZA INFECTION
SRP DEPENDENT COTRANSLATIONAL PROTEIN TARGETING TO MEMBRANE
REGULATION OF EXPRESSION OF SLITS AND ROBOS
SIGNALING BY ROBO RECEPTORS
METABOLISM OF AMINO ACIDS AND DERIVATIVES
RHOA GTPASE CYCLE
CHROMATIN MODIFYING ENZYMES
TRANSPORT OF MATURE TRANSCRIPT TO CYTOPLASM
RNA POLYMERASE II TRANSCRIPTION TERMINATION
Enriched pathways
Scr
Camkk2d
Camkk2
Erbb2
Nrg1
Vegfa
Map3k12
Synj2
Bhlhe40
Fgf5
perturbation
NES
-1 0 1 2 3
qvalue
<= 0.001
<= 0.01
<= 0.05

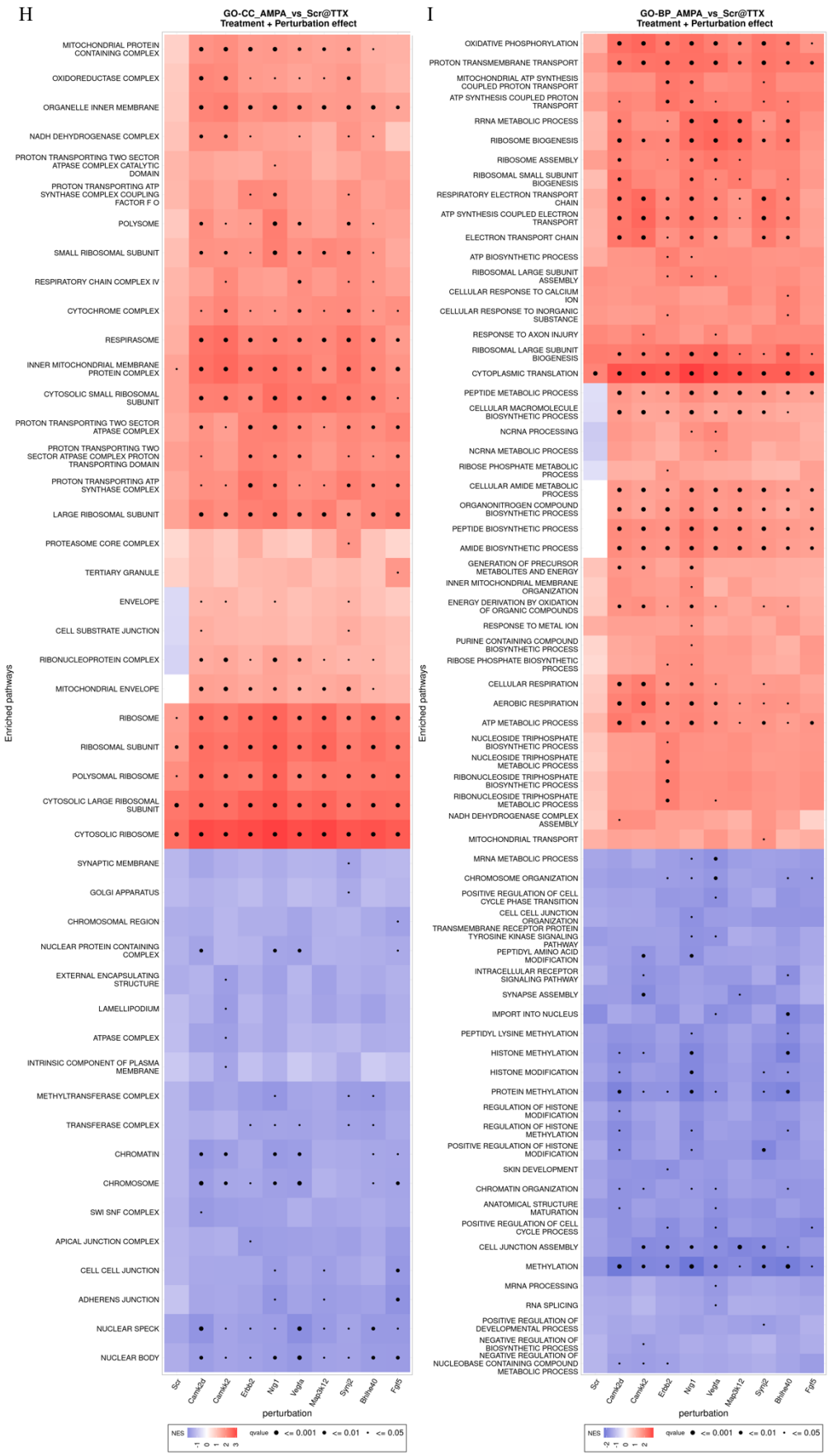
H
GO-CC_AMPA_vs_Scr@TTX
Treatment + Perturbation effect
MITOCHONDRIAL PROTEIN CONTAINING COMPLEX
OXIDOREDUCTASE COMPLEX
ORGANELLE INNER MEMBRANE
NADH DEHYDROGENASE COMPLEX
PROTON TRANSPORTING TWO SECTOR ATPASE COMPLEX CATALYTIC DOMAIN
PROTON TRANSPORTING ATP SYNTHASE COMPLEX COUPLING FACTOR F O
POLYSOME
SMALL RIBOSOMAL SUBUNIT
RESPIRATORY CHAIN COMPLEX IV
CYTOCHROME COMPLEX
RESPIRASOME
INNER MITOCHONDRIAL MEMBRANE PROTEIN COMPLEX
CYTOSOLIC SMALL RIBOSOMAL SUBUNIT
PROTON TRANSPORTING TWO SECTOR ATPASE COMPLEX
PROTON TRANSPORTING TWO SECTOR ATPASE COMPLEX PROTON TRANSPORTING DOMAIN
PROTON TRANSPORTING ATP SYNTHASE COMPLEX
LARGE RIBOSOMAL SUBUNIT
PROTEASOME CORE COMPLEX
TERTIARY GRANULE
ENVELOPE
CELL SUBSTRATE JUNCTION
RIBONUCLEOPROTEIN COMPLEX
MITOCHONDRIAL ENVELOPE
RIBOSOME
RIBOSOMAL SUBUNIT
POLYSOMAL RIBOSOME
CYTOSOLIC LARGE RIBOSOMAL SUBUNIT
CYTOSOLIC RIBOSOME
SYNAPTIC MEMBRANE
GOLGI APPARATUS
CHROMOSOMAL REGION
NUCLEAR PROTEIN CONTAINING COMPLEX
EXTERNAL ENCAPSULATING STRUCTURE
LAMELLIPODIUM
ATPASE COMPLEX
INTRINSIC COMPONENT OF PLASMA MEMBRANE
METHYLTRANSFERASE COMPLEX
TRANSFERASE COMPLEX
CHROMATIN
CHROMOSOME
SWI SNF COMPLEX
APICAL JUNCTION COMPLEX
CELL CELL JUNCTION
ADHERENS JUNCTION
NUCLEAR SPECK
NUCLEAR BODY
Enriched pathways
Scr
Camkd3
Camkk2
Erbb2
Nrg1
Vegfa
Map3k12
Syngap1
Bhlhe40
Fgf5
perturbation
NES
qvalue
<= 0.001
<= 0.01
<= 0.05
I
GO-BP_AMPA_vs_Scr@TTX
Treatment + Perturbation effect
OXIDATIVE PHOSPHORYLATION
PROTON TRANSMEMBRANE TRANSPORT
MITOCHONDRIAL ATP SYNTHESIS COUPLED PROTON TRANSPORT
ATP SYNTHESIS COUPLED PROTON TRANSPORT
RRNA METABOLIC PROCESS
RIBOSOME BIOGENESIS
RIBOSOME ASSEMBLY
RIBOSOMAL SMALL SUBUNIT BIOGENESIS
RESPIRATORY ELECTRON TRANSPORT CHAIN
ATP SYNTHESIS COUPLED ELECTRON TRANSPORT
ELECTRON TRANSPORT CHAIN
ATP BIOSYNTHETIC PROCESS
RIBOSOMAL LARGE SUBUNIT ASSEMBLY
CELLULAR RESPONSE TO CALCIUM ION
CELLULAR RESPONSE TO INORGANIC SUBSTANCE
RESPONSE TO AXON INJURY
RIBOSOMAL LARGE SUBUNIT BIOGENESIS
CYTOPLASMIC TRANSLATION
PEPTIDE METABOLIC PROCESS
CELLULAR MACROMOLECULE BIOSYNTHETIC PROCESS
NCRNA PROCESSING
NCRNA METABOLIC PROCESS
RIBOSE PHOSPHATE METABOLIC PROCESS
CELLULAR AMIDE METABOLIC PROCESS
ORGANONITROGEN COMPOUND BIOSYNTHETIC PROCESS
PEPTIDE BIOSYNTHETIC PROCESS
AMIDE BIOSYNTHETIC PROCESS
GENERATION OF PRECURSOR METABOLITES AND ENERGY
INNER MITOCHONDRIAL MEMBRANE ORGANIZATION
ENERGY DERIVATION BY OXIDATION OF ORGANIC COMPOUNDS
RESPONSE TO METAL ION
PURINE CONTAINING COMPOUND BIOSYNTHETIC PROCESS
RIBOSE PHOSPHATE BIOSYNTHETIC PROCESS
CELLULAR RESPIRATION
AEROBIC RESPIRATION
ATP METABOLIC PROCESS
NUCLEOSIDE TRIPHOSPHATE BIOSYNTHETIC PROCESS
NUCLEOSIDE TRIPHOSPHATE METABOLIC PROCESS
RIBONUCLEOSIDE TRIPHOSPHATE BIOSYNTHETIC PROCESS
RIBONUCLEOSIDE TRIPHOSPHATE METABOLIC PROCESS
NADH DEHYDROGENASE COMPLEX ASSEMBLY
MITOCHONDRIAL TRANSPORT
MRNA METABOLIC PROCESS
CHROMOSOME ORGANIZATION
POSITIVE REGULATION OF CELL CYCLE PHASE TRANSITION
CELL CELL JUNCTION ORGANIZATION
TRANSMEMBRANE RECEPTOR PROTEIN TYROSINE KINASE SIGNALING PATHWAY
PEPTIDYL AMINO ACID MODIFICATION
INTRACELLULAR RECEPTOR SIGNALING PATHWAY
SYNAPSE ASSEMBLY
IMPORT INTO NUCLEUS
PEPTIDYL LYSINE METHYLATION
HISTONE METHYLATION
HISTONE MODIFICATION
PROTEIN METHYLATION
REGULATION OF HISTONE MODIFICATION
REGULATION OF HISTONE METHYLATION
POSITIVE REGULATION OF HISTONE MODIFICATION
SKIN DEVELOPMENT
CHROMATIN ORGANIZATION
ANATOMICAL STRUCTURE MATURATION
POSITIVE REGULATION OF CELL CYCLE PROCESS
CELL JUNCTION ASSEMBLY
METHYLATION
MRNA PROCESSING
RNA SPLICING
POSITIVE REGULATION OF DEVELOPMENTAL PROCESS
NEGATIVE REGULATION OF BIOSYNTHETIC PROCESS
NEGATIVE REGULATION OF NUCLEOBASE CONTAINING COMPOUND METABOLIC PROCESS
Enriched pathways
Scr
Camkd3
Camkk2
Erbb2
Nrg1
Vegfa
Map3k12
Syngap1
Bhlhe40
Fgf5
perturbation
NES
qvalue
<= 0.001
<= 0.01
<= 0.05

Figure 33 Heatmap representation of Enrichment Score and Significance Values for Treatment and Perturbation combined effects compared to Scramble TTX samples across all perturbations

Heatmaps illustrate the enrichment score and significance values for treatment and perturbation effects compared to scramble TTX samples across various perturbations. The analysis includes:

A. Gene Ontology Molecular Functions (GO-MF) enrichment for DEGs in BIC samples.

B. Gene Ontology Cellular Components (GO-CC) enrichment for DEGs in BIC samples.

C. Reactome pathway enrichment for DEGs in BIC samples.

D. KEGG pathway enrichment for DEGs in BIC samples.

E. Gene Ontology Biological Processes (GO-BP) enrichment for DEGs in BIC samples.

F. Gene Ontology Molecular Functions (GO-MF) enrichment for DEGs in AMPA samples.

G. Reactome pathway enrichment for DEGs in AMPA samples.

H. Gene Ontology Cellular Components (GO-CC) enrichment for DEGs in AMPA samples.

I. Gene Ontology Biological Processes (GO-BP) enrichment for DEGs in AMPA samples.

4.2 Chapter 2

4.2.1 Identification of an optimal BDNF sensor

4.2.1.1 Quantitative analysis of potential BDNF sensors in primary cortical neurons

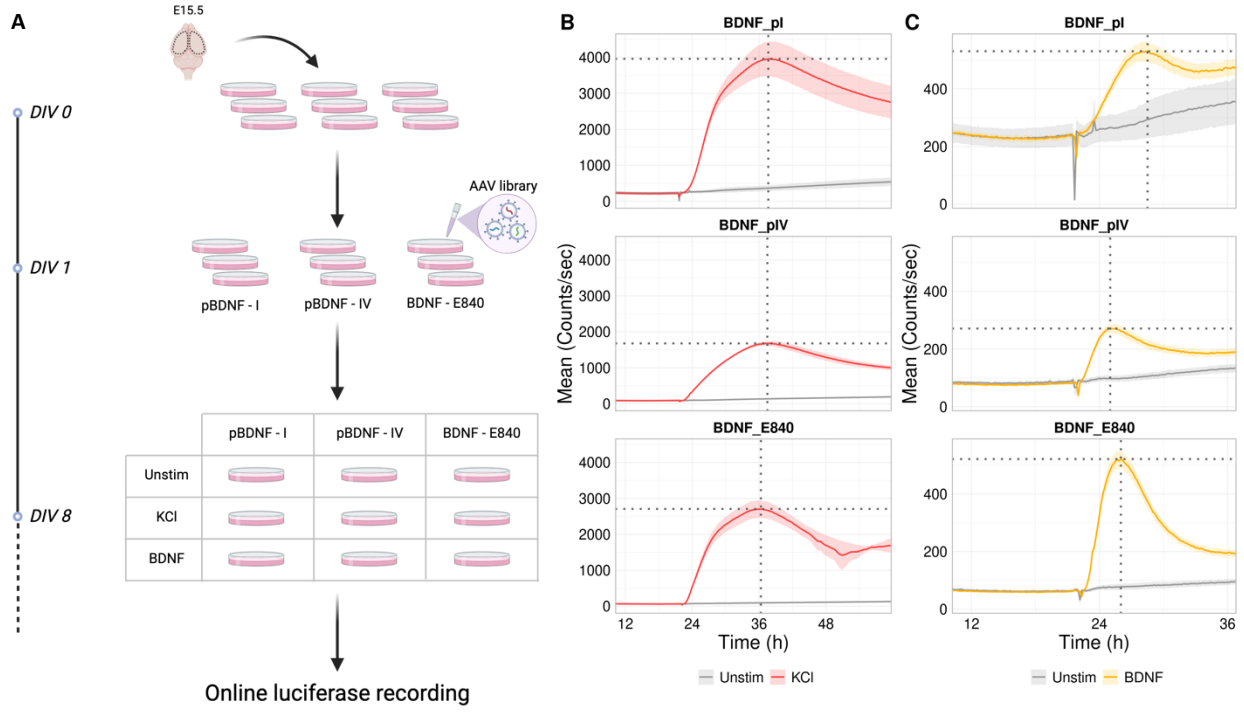

Figure 34 BDNF-E840 is identified to be the most effective BDNF sensor

(A) Schematic representation of cell culture experiment. Primary cortical neurons were harvested from E15.5 wild-type mouse and plated in 3.5cm dishes. Cultures were transduced with AAVs on *DIV1* and upon silencing with TTX cocktail and Luciferin at DIV7, they were separated onto 3 groups each and placed inside an incubator equipped with live luciferase recording module. Group 1,2,3 was treated with either 25mM KCl, 50 ng/µl BDNF or Vehicle and change in Luciferase count was recorded for 48 hr.

(B,C) Live luciferase recordings to monitor dynamics of luciferase activity in real-time which is a measure of sensor activity upon stimulated with either 25 mM KCl or 50 ng/ml BDNF and contrasted against sensor activity of unstimulated control. Grey dotted lines show x-intercept and y-intercept, representing the time at which the maximum luciferase counts were recorded and the corresponding count value.

To identify the most effective BDNF sensor, we generated three potential BDNF sensor TargetFinder AAV libraries. These libraries were then transduced into primary mouse cortical neuron cultures on *DIV1*. At *DIV7*, all cultures underwent silencing with a TTX cocktail to minimize background sensor activity. Additionally, 2µM Luciferin, the substrate for the Luciferase enzyme, was introduced into all cultures. Subsequently, cultures were placed inside an incubator equipped with a live luciferase recording module. After a 24-hour post-silencing period, cultures were stimulated with either 25mM KCl or 50 ng/ml BDNF. In parallel, a subset of cultures received treatment with warm, temperature-adjusted culture media as an unstimulated control. Each sensor + treatment condition was represented by three independent cultures in the cell culture

setup (Figure 34). The recording of cultures continued until the sensor activity reached a plateau.

Figure 34 B presents the temporal profiles of BDNF sensor activity following stimulation with 25mM KCl. Across all sensors, a peak in luciferase counts is observed around 12 hours post-stimulation. Notably, sensor strength varies among the tested sensors, with pBDNF-I exhibiting the highest maximum counts, followed by BDNF-E840 and pBDNF-IV. In Figure 34 C, the dynamics of BDNF sensor activity upon stimulation with 50 ng/ml BDNF are depicted. Post- stimulation, variations are observed in both the maximum luciferase counts and baseline sensor activity among different sensors. Notably, pBDNF-I displays elevated baseline sensor activity. As a result, the order of sensor strength is determined as follows: BDNF-E840 > pBDNF-I ≥ pBDNF-IV.

4.2.1.2 Evaluating optimum stimulation time for BDNF-E840 sensor

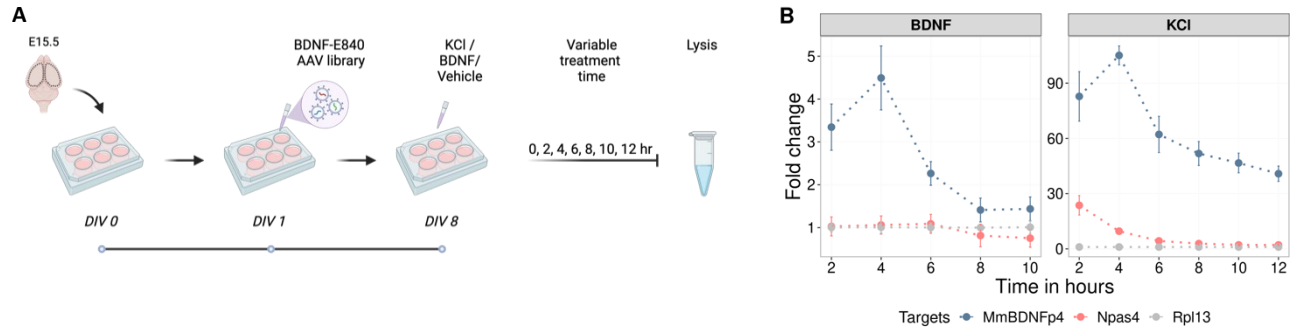

Figure 35 Temporal quantitative PCR was performed to identify adequate stimulation time

(A) Schematic representation of cell culture experiment. Primary cortical neurons were harvested from E15.5 wild-type mouse and plated in 6-well plate. Cultures were transduced with BDNF-E840 AAV library on *DIV1* and upon silencing with TTX cocktail at DIV7, they were separated onto 3 groups. Group 1,2,3 were treated with 25mM KCl, 50 ng/µl BDNF or Vehicle and RNA was harvested at 2, 4, 6, 8, 10 and 12 hr time-point.

(B) Quantitative real-time PCR (qRT-PCR) results for endogenous targets, pBDNF-IV transcript Npas4 and Rpl13 (housekeeping). Fold change has been calculated relative to 0 hour samples.

To assess the kinetics of endogenous and sensor-specific targets upon stimulation, quantitative real-time polymerase chain reaction (qRT-PCR) was conducted. Primary cortical neuron cultures were transduced with the BDNF-E840 AAV library on *DIV1*. Subsequently, on *DIV8*, an adequate number of cultures were stimulated with either 25mM KCl or 50 ng/ml BDNF. Cultures were lysed at every 2-hour interval, ranging from 0 hours up to 12 hours post-stimulation.

The qRT-PCR results revealed distinct expression profiles for different transcripts. *Bdnf* transcript driven by promoter IV exhibited a similar trend for both BDNF and KCl stimulation, with peak expression observed at 4 hours post-stimulation. In contrast, *Npas4* transcripts showed relative expression only upon KCl stimulation, with peak expression occurring at 2 hours.

4.2.2 TargetFinder assay with BDNF-E840 as sensor

4.2.2.1 Neuronal modulators of BDNF-E840 sensor

To identify neuronal modulators of the BDNF-E840 sensor, two independent TargetFinder assays were conducted using primary cortical neuron cultures derived from two separate E15.5 wild-type mice batches. For Batch 1, cultures were transduced with the AAV library on *DIV1* and divided into three groups. Each group consisted of three independent dishes, which were subsequently silenced using a TTX cocktail. On *DIV8*, the silenced cultures were treated with either vehicle, 25mM KCl, or 50 ng/ml BDNF. For Batch 2, transduced cultures were also divided into two groups, each containing four independent dishes, and silenced using a TTX cocktail. On *DIV8*, these cultures were treated with either vehicle or 25mM KCl.

Two hours post-stimulation, cultures from both batches were lysed, and RNA was harvested using a standard protocol. Enrichment PCR for the sensor barcode was performed on each library. After sample indexing and KAPA quantification, the samples were pooled together. The pooling strategy ensured that each sample from Batch 1 had a coverage of 10 million reads, while each sample from Batch 2 had a coverage of 20 million reads.

As a stimulation quality control in samples, qRT-PCR was performed against endogenous and sensor transcripts. In Batch 1, relative to Unstimulated samples, BDNF stimulated samples show a ~3-fold increase for *Luciferase* transcript and ~5-fold increase for *MmBDNF pIV* transcripts. Subsequently, for KCl stimulated samples there is a ~15-fold increase for *Luciferase* transcript and ~100-fold increase for *MmBDNF pIV* transcripts (Figure 2.3.C). Similarly for Batch 2 samples stimulation effect has been observed for KCl stimulated samples for both *MmBDNF pIV* transcripts and *Luciferase* transcripts.

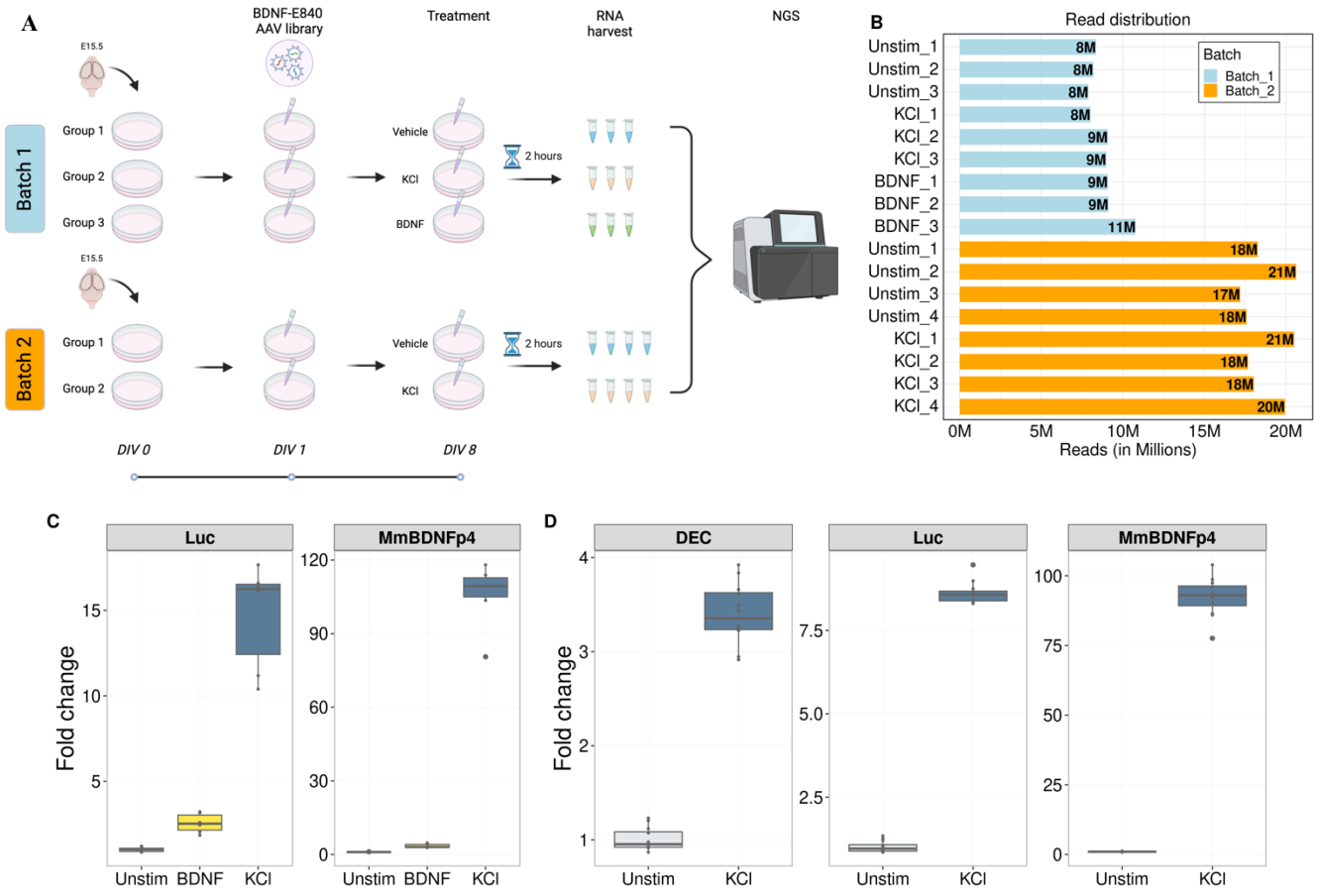

Figure 36 TargetFinder assay identifies modulators of BDNF-E840 sensor

(A) Schematic representation of cell culture experiment. Two independent primary cortical neurons cultures were prepared from E15.5 wild-type mouse and plated in 15 cm dishes. Cultures were transduced with BDNF-E840 AAV library on *DIV1* and upon silencing with TTX cocktail at DIV7, they were separated onto 3 groups for Batch1 (3 replicates each) and 2 groups for Batch2 (4 replicates each). Batch1 cultures were either treated with 25mM KCl, 50 ng/µl BDNF or Vehicle and RNA was harvested at 2hr. Batch1 cultures were either treated with 25mM KCl or Vehicle and RNA was harvested at 2hr. Upon cDNA synthesis, barcode enrichment PCR and adapter PCR samples were pooled and sequencing was performed.

(B) Raw read count distribution of different sample libraries. Batch 1 and Batch 2 samples were sequenced with a coverage of 10 million and 20 million each, respectively.

(C) Quantitative real-time PCR (qRT-PCR) for individual samples shows stimulation relative to Unstimulated control for Batch 1 against endogenous transcript, MmBDNF pIV and sensor specific transcript, Luciferase. Wilcox test was performed and p-value was less than 0.05

(D) qRT-PCR for Batch 2 samples showing stimulation. Wilcox test was performed and p-value is less than 0.05 .

4.2.2.2 TargetFinder assay BDNF-E840 samples quality assessment

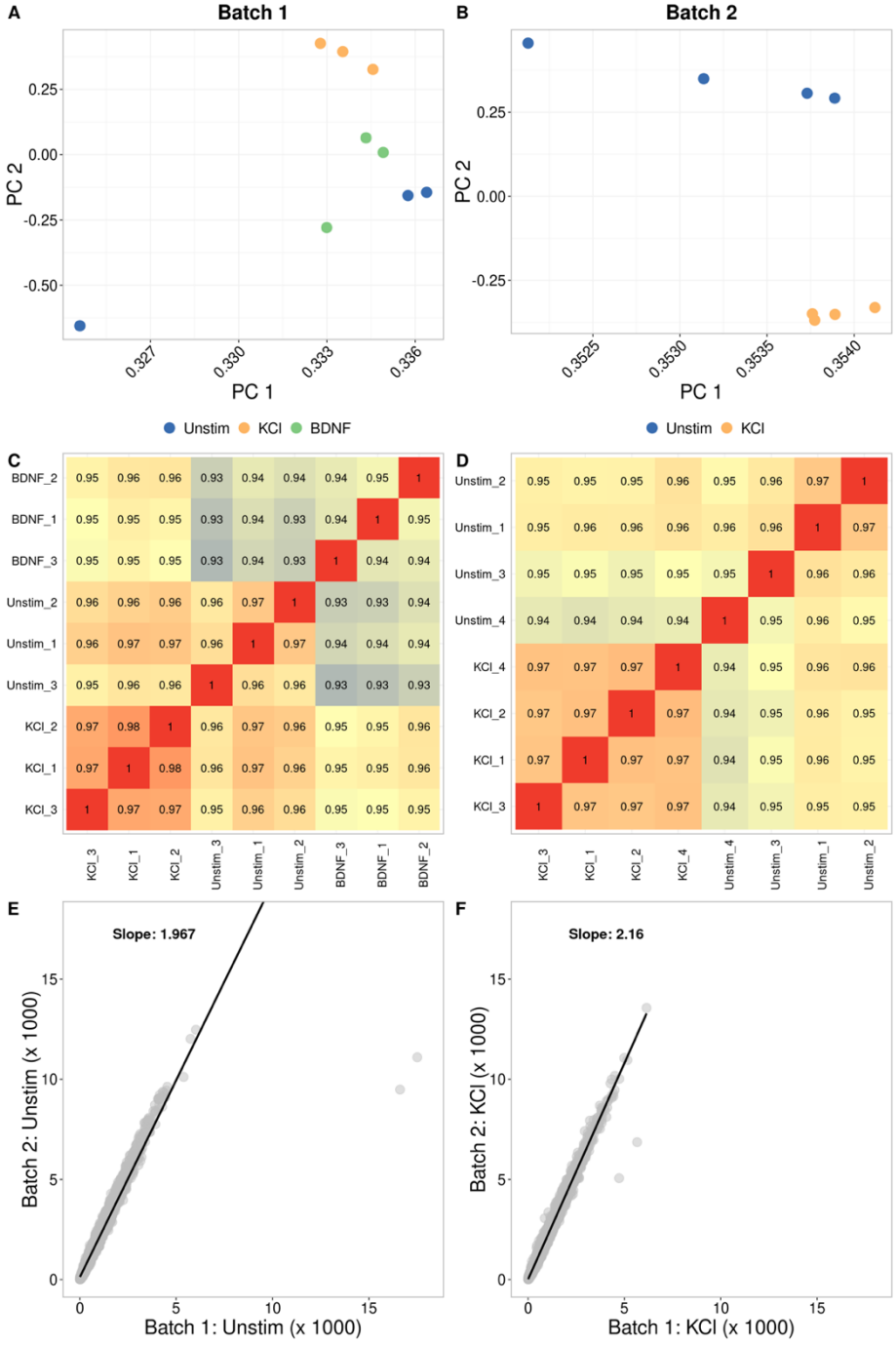

Figure 37 TargetFinder assay BDNF-E840 samples quality assessment

(A,B) PCA plots showing variability due to stimulation and sample replicates in principal component 1 and 2.

(C,D) Normalized read counts of samples are clustered hierarchically, and the Pearson correlation values between samples are shown in each tile of the heatmap.

(E) Linear correlation plot between average normalized counts of unstimulated sample from Batch 1 and Batch 2. Each point on the plot represents a pair of samples, and the slope of the linear regression line indicates the degree of correlation between the two batches.

(F) Linear correlation plot between average normalized counts of KCl sample from Batch 1 and Batch 2.

To ensure the removal of low-quality and less reliable sensor activity data points, a thorough quality assessment of samples and batches was conducted. Initially, pre-filtering was applied to the raw counts, where rows with a count of at least 10 for individual samples were filtered out. Subsequently, the raw counts underwent rlog transformation.

Principal Component Analysis (PCA) was then employed to scrutinize treatment covariates and potential technical variability among samples within each batch. PC1 and PC2 collectively accounted for over 98% of the variance in both batches. Unstimulated and stimulated (KCl and/or BDNF) sample replicates exhibited cohesive clustering, underscoring between replicates similarity. However, a single unstimulated sample from Batch 1 displayed elevated variance across both principal components (Figure 37 A).

Furthermore, sample-to-sample distances were computed to facilitate hierarchical clustering, elucidating similarities, and dissimilarities between samples. Conditional replicates demonstrated higher correlations, while correlations between conditions were subtly lower (Figure 37 C,D). Based on both PCA and correlation heatmap analyses, it was determined that all individual samples from both batches would proceed to the subsequent step (Figure A-D).

To quantify sensor activity count disparities between batches, the correlation of average normalized counts was computed. For the unstimulated condition, the degree of correlation was indicated by a regression line with a slope of 1.967, suggesting a strong correlation (Figure 37 E). This observation remained consistent for the KCl conditions, where the slope was 2.16 (Figure 37 F). These findings suggest that in addition to the intended sequencing coverage differences, both batches exhibit a high level of correlation.

4.2.2.3 Differential expression analysis to identify modulators of BDNF-E840 sensor

Differential expression analysis was conducted utilizing the *DESeq2* package with default parameters. To identify Differentially Sensor Modulators (DSMs), a volcano plot was employed, highlighting variations in fold change in sensor activity indicative of the type of modulator affecting the BDNF-E840 sensor. DSMs meeting the criteria of an absolute average fold change of >= 1 and a p-value <= 0.05 were considered significant. Based on the directionality of average fold change, DSMs were categorized as either "up" or "down," denoting negative or positive regulators of the BDNF-E840 sensor, respectively.

Remarkably, the TargetFinder assay revealed a prevalence of negative regulators compared to positive regulators in both KCl and BDNF samples. Furthermore, to visualize the intersections between the results of the three differential

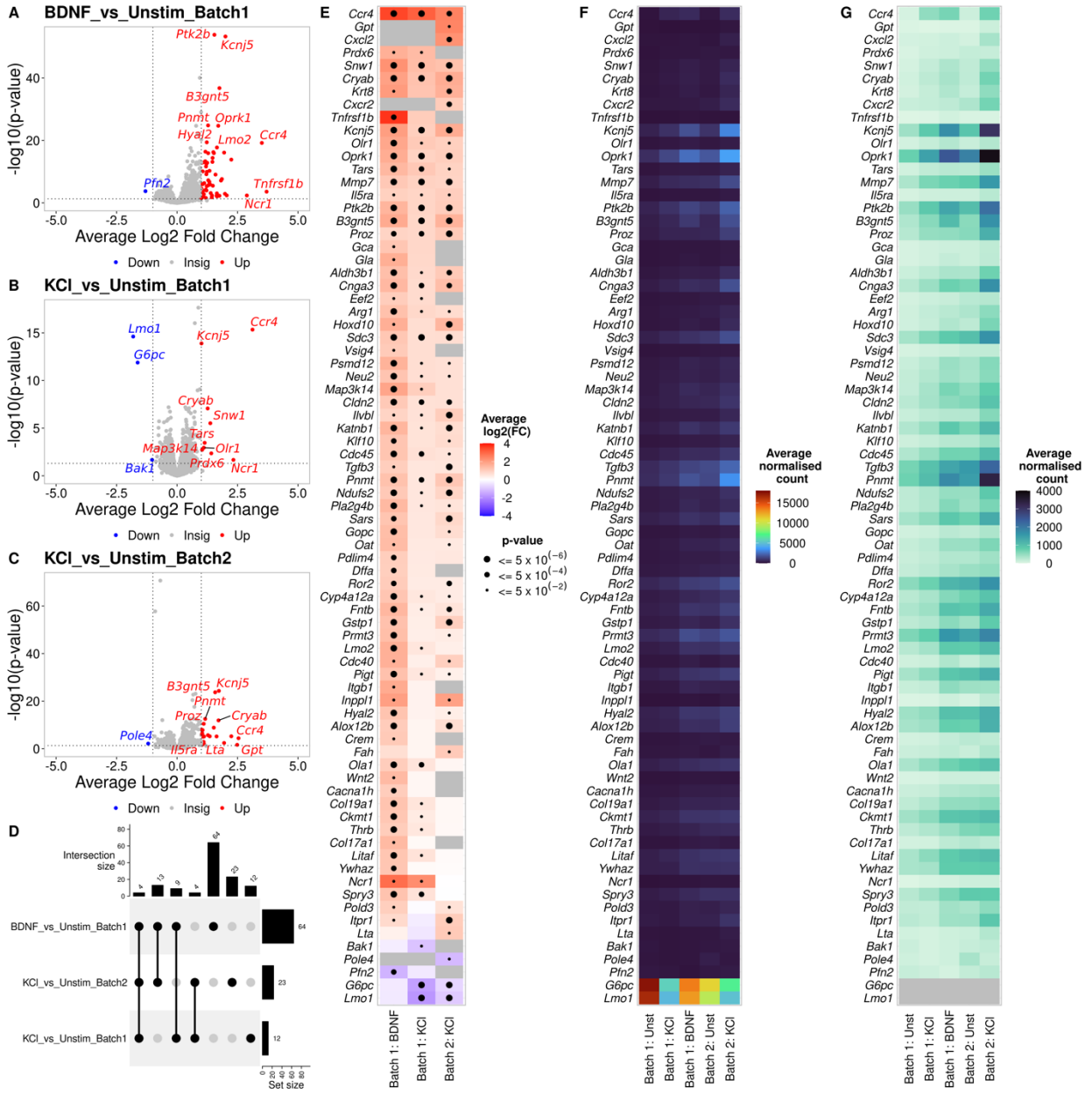

Figure 38 Differential Analysis identifies modulators of BDNF-E840 sensor.

Volcano plots showing results of differential analysis. Vertical and horizontal dotted lines indicate the average log2 fold change threshold and p-value threshold, respectively. Negative and positive modulators were depicted with red and blue respectively.

(A) KCl versus Unstimulated samples from Batch 1.

(B) KCl versus Unstimulated samples from Batch 2.

(C) BDNF versus Unstimulated samples from Batch 1.

(D) UpSet plot to shows DSMs overlap between 3 differential analyses.

(E) Average fold-change of DSMs from all 3 assays are represented by different color shades. Size of the dot represents level of significance.

(F, G) Average normalized read count of DSMs from all 3 assays are represented by different color shades.

analyses, UpSet plots were utilized. Notably, the KCl versus Unstimulated differential expression analysis exhibited a relatively low overlap of 8. Additionally, given KCl's recognized potency as a stimulant relative to BDNF, a greater number of DSMs were identified in the BDNF differential analysis.

However, these findings were unexpected, possibly attributable to biological variability among the animals or other unaccounted covariates. Further investigation may be warranted to elucidate the underlying factors contributing to these observations.

4.2.2.4 Over-Representation Analysis (ORA)

Over-Representation Analysis (ORA) was conducted on Differentially Sensor Modulators (DSMs) identified from the KCl and BDNF differential analyses. Given that most DSMs act as negative modulators of sensor activity, all the biological pathways show a positive enrichment ratio.

A noteworthy observation emerged from the analysis, indicating the presence of 13 shared DSMs between both differential analyses. Consequently, the enriched pathways predominantly encompassed neuron-specific categories, reflecting commonalities across both stimulation conditions.

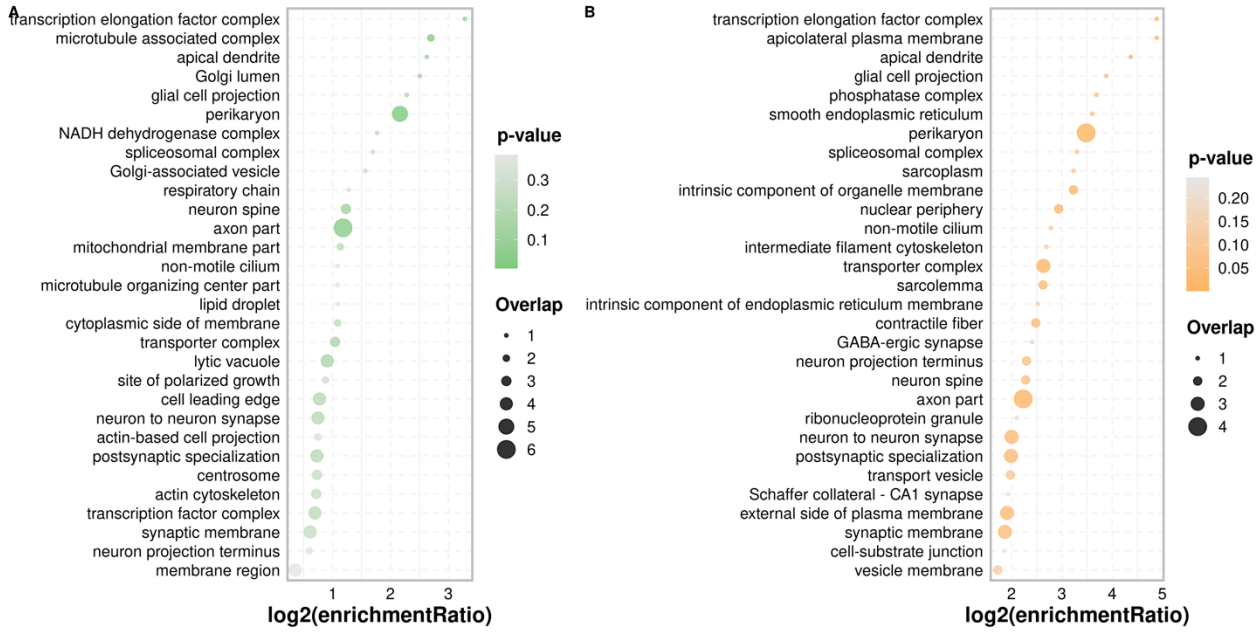

Figure 39 Dot plot showing results of Over-representation analysis.

(A) DSMs from Batch 1, BDNF vs Unstimulated samples were used.

(B) DSMs from Batch 2, KCl vs Unstimulated samples were used.

However, it is essential to note that the enriched pathways associated with DSMs from the BDNF differential analysis displayed relatively lower statistical significance compared to those from the KCl differential analysis. This discrepancy may signify distinct regulatory mechanisms or varying degrees of involvement in biological processes between the two conditions.

These findings underscore the complex interplay between different signaling pathways and the dynamic nature of cellular responses to external stimuli, shedding light on potential avenues for further investigation into the molecular mechanisms underlying sensor modulation by KCl and BDNF.

5 Discussion

5.1 Chapter 1

5.1.1 TargetFinder assay on E-SARE sensor identifies genetic modulators of neuronal activity from developmental perspective

In our investigation, we aimed to delve into the developmental nuances of synaptic plasticity through the utilization of the TargetFinder assay, employing E-SARE as the sensor. Building upon the foundational work by (Herholt et al., 2018) who initially delineated modulators of the E-SARE sensor, we sought to refine our understanding by introducing gene knockdown at an earlier developmental stage, specifically at *DIV1* within *in-vitro* primary mouse cortical neurons.

Our rationale for this developmental focus stems from the well-documented progression of primary neuronal cultures, where cells transition from a non-polar state to the emergence of primary neurites at *DIV1-3*, followed by the development of secondary and tertiary neurites by *DIV6-9* (Baj et al., 2014). By initiating knockdown interventions at *DIV1*, we aimed to capture the critical early stages of neuronal development and synaptic circuit establishment, recognizing the potential impact of modulators on these processes.

Building upon the lessons learned from previous iterations of the TargetFinder assay, we endeavored to refine our experimental approach. Notably, we identified a relatively higher number of modulators in our current screen, indicating the iterative improvement in our methodology. Initial assessments focused on the efficacy of differential sensor modulators (DSMs) knockdown, with the top 10 DSMs selected for further interrogation via shRNA-Perturb-seq experiments.

5.1.2 Optimization of shRNA-Perturb-seq methodology

In our initial exploratory experiments aimed at refining the shRNA-Perturb-seq methodology, we meticulously tailored our approach, drawing insights from established Perturb-seq protocols. We specifically focused on optimizing various aspects, including plasmid design (Datlinger et al., 2017), transduction techniques (Berry and Asokan, 2016), droplet-based single-nuclei RNA sequencing (Fischer and Ayers, 2021), and downstream data analysis (Dixit et al., 2016; Jin et al., 2020; Love et al., 2014; Santinha et al., 2023).

First, we focused on robust whole-cell expression of EGFP-Pert-BC transcript by using *hSyn1* promoter, facilitating its direct capture in the genomic transcriptome library and avoid the incomplete PCR amplification induced chimeras (Adamson et al.,

2016; Dixit et al., 2016; Jin et al., 2020). For approximately 30% of the cells, we directly captured Pert-BC from transcriptomic reads (Figure 20). Possibly with improved single nuclei protocol; we can improve the median genes per cell and that will improve the direct capture of Pert-BC (Section 4.1.3.3).

Subsequently, to achieve uniform knockdown levels across all cells. We meticulously investigated the optimal Multiplicity of Infection (MOI) to minimize the occurrence of multiple infections and possibly ensure a homogenous transcriptome profile (Section 4.1.2.2).

Finally, to effectively mitigate the potential confounding effects of cross-transduction by the perturbant we refined an in-suspension transduction protocol. Earlier studies used pooled libraries method for introducing perturbation (Adamson et al., 2016; Dixit et al., 2016; Jin et al., 2020; Replogle et al., 2022). However, we intentionally wanted to avoid library approach due to multiple transductions induced variance in transcriptomics profile and secondly due to barcode swapping during library preparation reported in many studies (Xie et al., 2018). We cannot claim where our approach stands compared to previous studies, however we observed approximately 15% cells were identified to carry different Pert-BC for shRNA targeting different transcripts (Figure 20).

5.1.3 shRNA-Perturb-seq quality assessment

After conducting single-cell RNA sequencing using the standard protocol from 10X Genomics, we assessed the distribution of reads for both transcriptomics and Dial-out PCR samples, finding them to align with expectations. Leveraging two different methods for perturbation to cell identity, we observed that Dial-out PCR yielded a relatively higher number of cell perturbation identities compared to direct capture from transcriptomics reads (Figure 20). This finding is consistent with prior research findings (Dixit et al., 2016; Jin et al., 2020), highlighting that robust expression of shRNA-BC alone may not suffice for direct capture from transcriptome reads. To ensure the reliability of our analysis, we exclusively utilized cells with non-conflicting perturbation identities for further investigation.

The median number of genes detected per cell averaged approximately 550 across all samples, given the nature of the assay focusing on single nuclei rather than whole cells. We were unable to reliably confirm knockdown efficacy through transcriptomic analysis. However, unpublished data from our laboratory indicate that using an Iodixanol gradient-based method significantly improves the quality of nuclei samples, thereby enhancing the overall quality of the transcriptomic libraries. Anyhow, all four samples passed standard quality control metrics (Figure 21) without any notable batch effects (Butler et al., 2018; Hao et al., 2021; Satija et al., 2015; Stuart et al., 2019).

5.1.4 Annotating Cell Types and Overcoming Challenges in Cluster Characterization

Moving forward, we proceeded to annotate cell types based on canonical marker gene expression, utilizing various published single-cell datasets to characterize clusters (Yao et al., 2021). While we successfully identified GABAergic neurons, astrocytes, and oligodendrocytes using marker genes, we encountered challenges in characterizing certain clusters (Figure 22 A-D). Notably, the Glutamatergic cluster proved difficult to characterize due to potential limitations in expressing canonical marker genes under *in-vitro* conditions. To address this, we employed the *FindMarker()* function of Seurat to conduct differential expression analysis between clusters (Figure 22 E), revealing unique marker genes for each cluster, which will serve as a template for further characterizing cell types in *in-vitro* mouse primary cortical neurons.

5.1.5 Treatment-Specific transcriptional responses

Given our focus on perturbed cells, we concentrated our efforts on the Glutamatergic neuron cluster, ensuring an adequate sample size for analysis. Initially, we validated the efficacy of treatments by comparing our scRNA-seq results with available RNAseq datasets from individually stimulated primary cortical cultures. Remarkably, we observed similar trends in the expression of the most known treatment-specific responding genes (Schaukowitch et al., 2017) in our single-cell dataset (Figure 23 D-F).

Furthermore, we assessed the performance of activity-regulated genes (Tyssowski et al., 2018), finding that the Perturb-seq assay effectively captured primary and secondary response genes. Notably, BIC and AMPA treatments exhibited distinct transcriptional profiles, indicative of specific cellular responses associated with different treatments (Figure 23 G-I).

5.1.6 Pseudo-bulk differential analysis identifies perturbation only and combined treatment and perturbation transcriptional response

In our analysis of perturbation effects, we initially conducted pseudo-bulk analysis followed by Principal Component Analysis (PCA) to assess the variance explained by each principal component (PC), focusing on PC1, PC2, and PC3. Notably, treatment effects were prominent in the first three PCs, with the BIC and AMPA treatment groups exhibiting distinct separation from the Unt and TTX groups (Figure 24).

Subsequently, we observed a relative lower fold change span in perturbation-only effects, indicating subtle perturbation effects (Figure 26). Interestingly, when

comparing differentially expressed genes (DEGs) between treatment groups, we found minimal overlap, suggesting that different treatment conditions trigger distinct pathways while modulating the same phenotype (Figure 28). This underscores the treatment-specific nature of perturbation effects, although we acknowledge the potential presence of false positives, necessitating individual validation for mechanistic insights.

Moreover, our analysis revealed a decent fold change span in perturbation and treatment effects, predominantly driven by treatment-specific DEGs (Figure 27). While there was a relatively higher overlap between differential analyses across treatment and perturbation groups, each individual perturbation and treatment group still exhibited many unique DEGs (Figure 29).

5.1.7 GSEA reveals Perturbation effect upon AMPA treatment

Further pathway analysis at the perturbation-only effect and perturbation + treatment effect levels uncovered enriched pathways associated with specific treatments. Notably, while AMPA treatment showed enriched pathways, BIC treatment did not (Figure 30). This observation aligns with the hypothesis that broad stimulation, as seen with BIC, may lead to increased transcription globally, diluting out pathway-specific genes and hence not meeting the significant threshold.

Additionally, KEGG pathway analysis revealed a positive enrichment of biochemical pathways associated with eukaryotic translation and energy metabolism across all perturbations (Figure 31 A). However, only perturbations with efficient knockdowns resulted in a significant q-value threshold. Conversely, all perturbations exhibited negative enrichment for neuron-specific pathways such as "Long term potentiation" and "Axon guidance." Notably, perturbations targeting calcium signaling pathways showed negative enrichment, suggesting potential regulatory roles of these genes in calcium signaling pathways (Figure 31 A, B).

Furthermore, GO-CC enrichment analysis predominantly showed negatively enriched neuron-specific pathways, with specific knockdowns resulting in negative enrichment of synaptic membrane and post-synaptic membrane regions (Figure 31 E). GO-BP and Reactome enrichment pathways displayed positive enrichment in metabolic and biochemical pathways due to perturbation (Figure 31 B). Interestingly, neurotransmitter receptors and post-synaptic signal transmission pathways were enriched upon knockdown of specific genes (Figure 31).

5.1.8 Differential Analysis and Pathway Enrichment results helps validating the modulators of E-SARE sensor

Lastly, we conducted perturbation and treatment differential analysis against either Untreated scramble or TTX scramble to validate our TargetFinder assay and

assess E-SARE modulators with or without basal activity. Our observations supported our hypothesis that perturbation leads to positive enrichment of pathways related to neurodevelopment relative to scramble control, indicating altered synaptic activity influenced by developmental genes (Figure 33). Moreover, perturbations affecting only neurodevelopmental pathways were positively enriched, while basal activity did not significantly alter pathway enrichment patterns.

5.1.9 Methodological Insights and Future Directions

This study stands out due to several distinctive features, particularly the use of shRNA for gene knockdown in mouse primary cortical neurons. In contrast, previous research has predominantly employed the CRISPR-Cas9 system for gene knockdown (Adamson et al., 2016; Dixit et al., 2016; Jin et al., 2020; Replogle et al., 2022; Santinha et al., 2023). Although further empirical validation is essential to understand the mechanistic effects of these perturbations, the limitations associated with shRNA knockdown cannot be ignored. Additionally, shRNA-PerturbSeq was used as a validation tool for the hits from the TargetFinder assay. Recent studies that employed an image-based readout have suggested it is more robust compared to an NGS-based readout (Boggess et al., 2024), primarily due to relatively high noise level using transcriptional sensor. Further empirical studies are required to compare these two methodologies.

5.2 Chapter 2

5.2.1 Characterization of BDNF-E840 as sensor

To evaluate the temporal performance of three candidate sensors in primary mouse cortical neurons was guided by prior knowledge and the need to identify an optimal sensor for subsequent experiments. Following protein read-out analysis, the enhancer -840 bp (BDNF-E840) sensor emerged as the most promising candidate due to its robust sensor strength (Figure 34 B,C). Importantly, this sensor was selected based on its novelty relative to the well-studied native *Bdnf* promoters I and IV, presenting an opportunity to explore previously unexplored aspects of BDNF signaling dynamics.

To ensure the reliability and reproducibility of our experimental assays, we performed additional optimization steps. Given that the TargetFinder read-out relies on next-generation sequencing, we conducted a temporal quantitative real-time PCR to determine the optimum lysis time for two endogenous genes. Interestingly, both BDNF and KCl stimulation elicited maximum fold-change of *Bdnf* gene expression at 4 hours post-stimulation. However, *Npas4*, a well-characterized gene associated with KCl stimulation, exhibited peak expression at 2 hours post-stimulation (Figure 35 B). Based on these findings, we fixed the stimulation time at 2 hours for subsequent assays to capture the maximum biological effects of BDNF and KCl stimulation.

5.2.2 TargetFinder assay with BDNF-E840 as sensor

Modulators for BDNF-E840 sensor were studied in 2 independent assays. The motivation behind this is to evaluate the reproducibility of the experiments and identify reliable modulators independent of common covariates like in-vitro cell culture, experimental conditions, and sequencing depth.

Quality control step was employed before NGS for treatment effect, qRT-PCR of individual samples were done. Although significant stimulation effect was observed in either assay, however *Luc* transcripts which is an indicator for sensor activity have a small difference between batches upon KCl stimulation.

Further into analysis quality assessment was performed on samples. Principal component analysis shows variance between treatment groups and low variance between replicates. Sample-to-sample correlation within treatment group is very high and cluster together. However, within treatment groups, correlation is not that low either. Both these observations indicate the subtle effect on change in Sensor activity upon stimulation.

We also took the opportunity of understanding the robustness of the assay with different batches of the experiment. Between batches, the covariates are *in-vitro* culture conditions and downstream sample handling keeping the AAV library and all other parts of the sample processing strictly common. We also added a covariate at the level of sequencing depth to understand if differences in sequencing depth also affect the assay's robustness. We have observed a strong linear correlation of average read counts between the batches irrespective of treatment.

Differential analysis between treatment (KCl or BDNF) group and unstimulated group was performed to identify drug-induced pathway modulators of BDNF-E840 sensor. Consistent with our observations from previous analysis, we identified modulators which upon knock down increase's sensor activity (Negative regulators). To our surprise, KCl being a stronger stimulant relative to BDNF promoter in the temporal luciferase assay (Figure 38 B,C and Figure 38 C,D), still the number of DSMs is considerably less in KCl versus Unstimulated differential analysis from both batches. Possibly reason of this observation is due to the strength off KCl stimulation leads to increase in transcriptomic profile globally. Hence, identifying DSMs using differential analysis is challenging. Nevertheless, the number of common DSMs and their directionality shows that is the Sensor performance is robust.

However, when we compared DSMs between the two batches for KCl versus Unstimulated, we found novel modulators in Batch 2. This discrepancy is appearing as a result of pre-filtering done before DESeq2 analysis and for certain DSMs could not qualify filtering threshold. This advocates for sequencing depth impact on these assay and hence extra caution about finding biological interpretation of these DSMs.

All 3 assays yield very few positive regulators of sensor. *G6pc* and *Lmo1* have one of the highest background sensor activities. *G6pc* (Glucose-6-phosphatase, catalytic subunit) is a key player in glucose homeostasis and energy metabolism. Upon induction by GDNF in SH-SY5Y cell lines, *G6pc* shows an upregulation and is implicated in endoplasmic reticulum-associated cell differentiation (Chen et al., 2017). In this study, knockdown of *G6pc* results in an increase in sensor activity. Perhaps this observation indicates a compensatory mechanism in cortical cultures upon G6pc knock down. On the other hand, *Lmo1* (LIM Domain Only 1) is a transcriptional regulator essential for embryonic development. In contrast to unstimulated groups upon KCl stimulation sensor activity goes down with significant fold change. LIM protein genes have been shown to be differentially regulated by neuronal activity (Hinks et al., 1997). The precise mechanisms by which *Lmo1* contributes to neurodevelopmental phenotypes are still under investigation. *Pfn2* (*Profilin 2)* is a positive regulator in BDNF assay. *Pfn2* has roles in regulating actin dynamics and cytoskeletal organization. In neurons, *Pfn2* plays a role in neuronal development and synaptic plasticity (maybe via vesicle trafficking and intracellular transport) (Pilo Boyl et al., 2007).

Ccr4, Cryab, Kcnj5, Snw1 are common negative regulators across all 3 screens. *Ccr4 (C-C Motif Chemokine Receptor 4)* is a Chemokine CC receptors regulates survival and outward chemotactic migration of progenitor cells during embryonic and postnatal CNS development (Dziembowska et al., 2005). Possibly *Ccr4* knockdown leads to activation of E840-Bdnf sensor as a compensatory mechanism. Not enough related studies were found for *Cryab, Kcnj5 and Snw1* knockdown *and Bdnf* expression.

Further empirical validation is required to understand the DSMs relation to E840-Bdnf sensor activity.

5.3 Limitations

5.3.1 Sensitivity and Specificity of Genetic Sensors

One significant limitation is the sensitivity and specificity of the genetic sensors used in the assay. Genetic sensors like E-SARE and BDNF-E840 rely on the expression of reporter genes to indicate neuronal activity. However, the reporter gene expression may not fully capture the dynamic and complex nature of neuronal activity and synaptic plasticity. This can result in a partial or skewed representation of the true biological responses, potentially leading to false positives or negatives in identifying modulators.

5.3.2 Temporal Resolution and Timing of Interventions

Another limitation is the temporal resolution of the assay. The timing of gene knockdown interventions at *DIV1* and subsequent measurements may not perfectly align with the critical windows of neuronal development and synaptic changes. The fixed time points for stimulation and analysis may miss transient or delayed responses (Figure 23 G-I; 35 B; 38), limiting the assay's ability to capture the full spectrum of gene expression changes over time.

5.3.3 Variability in *in-vitro* Culture Conditions

Variability in *in-vitro* culture conditions can also impact the reproducibility and reliability of the findings (Figure 38). Differences in culture medium composition, cell density, and handling procedures can introduce variability that affects neuronal development and gene expression profiles. Although steps were taken to standardize conditions, inherent biological variability remains a challenge.

5.3.4 Technical Limitations of shRNA-Mediated Knockdown

The use of shRNA for gene knockdown presents its own set of limitations. shRNA-mediated knockdown can lead to off-target effects, where unintended genes are silenced, potentially confounding the results. Additionally, the efficiency of shRNA

knockdown can vary, resulting in incomplete gene silencing that may not fully reveal the functional role of the targeted genes.

5.3.5 Limitations in Single-Cell RNA Sequencing

Single-cell RNA sequencing, while powerful, has limitations in capturing the complete transcriptomic landscape of individual cells. The average number of genes detected per cell was relatively low (around 550 genes), which may omit important gene expression changes and lead to incomplete data interpretation (Figure 21). Furthermore, the resolution of single-cell data may not be sufficient to distinguish closely related cell types or subtle phenotypic differences (Figure 26-33).

5.3.6 Transition from NGS to Image-Based Readouts in Single-Cell Assays

Comprehended from (Chen et al., 2023)

Higher Spatial Resolution: Image-based techniques allow for the visualization of gene expression at a single-cell level with high spatial resolution. This can provide more detailed insights into cellular morphology and the spatial organization of gene expression patterns, which are often lost in bulk sequencing approaches.

Dynamic and Temporal Measurements: Live-cell imaging enables real-time monitoring of cellular processes and gene expression changes over time. This dynamic observation can capture transient and immediate responses to stimuli, providing a more comprehensive temporal profile of cellular activities.

Reduction of Sequencing Bias: Image-based methods can minimize the biases introduced during sample preparation, amplification, and sequencing in NGS. This can lead to more accurate quantification of gene expression levels and reduce the occurrence of false positives or negatives.

References

Adamson, Britt, Thomas M. Norman, Marco Jost, Min Y. Cho, James K. Nuñez, Yuwen Chen, Jacqueline E. Villalta, et al. "A Multiplexed Single-Cell CRISPR Screening Platform Enables Systematic Dissection of the Unfolded Protein Response." Cell 167, no. 7 (December 15, 2016): 1867-1882.e21. https://doi.org/10.1016/j.cell.2016.11.048.

Adil, Asif, Vijay Kumar, Arif Tasleem Jan, and Mohammed Asger. "Single-Cell Transcriptomics: Current Methods and Challenges in Data Acquisition and Analysis." Frontiers in Neuroscience 15 (2021): 591122. https://doi.org/10.3389/fnins.2021.591122.

Ahmed, Mai, Julien Muffat, and Yun Li. "Understanding Neural Development and Diseases Using CRISPR Screens in Human Pluripotent Stem Cell-Derived Cultures." Frontiers in Cell and Developmental Biology 11 (2023): 1158373. https://doi.org/10.3389/fcell.2023.1158373.

Aid, Tamara, Anna Kazantseva, Marko Piirsoo, Kaia Palm, and Tõnis Timmusk. "Mouse and Rat BDNF Gene Structure and Expression Revisited." Journal of Neuroscience Research 85, no. 3 (February 15, 2007): 525–35. https://doi.org/10.1002/jnr.21139.

Alberts B, Johnson A, Lewis J, et al. Molecular Biology of the Cell. 4th edition. New York: Garland Science, 2002. https://www.ncbi.nlm.nih.gov/books/NBK21054/.

Ali, Muhammad, Tianxia Yang, Hai He, and Yu Zhang. "Plant Biotechnology Research with Single-Cell Transcriptome: Recent Advancements and Prospects." Plant Cell Reports 43, no. 3 (February 21, 2024): 75. https://doi.org/10.1007/s00299-024-03168-0.

Ancot, F., B. Foveau, J. Lefebvre, C. Leroy, and D. Tulasne. "Proteolytic Cleavages Give Receptor Tyrosine Kinases the Gift of Ubiquity." Oncogene 28, no. 22 (June 4, 2009): 2185–95. https://doi.org/10.1038/onc.2009.88.

Baj, Gabriele, Angela Patrizio, Alberto Montalbano, Marina Sciancalepore, and Enrico Tongiorgi. "Developmental and Maintenance Defects in Rett Syndrome Neurons Identified by a New Mouse Staging System in Vitro." *Frontiers in Cellular Neuroscience* 8 (2014): 18. https://doi.org/10.3389/fncel.2014.00018.

Beirute-Herrera, Julianne, Beatriz López-Amo Calvo, Frank Edenhofer, and Christopher Esk. "The Promise of Genetic Screens in Human in Vitro Brain Models." Biological Chemistry 405, no. 1 (January 29, 2024): 13–24. https://doi.org/10.1515/hsz-2023-0174.

Berry, Garrett Edward, and Aravind Asokan. "Cellular Transduction Mechanisms of Adeno-Associated Viral Vectors." Current Opinion in Virology 21 (December 2016): 54–60. https://doi.org/10.1016/j.coviro.2016.08.001.

Bito, H., K. Deisseroth, and R. W. Tsien. "CREB Phosphorylation and Dephosphorylation: A Ca(2+)- and Stimulus Duration-Dependent Switch for Hippocampal Gene Expression." Cell 87, no. 7 (December 27, 1996): 1203–14. https://doi.org/10.1016/s0092-8674(00)81816-4.

Boggess, Steven C., Vaidehi Gandhi, Ming-Chi Tsai, Joanna Yu-Ying Chou, Xiaoyu Hu, Lin Yadanar, Noam Teyssier, et al. "A Massively Parallel CRISPR-Based Screening Platform for Modifiers of Neuronal Activity." bioRxiv, January 1, 2024, 2024.02.28.582546. https://doi.org/10.1101/2024.02.28.582546.

Butler, Andrew, Paul Hoffman, Peter Smibert, Efthymia Papalexi, and Rahul Satija. "Integrating Single-Cell Transcriptomic Data across Different Conditions, Technologies, and Species." Nature Biotechnology 36, no. 5 (June 2018): 411–20. https://doi.org/10.1038/nbt.4096.

Chen, Jing, Ting Wang, Xiao-Yan Zhou, Chuan-Xi Tang, and Dian-Shuai Gao. "Glucose-6-Phosphatase-α Participates in Dopaminergic Differentiation." Neurological Research 39, no. 10 (October 2017): 869–76. https://doi.org/10.1080/01616412.2017.1348681.

Chen, Tsai-Ying, Li You, Jose Angelito U. Hardillo, and Miao-Ping Chien. "Spatial Transcriptomic Technologies." Cells 12, no. 16 (August 10, 2023): 2042. https://doi.org/10.3390/cells12162042.

Chen, Wen G., Anne E. West, Xu Tao, Gabriel Corfas, Marilyn N. Szentirmay, Michele Sawadogo, Charles Vinson, and Michael E. Greenberg. "Upstream Stimulatory Factors Are Mediators of Ca2+-Responsive Transcription in Neurons." The Journal of Neuroscience: The Official Journal of the Society for Neuroscience 23, no. 7 (April 1, 2003): 2572–81. https://doi.org/10.1523/JNEUROSCI.23-07-02572.2003.

Datlinger, Paul, André F. Rendeiro, Christian Schmidl, Thomas Krausgruber, Peter Traxler, Johanna Klughammer, Linda C. Schuster, Amelie Kuchler, Donat Alpar, and Christoph Bock. "Pooled CRISPR Screening with Single-Cell Transcriptome Readout." Nature Methods 14, no. 3 (March 2017): 297–301. https://doi.org/10.1038/nmeth.4177.

Dixit, Atray, Oren Parnas, Biyu Li, Jenny Chen, Charles P. Fulco, Livnat Jerby-Arnon, Nemanja D. Marjanovic, et al. "Perturb-Seq: Dissecting Molecular Circuits with Scalable Single-Cell RNA Profiling of Pooled Genetic Screens." Cell 167, no. 7 (December 15, 2016): 1853-1866.e17. https://doi.org/10.1016/j.cell.2016.11.038.

Dolmetsch, R. E., U. Pajvani, K. Fife, J. M. Spotts, and M. E. Greenberg. "Signaling to the Nucleus by an L-Type Calcium Channel-Calmodulin Complex through the MAP Kinase Pathway." Science (New York, N.Y.) 294, no. 5541 (October 12, 2001): 333–39. https://doi.org/10.1126/science.1063395.

Dziembowska, M., T. N. Tham, P. Lau, S. Vitry, F. Lazarini, and M. Dubois-Dalcq. "A Role for CXCR4 Signaling in Survival and Migration of Neural and Oligodendrocyte Precursors." Glia 50, no. 3 (May 2005): 258–69. https://doi.org/10.1002/glia.20170.

Fischer, Juliane, and Thomas Ayers. "Single Nucleus RNA-Sequencing: How It's Done, Applications and Limitations." Emerging Topics in Life Sciences 5, no. 5 (November 12, 2021): 687–90. https://doi.org/10.1042/ETLS20210074.

Fujii, Hajime, Masatoshi Inoue, Hiroyuki Okuno, Yoshikazu Sano, Sayaka Takemoto-Kimura, Kazuo Kitamura, Masanobu Kano, and Haruhiko Bito. "Nonlinear Decoding and Asymmetric Representation of Neuronal Input Information by CaMKIIα and Calcineurin." Cell Reports 3, no. 4 (April 25, 2013): 978–87. https://doi.org/10.1016/j.celrep.2013.03.033.

Gorba, T., and P. Wahle. "Expression of TrkB and TrkC but Not BDNF mRNA in Neurochemically Identified Interneurons in Rat Visual Cortex in Vivo and in Organotypic Cultures." The European Journal of Neuroscience 11, no. 4 (April 1999): 1179–90. https://doi.org/10.1046/j.1460-9568.1999.00551.x.

Guzowski, J. F., B. L. McNaughton, C. A. Barnes, and P. F. Worley. "Environment-Specific Expression of the Immediate-Early Gene Arc in Hippocampal Neuronal Ensembles." Nature Neuroscience 2, no. 12 (December 1999): 1120–24. https://doi.org/10.1038/16046.

Han, Yingying, Dan Wang, Lushan Peng, Tao Huang, Xiaoyun He, Junpu Wang, and Chunlin Ou. "Single-Cell Sequencing: A Promising Approach for Uncovering the Mechanisms of Tumor Metastasis." Journal of Hematology & Oncology 15, no. 1 (May 12, 2022): 59. https://doi.org/10.1186/s13045-022-01280-w.

Hanson, I. M., A. Seawright, and V. van Heyningen. "The Human BDNF Gene Maps between FSHB and HVBS1 at the Boundary of 11p13-P14." Genomics 13, no. 4 (August 1992): 1331–33. https://doi.org/10.1016/0888-7543(92)90060-6.

Hao, Yuhan, Stephanie Hao, Erica Andersen-Nissen, William M. Mauck, Shiwei Zheng, Andrew Butler, Maddie J. Lee, et al. "Integrated Analysis of Multimodal Single-Cell Data." Cell 184, no. 13 (June 24, 2021): 3573-3587.e29. https://doi.org/10.1016/j.cell.2021.04.048.

Herholt, Alexander, Ben Brankatschk, Nirmal Kannaiyan, Sergi Papiol, Sven P. Wichert, Michael C. Wehr, and Moritz J. Rossner. "Pathway Sensor-Based Functional Genomics Screening Identifies Modulators of Neuronal Activity." Scientific Reports 8, no. 1 (December 4, 2018): 17597. https://doi.org/10.1038/s41598-018-36008-9.

Herholt, Alexander, Vivek K. Sahoo, Luksa Popovic, Michael C. Wehr, and Moritz J. Rossner. "Dissecting Intercellular and Intracellular Signaling Networks with Barcoded Genetic Tools." Current Opinion in Chemical Biology 66 (February 1, 2022): 102091. https://doi.org/10.1016/j.cbpa.2021.09.002.

Hing, Benjamin, Leela Sathyaputri, and James B. Potash. "A Comprehensive Review of Genetic and Epigenetic Mechanisms That Regulate BDNF Expression and Function with Relevance to Major Depressive Disorder." American Journal of Medical Genetics. Part B, Neuropsychiatric Genetics: The Official Publication of the International Society of Psychiatric Genetics 177, no. 2 (March 2018): 143–67. https://doi.org/10.1002/ajmg.b.32616.

Hinks, G. L., B. Shah, S. J. French, L. S. Campos, K. Staley, J. Hughes, and M. V. Sofroniew. "Expression of LIM Protein Genes Lmo1, Lmo2, and Lmo3 in Adult Mouse Hippocampus and Other Forebrain Regions: Differential Regulation by Seizure Activity." The Journal of Neuroscience: The Official Journal of the Society for Neuroscience 17, no. 14 (July 15, 1997): 5549–59. https://doi.org/10.1523/JNEUROSCI.17-14-05549.1997.

Huang, Eric J., and Louis F. Reichardt. "Trk Receptors: Roles in Neuronal Signal Transduction." Annual Review of Biochemistry 72 (2003): 609–42. https://doi.org/10.1146/annurev.biochem.72.121801.161629.

Inoue, Masatoshi, Nan Yagishita-Kyo, Mio Nonaka, Takashi Kawashima, Hiroyuki Okuno, and Haruhiko Bito. "Synaptic Activity-Responsive Element (SARE): A Unique Genomic Structure with

an Unusual Sensitivity to Neuronal Activity." Communicative & Integrative Biology 3, no. 5 (September 2010): 443–46. https://doi.org/10.4161/cib.3.5.12287.

Islam, Saiful, Una Kjällquist, Annalena Moliner, Pawel Zajac, Jian-Bing Fan, Peter Lönnerberg, and Sten Linnarsson. "Characterization of the Single-Cell Transcriptional Landscape by Highly Multiplex RNA-Seq." Genome Research 21, no. 7 (July 2011): 1160–67. https://doi.org/10.1101/gr.110882.110.

Jaitin, Diego Adhemar, Assaf Weiner, Ido Yofe, David Lara-Astiaso, Hadas Keren-Shaul, Eyal David, Tomer Meir Salame, Amos Tanay, Alexander van Oudenaarden, and Ido Amit. "Dissecting Immune Circuits by Linking CRISPR-Pooled Screens with Single-Cell RNA-Seq." Cell 167, no. 7 (December 15, 2016): 1883-1896.e15. https://doi.org/10.1016/j.cell.2016.11.039.

Jiang, Xueying, Feng Tian, Yang Du, Neal G. Copeland, Nancy A. Jenkins, Lino Tessarollo, Xuan Wu, et al. "BHLHB2 Controls Bdnf Promoter 4 Activity and Neuronal Excitability." The Journal of Neuroscience: The Official Journal of the Society for Neuroscience 28, no. 5 (January 30, 2008): 1118–30. https://doi.org/10.1523/JNEUROSCI.2262-07.2008.

Jin, Xin, Sean K. Simmons, Amy Guo, Ashwin S. Shetty, Michelle Ko, Lan Nguyen, Vahbiz Jokhi, et al. "In Vivo Perturb-Seq Reveals Neuronal and Glial Abnormalities Associated with Autism Risk Genes." Science (New York, N.Y.) 370, no. 6520 (November 27, 2020): eaaz6063. https://doi.org/10.1126/science.aaz6063.

Jovic, Dragomirka, Xue Liang, Hua Zeng, Lin Lin, Fengping Xu, and Yonglun Luo. "Single-Cell RNA Sequencing Technologies and Applications: A Brief Overview." Clinical and Translational Medicine 12, no. 3 (March 2022): e694. https://doi.org/10.1002/ctm2.694.

Kawashima, Takashi, Kazuo Kitamura, Kanzo Suzuki, Mio Nonaka, Satoshi Kamijo, Sayaka Takemoto-Kimura, Masanobu Kano, Hiroyuki Okuno, Kenichi Ohki, and Haruhiko Bito. "Functional Labeling of Neurons and Their Projections Using the Synthetic Activity–Dependent Promoter E-SARE." Nature Methods 10, no. 9 (September 2013): 889–95. https://doi.org/10.1038/nmeth.2559.

Kawashima, Takashi, Hiroyuki Okuno, Mio Nonaka, Aki Adachi-Morishima, Nan Kyo, Michiko Okamura, Sayaka Takemoto-Kimura, Paul F. Worley, and Haruhiko Bito. "Synaptic Activity-Responsive Element in the Arc/Arg3.1 Promoter Essential for Synapse-to-Nucleus Signaling in Activated Neurons." Proceedings of the National Academy of Sciences of the United States of America 106, no. 1 (January 6, 2009): 316–21. https://doi.org/10.1073/pnas.0806518106.

Kerschensteiner, M., E. Gallmeier, L. Behrens, V. V. Leal, T. Misgeld, W. E. Klinkert, R. Kolbeck, et al. "Activated Human T Cells, B Cells, and Monocytes Produce Brain-Derived Neurotrophic Factor in Vitro and in Inflammatory Brain Lesions: A Neuroprotective Role of Inflammation?" The Journal of Experimental Medicine 189, no. 5 (March 1, 1999): 865–70. https://doi.org/10.1084/jem.189.5.865.

Lessmann, Volkmar, Kurt Gottmann, and Marzia Malcangio. "Neurotrophin Secretion: Current Facts and Future Prospects." Progress in Neurobiology 69, no. 5 (April 2003): 341–74. https://doi.org/10.1016/s0301-0082(03)00019-4.

Liao, Yuxing, Jing Wang, Eric J. Jaehnig, Zhiao Shi, and Bing Zhang. "WebGestalt 2019: Gene Set Analysis Toolkit with Revamped UIs and APIs." Nucleic Acids Research 47, no. W1 (July 2, 2019): W199–205. https://doi.org/10.1093/nar/gkz401.

Link, W., U. Konietzko, G. Kauselmann, M. Krug, B. Schwanke, U. Frey, and D. Kuhl. "Somatodendritic Expression of an Immediate Early Gene Is Regulated by Synaptic Activity." Proceedings of the National Academy of Sciences of the United States of America 92, no. 12 (June 6, 1995): 5734–38. https://doi.org/10.1073/pnas.92.12.5734.

Lipsky, R. H., K. Xu, D. Zhu, C. Kelly, A. Terhakopian, A. Novelli, and A. M. Marini. "Nuclear Factor kappaB Is a Critical Determinant in N-Methyl-D-Aspartate Receptor-Mediated Neuroprotection." Journal of Neurochemistry 78, no. 2 (July 2001): 254–64. https://doi.org/10.1046/j.1471-4159.2001.00386.x.

Love, Michael I., Wolfgang Huber, and Simon Anders. "Moderated Estimation of Fold Change and Dispersion for RNA-Seq Data with DESeq2." Genome Biology 15, no. 12 (2014): 550. https://doi.org/10.1186/s13059-014-0550-8.

Lyford, G. L., K. Yamagata, W. E. Kaufmann, C. A. Barnes, L. K. Sanders, N. G. Copeland, D. J. Gilbert, N. A. Jenkins, A. A. Lanahan, and P. F. Worley. "Arc, a Growth Factor and Activity-Regulated Gene, Encodes a Novel Cytoskeleton-Associated Protein That Is Enriched in Neuronal Dendrites." Neuron 14, no. 2 (February 1995): 433–45. https://doi.org/10.1016/0896-6273(95)90299-6.

Ma, Xiao, Fiona J. Mandausch, Yuxin Wu, Vivek K. Sahoo, Wenbo Ma, Giovanna Leoni, Madalina Hostiuc, et al. "Comprehensive Split TEV Based Protein-Protein Interaction Screening Reveals TAOK2 as a Key Modulator of Hippo Signalling to Limit Growth." Cellular Signalling 113 (January 1, 2024): 110917. https://doi.org/10.1016/j.cellsig.2023.110917.

Macosko, Evan Z., Anindita Basu, Rahul Satija, James Nemesh, Karthik Shekhar, Melissa Goldman, Itay Tirosh, et al. "Highly Parallel Genome-Wide Expression Profiling of Individual Cells Using Nanoliter Droplets." Cell 161, no. 5 (May 21, 2015): 1202–14. https://doi.org/10.1016/j.cell.2015.05.002.

Małczyńska, Paulina, Zofia Piotrowicz, Dorota Drabarek, Józef Langfort, and Małgorzata Chalimoniuk. "[The role of the brain-derived neurotrophic factor (BDNF) in neurodegenerative processes and in the neuroregeneration mechanisms induced by increased physical activity]." Postepy Biochemii 65, no. 1 (March 22, 2019): 2–8. https://doi.org/10.18388/pb.2019_251.

Matsumoto, Tomoya, Stefanie Rauskolb, Martin Polack, Johannes Klose, Roland Kolbeck, Martin Korte, and Yves-Alain Barde. "Biosynthesis and Processing of Endogenous BDNF: CNS Neurons Store and Secrete BDNF, Not pro-BDNF." Nature Neuroscience 11, no. 2 (February 2008): 131–33. https://doi.org/10.1038/nn2038.

McClung, Colleen A., and Eric J. Nestler. "Neuroplasticity Mediated by Altered Gene Expression." Neuropsychopharmacology: Official Publication of the American College of Neuropsychopharmacology 33, no. 1 (January 2008): 3–17. https://doi.org/10.1038/sj.npp.1301544.

Minichiello, Liliana, Anna Maria Calella, Diego L. Medina, Tobias Bonhoeffer, Rüdiger Klein, and Martin Korte. "Mechanism of TrkB-Mediated Hippocampal Long-Term Potentiation." Neuron 36, no. 1 (September 26, 2002): 121–37. https://doi.org/10.1016/s0896-6273(02)00942-x.

Mowla, S. J., H. F. Farhadi, S. Pareek, J. K. Atwal, S. J. Morris, N. G. Seidah, and R. A. Murphy. "Biosynthesis and Post-Translational Processing of the Precursor to Brain-Derived Neurotrophic Factor." The Journal of Biological Chemistry 276, no. 16 (April 20, 2001): 12660–66. https://doi.org/10.1074/jbc.M008104200.

Orefice, Lauren L., Emily G. Waterhouse, John G. Partridge, Rupa R. Lalchandani, Stefano Vicini, and Baoji Xu. "Distinct Roles for Somatically and Dendritically Synthesized Brain-Derived Neurotrophic Factor in Morphogenesis of Dendritic Spines." The Journal of Neuroscience: The Official Journal of the Society for Neuroscience 33, no. 28 (July 10, 2013): 11618–32. https://doi.org/10.1523/JNEUROSCI.0012-13.2013.

Paoletti, Pierre, Camilla Bellone, and Qiang Zhou. "NMDA Receptor Subunit Diversity: Impact on Receptor Properties, Synaptic Plasticity and Disease." Nature Reviews. Neuroscience 14, no. 6 (June 2013): 383–400. https://doi.org/10.1038/nrn3504.

Picelli, Simone, Åsa K. Björklund, Omid R. Faridani, Sven Sagasser, Gösta Winberg, and Rickard Sandberg. "Smart-Seq2 for Sensitive Full-Length Transcriptome Profiling in Single Cells." Nature Methods 10, no. 11 (November 2013): 1096–98. https://doi.org/10.1038/nmeth.2639.

Pilo Boyl, Pietro, Alessia Di Nardo, Christophe Mulle, Marco Sassoè-Pognetto, Patrizia Panzanelli, Andrea Mele, Matthias Kneussel, et al. "Profilin2 Contributes to Synaptic Vesicle Exocytosis, Neuronal Excitability, and Novelty-Seeking Behavior." The EMBO Journal 26, no. 12 (June 20, 2007): 2991–3002. https://doi.org/10.1038/sj.emboj.7601737.

Pruunsild, Priit, Anna Kazantseva, Tamara Aid, Kaia Palm, and Tõnis Timmusk. "Dissecting the Human BDNF Locus: Bidirectional Transcription, Complex Splicing, and Multiple Promoters." Genomics 90, no. 3 (September 2007): 397–406. https://doi.org/10.1016/j.ygeno.2007.05.004.

Pruunsild, Priit, Mari Sepp, Ester Orav, Indrek Koppel, and Tõnis Timmusk. "Identification of Cis-Elements and Transcription Factors Regulating Neuronal Activity-Dependent Transcription of Human BDNF Gene." The Journal of Neuroscience: The Official Journal of the Society for Neuroscience 31, no. 9 (March 2, 2011): 3295–3308. https://doi.org/10.1523/JNEUROSCI.4540-10.2011.

Przybyla, Laralynne, and Luke A. Gilbert. "A New Era in Functional Genomics Screens." Nature Reviews. Genetics 23, no. 2 (February 2022): 89–103. https://doi.org/10.1038/s41576-021-00409-w.

Ramsköld, Daniel, Shujun Luo, Yu-Chieh Wang, Robin Li, Qiaolin Deng, Omid R. Faridani, Gregory A. Daniels, et al. "Full-Length mRNA-Seq from Single-Cell Levels of RNA and Individual Circulating Tumor Cells." Nature Biotechnology 30, no. 8 (August 2012): 777–82. https://doi.org/10.1038/nbt.2282.

Rauscher, Benedikt, Erica Valentini, Ulrike Hardeland, and Michael Boutros. "Phenotype Databases for Genetic Screens in Human Cells." Journal of Biotechnology 261 (November 10, 2017): 63–69. https://doi.org/10.1016/j.jbiotec.2017.06.008.

Replogle, Joseph M., Reuben A. Saunders, Angela N. Pogson, Jeffrey A. Hussmann, Alexander Lenail, Alina Guna, Lauren Mascibroda, et al. "Mapping Information-Rich Genotype-Phenotype Landscapes with Genome-Scale Perturb-Seq." Cell 185, no. 14 (July 7, 2022): 2559-2575.e28. https://doi.org/10.1016/j.cell.2022.05.013.

Rocamora, N., E. Welker, M. Pascual, and E. Soriano. "Upregulation of BDNF mRNA Expression in the Barrel Cortex of Adult Mice after Sensory Stimulation." The Journal of Neuroscience: The Official Journal of the Society for Neuroscience 16, no. 14 (July 15, 1996): 4411–19. https://doi.org/10.1523/JNEUROSCI.16-14-04411.1996.

Santinha, Antonio J., Esther Klingler, Maria Kuhn, Rick Farouni, Sandra Lagler, Georgios Kalamakis, Ulrike Lischetti, Denis Jabaudon, and Randall J. Platt. "Transcriptional Linkage Analysis with in Vivo AAV-Perturb-Seq." Nature 622, no. 7982 (October 2023): 367–75. https://doi.org/10.1038/s41586-023-06570-y.

Satija, Rahul, Jeffrey A. Farrell, David Gennert, Alexander F. Schier, and Aviv Regev. "Spatial Reconstruction of Single-Cell Gene Expression Data." Nature Biotechnology 33, no. 5 (May 2015): 495–502. https://doi.org/10.1038/nbt.3192.

Schaukowitch, Katie, Austin L. Reese, Seung-Kyoon Kim, Gokhul Kilaru, Jae-Yeol Joo, Ege T. Kavalali, and Tae-Kyung Kim. "An Intrinsic Transcriptional Program Underlying Synaptic Scaling during Activity Suppression." Cell Reports 18, no. 6 (February 7, 2017): 1512–26. https://doi.org/10.1016/j.celrep.2017.01.033.

Shaywitz, A. J., and M. E. Greenberg. "CREB: A Stimulus-Induced Transcription Factor Activated by a Diverse Array of Extracellular Signals." Annual Review of Biochemistry 68 (1999): 821–61. https://doi.org/10.1146/annurev.biochem.68.1.821.

Shieh, P. B., S. C. Hu, K. Bobb, T. Timmusk, and A. Ghosh. "Identification of a Signaling Pathway Involved in Calcium Regulation of BDNF Expression." Neuron 20, no. 4 (April 1998): 727–40. https://doi.org/10.1016/s0896-6273(00)81011-9.

Simms, Brett A., and Gerald W. Zamponi. "Neuronal Voltage-Gated Calcium Channels: Structure, Function, and Dysfunction." Neuron 82, no. 1 (April 2, 2014): 24–45. https://doi.org/10.1016/j.neuron.2014.03.016.

Steward, O., C. S. Wallace, G. L. Lyford, and P. F. Worley. "Synaptic Activation Causes the mRNA for the IEG Arc to Localize Selectively near Activated Postsynaptic Sites on Dendrites." Neuron 21, no. 4 (October 1998): 741–51. https://doi.org/10.1016/s0896-6273(00)80591-7.

Stuart, Tim, Andrew Butler, Paul Hoffman, Christoph Hafemeister, Efthymia Papalexi, William M. Mauck, Yuhan Hao, Marlon Stoeckius, Peter Smibert, and Rahul Satija. "Comprehensive Integration of Single-Cell Data." Cell 177, no. 7 (June 13, 2019): 1888-1902.e21. https://doi.org/10.1016/j.cell.2019.05.031.

Tabuchi, Akiko, Hidemichi Sakaya, Tomochika Kisukeda, Hiroshi Fushiki, and Masaaki Tsuda. "Involvement of an Upstream Stimulatory Factor as Well as cAMP-Responsive Element-Binding Protein in the Activation of Brain-Derived Neurotrophic Factor Gene Promoter I." The Journal of Biological Chemistry 277, no. 39 (September 27, 2002): 35920–31. https://doi.org/10.1074/jbc.M204784200.

Tang, Fuchou, Catalin Barbacioru, Yangzhou Wang, Ellen Nordman, Clarence Lee, Nanlan Xu, Xiaohui Wang, et al. "mRNA-Seq Whole-Transcriptome Analysis of a Single Cell." Nature Methods 6, no. 5 (May 2009): 377–82. https://doi.org/10.1038/nmeth.1315.

Tao, X., S. Finkbeiner, D. B. Arnold, A. J. Shaywitz, and M. E. Greenberg. "Ca2+ Influx Regulates BDNF Transcription by a CREB Family Transcription Factor-Dependent Mechanism." Neuron 20, no. 4 (April 1998): 709–26. https://doi.org/10.1016/s0896-6273(00)81010-7.

Tao, Xu, Anne E. West, Wen G. Chen, Gabriel Corfas, and Michael E. Greenberg. "A Calcium-Responsive Transcription Factor, CaRF, That Regulates Neuronal Activity-Dependent Expression of BDNF." Neuron 33, no. 3 (January 31, 2002): 383–95. https://doi.org/10.1016/s0896-6273(01)00561-x.

Tejeda, Gonzalo S., and Margarita Díaz-Guerra. "Integral Characterization of Defective BDNF/TrkB Signalling in Neurological and Psychiatric Disorders Leads the Way to New Therapies." International Journal of Molecular Sciences 18, no. 2 (January 28, 2017): 268. https://doi.org/10.3390/ijms18020268.

Thomas, Gareth M., and Richard L. Huganir. "MAPK Cascade Signalling and Synaptic Plasticity." Nature Reviews Neuroscience 5, no. 3 (March 2004): 173–83. https://doi.org/10.1038/nrn1346.

Thomas, Kerrie, and Alun Davies. "Neurotrophins: A Ticket to Ride for BDNF." Current Biology: CB 15, no. 7 (April 12, 2005): R262-264. https://doi.org/10.1016/j.cub.2005.03.023.

Tirassa, P., L. Manni, C. Stenfors, T. Lundeberg, and L. Aloe. "RT-PCR ELISA Method for the Analysis of Neurotrophin mRNA Expression in Brain and Peripheral Tissues." Journal of Biotechnology 84, no. 3 (December 28, 2000): 259–72. https://doi.org/10.1016/s0168-1656(00)00370-9.

Tyssowski, Kelsey M., Nicholas R. DeStefino, Jin-Hyung Cho, Carissa J. Dunn, Robert G. Poston, Crista E. Carty, Richard D. Jones, et al. "Different Neuronal Activity Patterns Induce Different Gene Expression Programs." Neuron 98, no. 3 (May 2, 2018): 530-546.e11. https://doi.org/10.1016/j.neuron.2018.04.001.

Van de Sande, Bram, Joon Sang Lee, Euphemia Mutasa-Gottgens, Bart Naughton, Wendi Bacon, Jonathan Manning, Yong Wang, et al. "Applications of Single-Cell RNA Sequencing in Drug Discovery and Development." Nature Reviews. Drug Discovery 22, no. 6 (June 2023): 496–520. https://doi.org/10.1038/s41573-023-00688-4.

Vashishta, Aruna, Agata Habas, Priit Pruunsild, Jing-Juan Zheng, Tõnis Timmusk, and Michal Hetman. "Nuclear Factor of Activated T-Cells Isoform C4 (NFATc4/NFAT3) as a Mediator of Antiapoptotic Transcription in NMDA Receptor-Stimulated Cortical Neurons." The Journal of Neuroscience: The Official Journal of the Society for Neuroscience 29, no. 48 (December 2, 2009): 15331–40. https://doi.org/10.1523/JNEUROSCI.4873-09.2009.

Wang, Jing, Suhas Vasaikar, Zhiao Shi, Michael Greer, and Bing Zhang. "WebGestalt 2017: A More Comprehensive, Powerful, Flexible and Interactive Gene Set Enrichment Analysis Toolkit." Nucleic Acids Research 45, no. W1 (July 3, 2017): W130–37. https://doi.org/10.1093/nar/gkx356.

Woo, Newton H., Henry K. Teng, Chia-Jen Siao, Cristina Chiaruttini, Petti T. Pang, Teresa A. Milner, Barbara L. Hempstead, and Bai Lu. "Activation of p75NTR by proBDNF Facilitates Hippocampal Long-Term Depression." Nature Neuroscience 8, no. 8 (August 2005): 1069–77. https://doi.org/10.1038/nn1510.

Wu, Tianzhi, Erqiang Hu, Shuangbin Xu, Meijun Chen, Pingfan Guo, Zehan Dai, Tingze Feng, et al. "clusterProfiler 4.0: A Universal Enrichment Tool for Interpreting Omics Data." Innovation (Cambridge (Mass.)) 2, no. 3 (August 28, 2021): 100141. https://doi.org/10.1016/j.xinn.2021.100141.

Xie, Shiqi, Anne Cooley, Daniel Armendariz, Pei Zhou, and Gary C. Hon. "Frequent sgRNA-Barcode Recombination in Single-Cell Perturbation Assays." PloS One 13, no. 6 (2018): e0198635. https://doi.org/10.1371/journal.pone.0198635.

Yang, Jianmin, Lauren C. Harte-Hargrove, Chia-Jen Siao, Tina Marinic, Roshelle Clarke, Qian Ma, Deqiang Jing, et al. "proBDNF Negatively Regulates Neuronal Remodeling, Synaptic Transmission, and Synaptic Plasticity in Hippocampus." Cell Reports 7, no. 3 (May 8, 2014): 796–806. https://doi.org/10.1016/j.celrep.2014.03.040.

Yang, Jianmin, Chia-Jen Siao, Guhan Nagappan, Tina Marinic, Deqiang Jing, Kelly McGrath, Zhe-Yu Chen, et al. "Neuronal Release of proBDNF." Nature Neuroscience 12, no. 2 (February 2009): 113–15. https://doi.org/10.1038/nn.2244.

Yao, Zizhen, Cindy T. J. van Velthoven, Thuc Nghi Nguyen, Jeff Goldy, Adriana E. Sedeno-Cortes, Fahimeh Baftizadeh, Darren Bertagnolli, et al. "A Taxonomy of Transcriptomic Cell Types across the Isocortex and Hippocampal Formation." Cell 184, no. 12 (June 10, 2021): 3222-3241.e26. https://doi.org/10.1016/j.cell.2021.04.021.

Yeh, Che-Ming, Chiung-Chun Huang, and Kuei-Sen Hsu. "Prenatal Stress Alters Hippocampal Synaptic Plasticity in Young Rat Offspring through Preventing the Proteolytic Conversion of Pro-Brain-Derived Neurotrophic Factor (BDNF) to Mature BDNF." The Journal of Physiology 590, no. 4 (February 15, 2012): 991–1010. https://doi.org/10.1113/jphysiol.2011.222042.

You, He, and Bai Lu. "Diverse Functions of Multiple Bdnf Transcripts Driven by Distinct Bdnf Promoters." Biomolecules 13, no. 4 (April 6, 2023): 655. https://doi.org/10.3390/biom13040655.

Yu, Guangchuang, Li-Gen Wang, Yanyan Han, and Qing-Yu He. "clusterProfiler: An R Package for Comparing Biological Themes among Gene Clusters." Omics: A Journal of Integrative Biology 16, no. 5 (May 2012): 284–87. https://doi.org/10.1089/omi.2011.0118.

Zhai, Shenyu, Eugene D. Ark, Paula Parra-Bueno, and Ryohei Yasuda. "Long-Distance Integration of Nuclear ERK Signaling Triggered by Activation of a Few Dendritic Spines." Science (New York, N.Y.) 342, no. 6162 (November 29, 2013): 1107–11. https://doi.org/10.1126/science.1245622.

Acknowledgements

First and foremost, I would like to express my deepest gratitude to my advisor, Prof. Dr. Moritz Rossner, for his exceptional guidance, continuous support, and unwavering encouragement throughout my research journey. His insightful feedback and expertise have been invaluable in shaping this thesis.

I am profoundly grateful to the PDZnet, H2020-MSCA-ITN-2015 (Project no. 675341) and SZTest, H2020-MSCA-RISE-2016 (Project no. 734791) for their generous financial support, which made this research possible. Their commitment to advancing scientific knowledge and innovation is truly commendable.

I extend my heartfelt thanks to the *Klinik und Poliklinik für Psychiatrie und Psychotherapie* at LMU Klinikum, LMU München. The collaborative and intellectually stimulating environment provided by the department has been instrumental in the successful completion of my research. I would like to acknowledge the administrative and technical staff for their assistance and support throughout my studies.

A special thanks to my colleagues and fellow researchers, whose camaraderie and collaborative spirit have made this journey enjoyable and enriching. In particular, I would like to mention Nirmal Kannyian, Dr. Alexander Mouris, Dr. Michael Wehr and Dr. Sven Wichert for their valuable feedback, insightful discussions, and unwavering support.

I am also deeply appreciative of Beate Kauschat and Nadia Gabellini for their exceptional assistance with maintaining cell culture facility, Dr. Niels Jensen, Wilma Vogel, Jessica Bly and Pia Pickelmann for maintaining Animal facility and setting up breeding's and Stefanie Behrens and Lotte Lenz for their help in running the NGS facility.

I would like to acknowledge the significant contribution of the animals that were sacrificed in the study. Their role in advancing scientific research is deeply respected and appreciated.

Last but not least, I am forever indebted to my family and friends for their unconditional support and encouragement throughout this journey. Their belief in me has been a constant source of motivation.

Thank you all for being an integral part of this journey.